AERODYNAMIC PRELIMINARY ANALYSIS SYSTEM II

PART I THEORY

By E. Bonner, W. Clever, K. Dunn

North American Aircraft Division, Rockwell International

SUMMARY

An aerodynamic analysis system based on potential theory with edge consideration at subsonic/supersonic speeds and impact type finite element solutions at hypersonic conditions is described. Three-dimensional configurations having multiple non-planar surfaces of arbitrary planform and bodies of non-circular contour may be analyzed. Static, rotary, and control longitudinal and lateral-directional characteristics may be generated.

The analysis has been implemented on a time sharing system in conjunction with an input tablet digitizer and an interactive graphics input/output display and editing terminal to maximize its responsiveness to the preliminary analysis problem. CDC 175 computation time of 45 CPU seconds/Mach number at subsonic-supersonic speeds and 1 CPU second/Mach number/attitude at hypersonic conditions for a typical simulation indicates that program provides an efficient analysis for systematically performing various aerodynamic configuration tradeoff and evaluation studies.

TABLE OF CONTENTS

INTRODUCTION

Aerodynamic numerical analysis has developed to a point where evaluation of complete aircraft configurations by a single program is possible. Programs designed for this purpose in fact currently exist, but are limited in scope and abound with subtleties requiring the user to be highly experienced. Many of the difficulties are attributable to the numerical sensitivity of the associated solution. In preliminary design stages, some degree of approximation is acceptable in the interest of modest turn-around time, reduced computational costs, simplification of input, and stability and generality of results. The importance of short elapsed time stems from the necessity to systematically survey a large number of candidate advanced configurations or major component geometric parameters in a timely manner. Modest computational cost allows a greater number of configurations and/or conditions to be economically investigated.

One approach in this spirit is to employ panel approximations which reduce the member of simultaneous equations required to satisfy flow boundary conditions. Surface chord plane formulations, locally two dimensional crossflow body solutions and non-interfering panel simplifications are examples of approximations which can be used for this purpose.

Finite element analysis when combined with realistic assessment of limitations and estimated viscous characteristics provides a valuable tool for analyzing general aircraft configurations and aerodynamic interactions at modest attitudes for subsonic/supersonic speeds and evaluation of compressible non-linearities at high Mach numbers.

LIST OF SYMBOLS

A	Projected oblique cross section area
A_{ij}	Influence coefficient. Normalwash at control point i due to vortex panel j of unit strength
A_i	Area of quadrilateral panel i
b	Reference span
c	Local chord
$\bar{c}$	Reference chord
c_{AVG}	Average chord
C_d	Section drag coefficient
C_D	Drag coefficient
C_F	Flat plate skin friction coefficient
C_i	Boundary condition for control point i
C_ℓ	Section lift coefficient
C_ℓ, C_m, C_n	Rolling, pitching and yawing moment coefficients
C_L	Lift coefficient
C_n	Section normal force coefficient
C_P	Pressure coefficient $(P-P_\infty)/q$
$C_{P_{NET}}$	Net pressure coefficient $(P_\ell-P_u)/q$ and vortex panel strength
C_X, C_Y, C_Z	Axial, side, normal force coefficient

LIST OF SYMBOLS (CONTINUED)

C^*	$\frac{\mu^*}{\mu_\infty}\frac{T_\infty}{T^*}$
F_X, F_Y, F_Z	Force components
$g(x)$	Axisymmetric outer solution to potential equation
h	Radius of curvature of cross sectional boundary
$\bar{i}, \bar{j}, \bar{k}$	Unit vectors in x,y,z direction respectively
K	Drag due to lift factor or skin friction thickness correction factor
K_S	Equivalent distributed sand gain height or attainable suction fraction
ℓ	Effective length
$\ell(i,n)$	Length of segment i, i+1 of contour C_n
L	Equivalent body length or geometric length
L/d	Body fineness ratio
M	Mach number
M_X, M_Y, M_Z	Moment components
n	Unit normal
p,q,r	Rolling, pitching and yawing velocity about x, y and z
$\hat{p},\hat{q},\hat{r}$	Nondimensional angular velocities pb/2U, qc̄/2U and rb/2U
P	Pressure
P_r	Prandtl number

LIST OF SYMBOLS (CONTINUED)

q	Free stream dynamic pressure $1/2 \rho U^2$
r	Recovery factor
R	Unit Reynolds number or radius of curvature
$R_{[\ ]}$	Reynolds number based on [ ]
$\mathcal{R}$	Gas constant
s	Segment arc length
S	Body cross sectional area or surface area
S_{REF}	Reference area
T	Static temperature °R or tangent of quadrilateral panel leading edge sweep
t/c	Airfoil thickness ratio
u,v,w	x,y,z nondimensional components of perturbation velocity
U	Freestream velocity
V	Jet velocity
W	Complex potential function
x,y,z	Body axis coordinate system
x,r,θ	Cylindrical coordinate system
Z	Complex number y+iz
α	Angle of attack
α_i	Local angle of attack at surface control point i
β	Angle of sideslip or $\sqrt{\lvert 1-M^2 \rvert}$

LIST OF SYMBOLS (CONTINUED)

γ	Vorticity strength per unit length or ratio of specific heats
Γ	Horseshoe vortex strength in Trefftz plane
δ	Deflection or impact angle
η	Lateral surface coordinate
$\frac{\delta \nu}{\delta x}$	Body slope
θ	Dihedral angle of quadrilateral panel or boundary layer momentum thickness
Λ	Sweep angle
μ	Absolute viscosity
ν	Kinematic viscosity, μ/ρ
ρ	Density
σ	Source density
T	Side edge rotation factor
ϕ	Perturbation velocity potential
Φ	Total velocity potential
ψ	See figure 3
Ω	Leading edge rotation factor

Subscript

c	camber
CG	center of gravity
F	friction
ℓ	lower surface

LE	leading edge
r	recovery
t	thickness
T	tip
TRAN	transition point
u	upper surface
v	vortex
w	wave
∞	freestream condition

Superscripts

'	first derivative or quantity based on effective origin
''	second derivative
*	Eckert reference temperature condition

SUBSONIC/SUPERSONIC

The arbitrary configurations which may be treated by the analysis are simulated by a distribution of source and vortex singularities. Each of these singularities satisfies the linearized small perturbation potential equation of motion

$$\beta^2 \phi_{xx} + \phi_{yy} + \phi_{zz} = 0$$

The singularity strengths are obtained by satisfying the condition that the flow is tangent to the local surface:

$$\frac{\partial \Phi}{\partial n} = 0$$

All of the resulting velocities and pressures throughout the flow may be obtained when the singularity strengths are known. A configuration is composed of bodies, interference shells and aerodynamic surfaces (wings, canards, tails etc.). The following types of singularites are used to represent each.

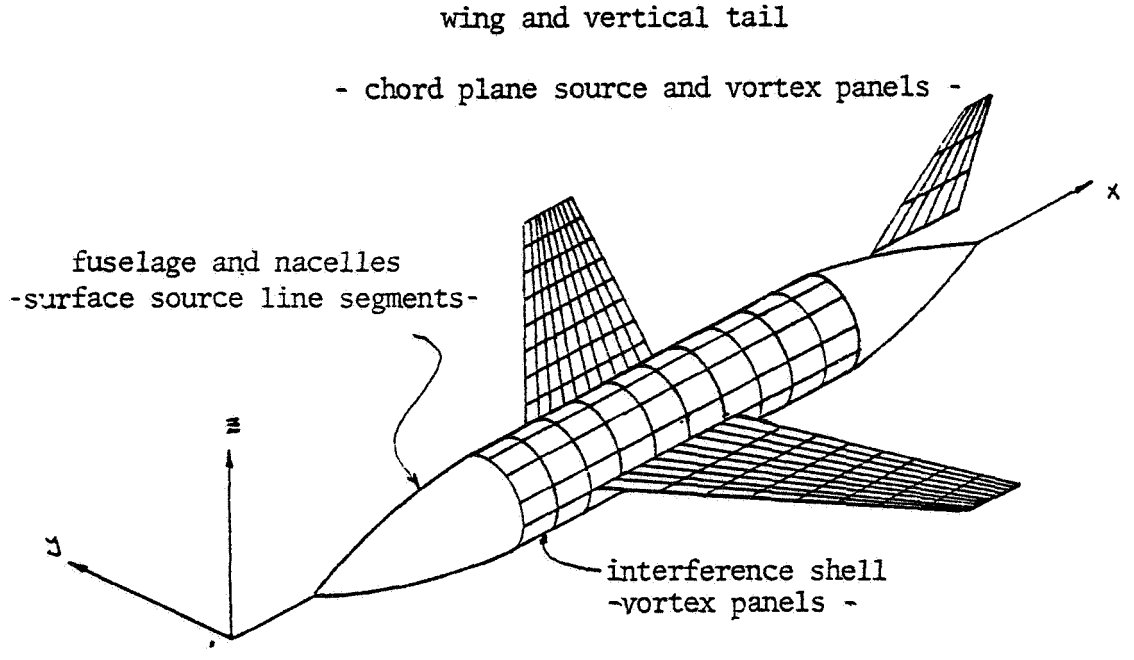

The first step in the solution procedure consists of obtaining the strengths of the singularities simulating the fuselage and nacelles, from an isolated body solution. The present analysis uses slender-body theory to

predict the surface and near field properties. The solution is composed of a compressible axisymmetric component for a body of revolution of the same crossectional area and an incompressible crossflow component, ϕ, satisfying the local three dimensional boundary conditions in the (y,z) plane. The crossflow is a solution of Laplace's equation

$$\phi_{yy} + \phi_{zz} = 0$$

A two-dimensional surface source distribution formulation is used to obtain this solution. When the body singularity strengths are determined, the perturbation velocities which they induce on the aerodynamic surfaces, or other regions of the field, are evaluated.

The assumptions of thin airfoil theory allow the effects of thickness and lift on aerodynamic surfaces to be considered independently. Therefore, the effects of the aerodynamic surfaces can be simulated by source and vortex singularities accounting for the effects of thickness and lift, respectively. The source and vortex distributions used in this program are in the form of quadrilateral panels having a constant source or vortex strength. The vortex panels have a system of trailing vorticies extending undeflected to downstream infinity. The use of a chordwise linearly varying source panel is provided as an option to eliminate singularities associated with sonic panel edges at supersonic Mach numbers.
The panels are planar, that is they have no incidence to the free stream (although dihedral may be included), since thin airfoil theory allows the transfer of the singularities and boundary conditions to the plane of the mean chord. These boundary conditions are satisfied at a single control point on each panel. For thickness, the control point is located at the panel centroid while the effects of twist, camber, and angle of attack are satisfied at the spanwise centroid of each vortex panel and at 87.5 percent of its chord.

A cylindrical, non-circular, interference shell, composed entirely of vortex panels, is used to account for the interference effects of the aerodynamic surfaces on the fuselage and nacelles. The boundary conditions on an interference shell are such that the velocity normal to the shell induced by all singularities, except those of the body which it surrounds, is zero. The boundary conditions are satisfied at the usual control points for vortex panels.

The following sections define the details of the solution procedure. Included are discussions of the isolated body analysis, surface finite element analysis considering edge effects, and evaluation of aerodynamic characteristics including drag. References are cited for the reader interested in further pursuing a particular point.

BODY SOLUTION

According to slender body theory[1,2] the flow disturbance near a sufficiently regular three-dimensional body may be represented by a perturbation potential of the form

$$\phi = \varphi(y,z;x) + g(x) \tag{1}$$

$\varphi(y,z;x)$ is a solution of the 2-D Laplace equation in the y, z cross flow plane satisfying the following boundary conditions

$$\nabla\varphi = jv + kw = 0$$

$$\frac{\partial \varphi}{\partial n} = 0 \qquad \text{on } C(x) \tag{2}$$

C(x) and n, are defined in figure 1 . A general solution for φ may be written as the real part of a complex potential function W(Z) with $Z = y + iz$.

$$\varphi = \mathrm{Re}\, W = \mathrm{Re}\left\{ A_0(x) \ln Z + \sum_{m=1}^{\infty} A_m(x) Z^{-m} \right\}$$

A useful alternative representation of φ and W is obtainable with the aid of Green's theorem[3]

$$\varphi = \mathrm{Re}\, W = -2\,\mathrm{Re} \oint_{c(x)} \sigma(\zeta) \ln(Z-\zeta)\, d\Delta \tag{3}$$

where $\sigma(\zeta)$ is a "source" density for values of $\zeta = y_c + iz_c$, (y_c, z_c) being coordinates of a point on the contour c(x).

The function g(x) is obtained by matching ϕ of equation (1) which is valid in the neighborhood of the body with an appropriate "outer" solution. g(x) is then found to depend explicitly on the Mach number M and longitudinal variation of cross-sectional areas S(x)

$$g(x) = \frac{1}{2\pi}\left\{ S'(x)\ln(\tfrac{1}{2}\beta) - \tfrac{1}{2}\int_0^x S''(t)\ln(x-t)\,dt + \tfrac{1}{2}\int_x^1 S''(t)\ln(t-x)\,dt \right.$$
$$\left. - \tfrac{1}{2}S'(0)\ln x - \tfrac{1}{2}S'(1)\ln(1-x) \right\} \qquad M<1$$
$$g(x) = \frac{1}{2\pi}\left\{ S'(x)\ln(\tfrac{1}{2}\beta) - \int_0^x S''(t)\ln(x-t)\,dt \right\} \qquad M>1 \tag{4}$$

where

$$\beta = \sqrt{|1-M^2|}$$

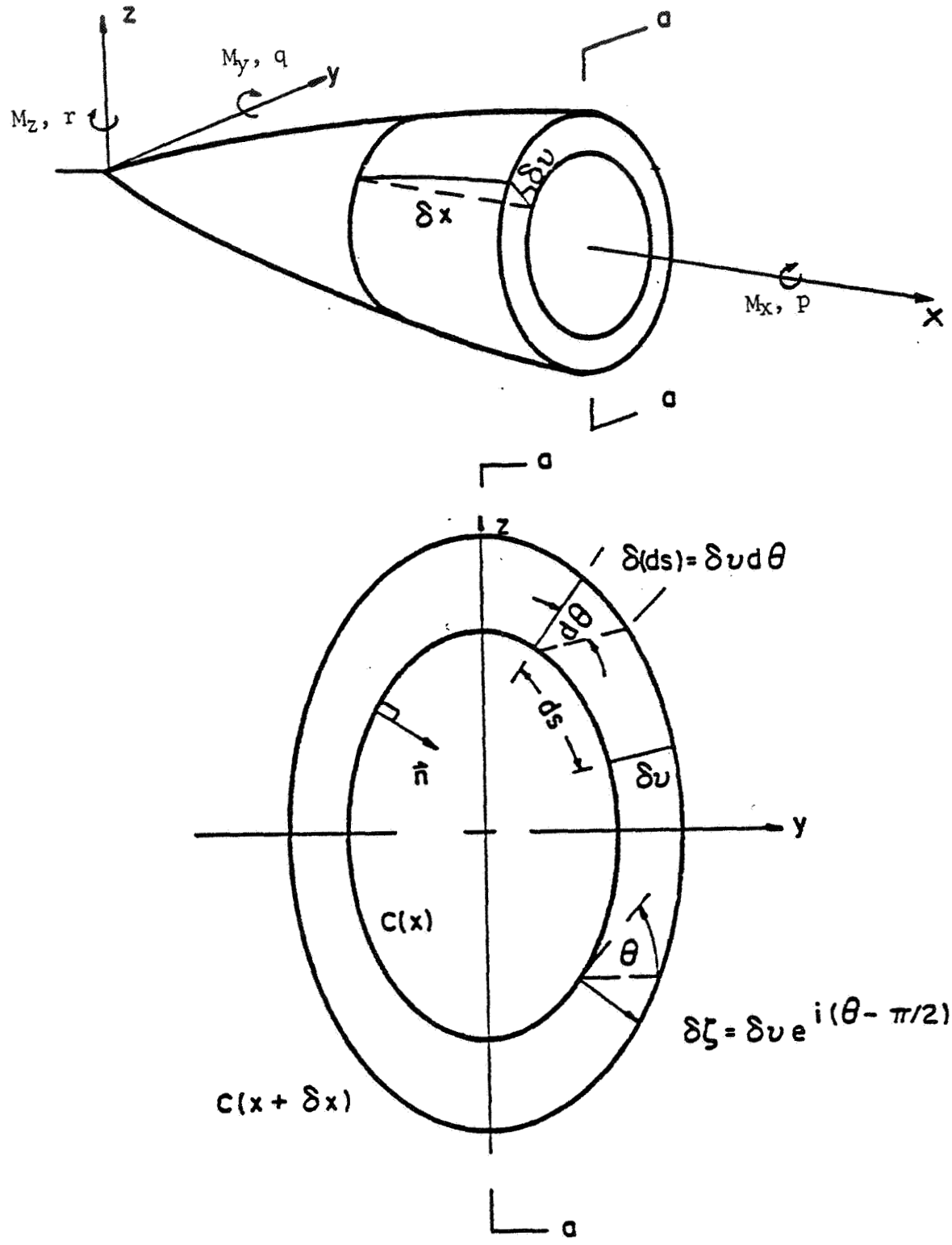

Figure 1. Body Slope and Cross-sectional Variables

The body axis perturbation velocities are obtained by differentiation of equation (1)

$$u = \phi_x = \phi_x + g'(x)$$

$$v = \phi_y$$

$$w = \phi_z$$

At supersonic speeds, zone of influence considerations require that $u = v = w = 0$ for $x - \beta r < 0$.

Solution of the preceding equations is based on an extension of the method of reference 3.

CROSS FLOW COMPONENT

The reduction of computations to a numerical procedure utilizes the integral representation of ϕ given in equation (3) by discretization of the cross sectional boundary into a large number of short linear segments (figure 2) over each of which the source density σ is assumed constant at a value determined by boundary conditions.

Computation of $\sigma(i,n)$ over the segment i, i+1 proceeds by applying the boundary condition equation (2) at each segment of C_n. If $\nabla\phi = \vec{q} = \vec{j}v + \vec{k}w$ represents the velocity vector, the corresponding complex velocity in the cross flow plane is obtained by differentiation of W in equation (3) with respect to Z:

$$v - i w = -2 \oint \frac{\sigma(\zeta)}{Z - \zeta} \, d\zeta \qquad (5)$$

The contribution by the sources located on segment i, i+1 to the velocity at $P_{j,n}$ is first evaluated. Noting that i, i+1 makes an angle $\theta(i,n)$ with respect to the horizontal axis, we have

$$d\zeta = ds \, e^{i\theta(i,n)}$$

and the contribution to the integral in equation (5) may be written:

$$\Delta \left\{ v(j,n) \;\; i\,w(j,n) \right\} = -2\sigma(i,n) \, e^{-i\theta(i,n)} \int_{\zeta_{i,n}}^{\zeta_{i+1,n}} \frac{d\zeta}{Z_{j,n} - \zeta}$$

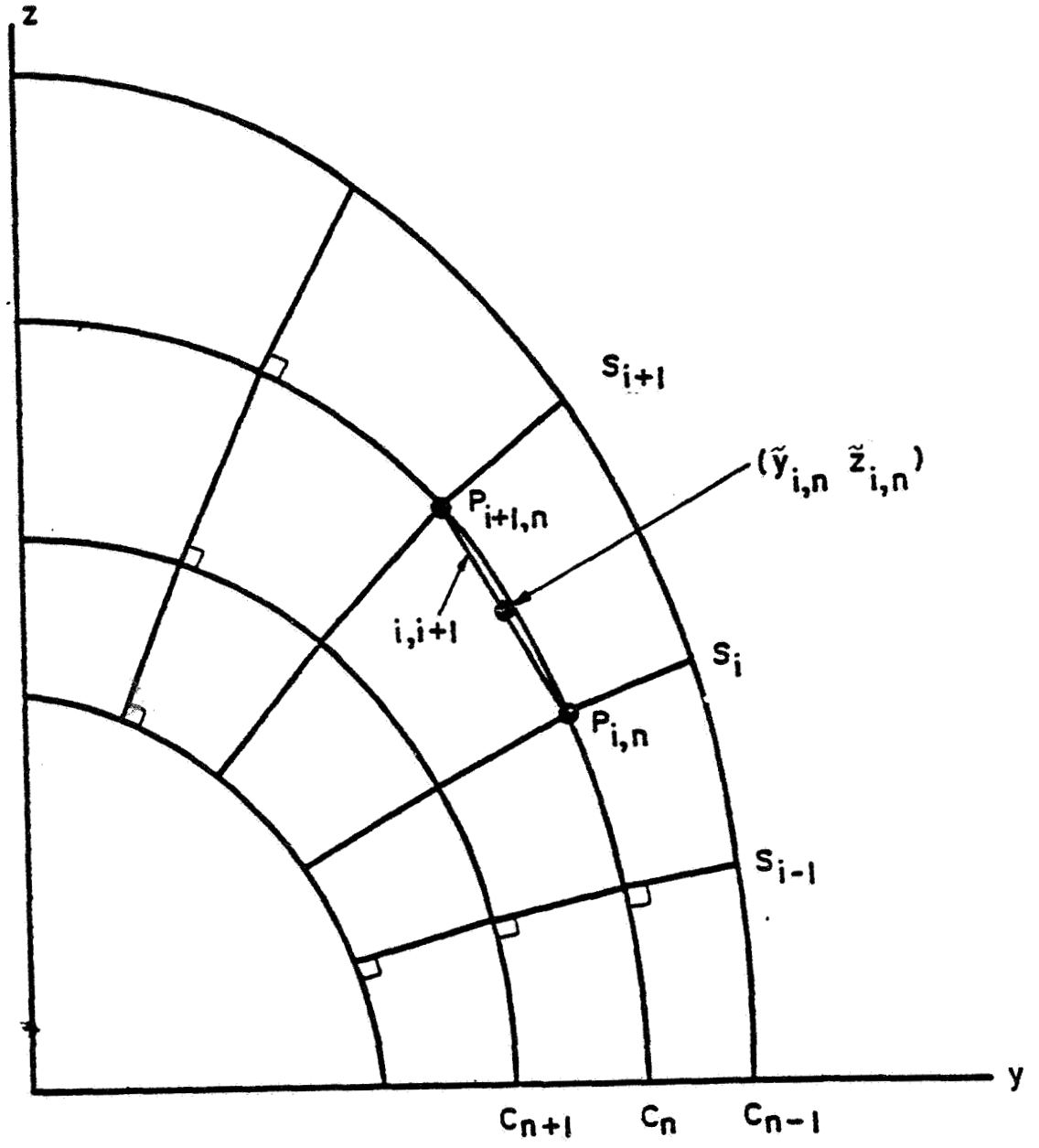

Figure 2. Cross-section Boundary Segmenting Scheme

After integration of the last term and summation over all contributing segments, the result may be written

$$v(j,n) - i\,w(j,n) = -2 \sum_{i} \sigma(i,n) e^{-i\theta(i,n)} \left\{ \ln \frac{R(i+1,j,n)}{R(i,j,n)} + i\,\delta(i,j,n) \right\} \qquad (6)$$

in which, referring to figure 3 , the quantities $R(i,j,n)$ and $\delta(i,j,n)$ are defined by the relationships

$$R(i,j,n)\, e^{i\psi(i,j,n)} = \tilde{z}_{j,n} - z_{i,n}$$

$$\delta(i,j,n) = \tilde{\psi}(i,j,n) - \psi(i,j,n) .$$

To insure uniqueness of the complex velocity, care must be exercised in assigning values to the angles $\psi(i,j,n)$ and $\tilde{\psi}(i,j,n)$. Referring to figure 3 , these are measured counter-clockwise from the positive y axis so that when facing from $P_{i,n}$ to $P_{i+1,n}$, a point $\tilde{P}_{j,n}$ just to the left of i,i+1 shall define an angle $\psi(i,j,n) = \theta(i,n)$. As $\tilde{P}_{j,n}$ traverses a path around $P_{i,n}$ to a point just to the right of i,i+1, $\psi(i,j,n)$ increases from $\theta(i,n)$ to $\theta(i,n) + 2\pi$. The same holds true for $\tilde{\psi}(i,j,n)$ as $\tilde{P}_{j,n}$ traverses a path around $P_{i+1,n}$. In consequence of these definitions $\delta(i,j,n)$ becomes $-\pi$ when approaching i,i+1 from the right and π when approaching from the left. This discontinuity reflects that exhibited by the stream function upon traversing any closed path which encloses a distribution of finite sources.

From the boundary condition equation (2), we have

$$-\left(\frac{\partial \phi}{\partial n}\right)_{j,n} = v(j,n) \sin\theta(j,n) - w(j,n) \cos\theta(j,n)$$

After substitution of v and w from equation (6), this last expression becomes

$$-\left(\frac{\partial \phi}{\partial n}\right)_{j,n} = \sum_{i} a(j,i)\, \sigma(i,n) \qquad (7)$$

where

$$a(j,i) = 2 \left\{ \sin[\theta(j,n) - \theta(i,n)] \ln \frac{R(i+1,j,n)}{R(i,j,n)} + \delta(i,j,n) \cos[\theta(j,n) - \theta(i,n)] \right\}$$

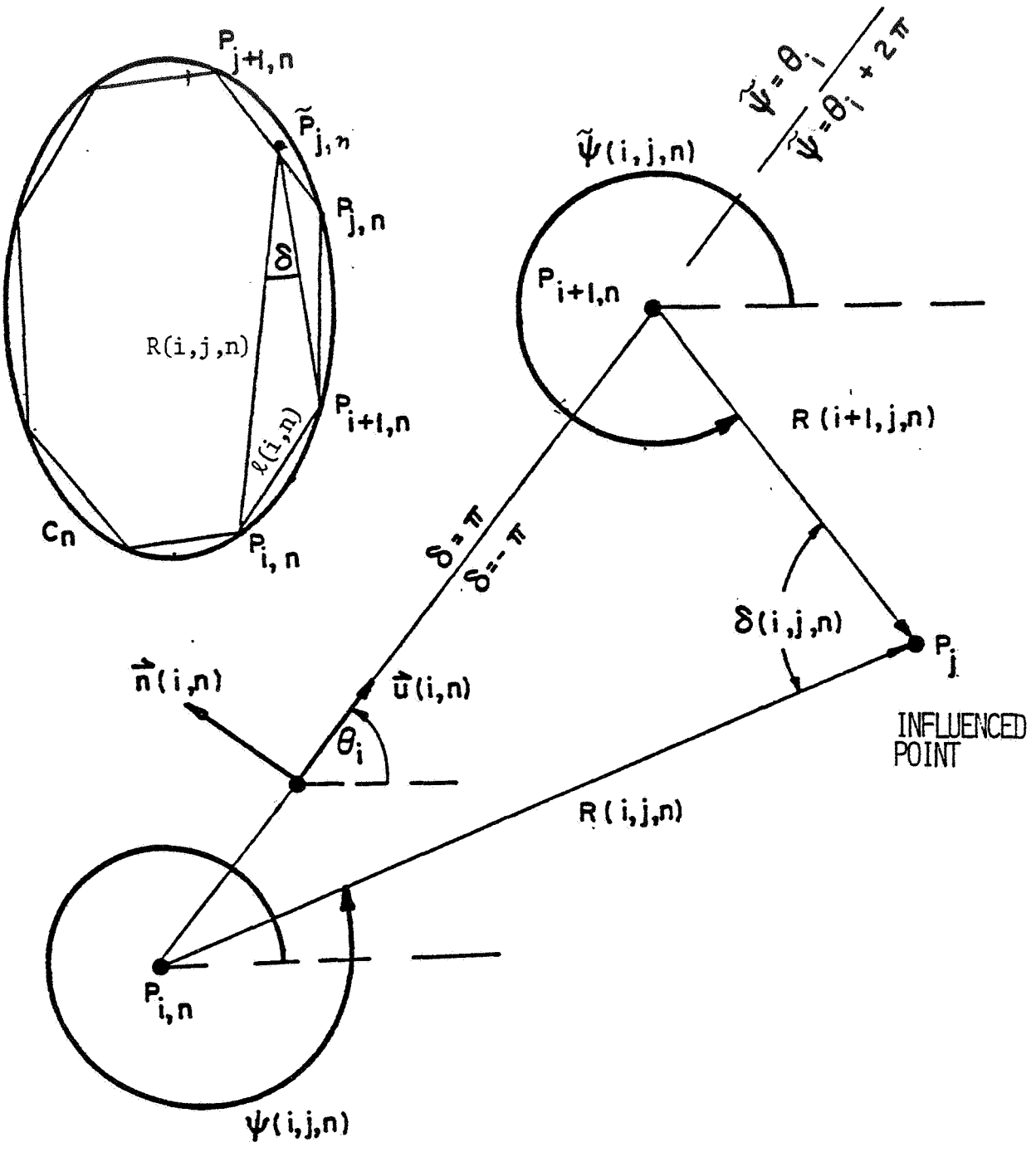

Figure 3. Details of Variables Pertaining to Segment i,i+1 of Boundary C_n

The surface normal perturbation velocity $-(\partial\varphi/\partial n)_{j,m}$ may be written in terms of the body slope $(\partial\nu/\partial x)_{j,m}$, the angles of attack α, and sideslip β and the angular velocities p,q,r as

$$-\left(\frac{\partial\varphi}{\partial n}\right)_{j,m} = \left(\frac{\partial\nu}{\partial x}\right)_{j,m} + \left[\alpha + \frac{1}{U}\, q(x-x_{cg}) + \frac{1}{U}\, py\right]\cos\theta(j,m)$$

$$+ \left[\beta - \frac{1}{U}\, r(x-x_{cg}) + \frac{p}{U}\,(z-z_{cg})\right]\sin\theta(j,m)$$

Satisfying equation 7 at each of the points $\tilde{P}_{j,n}$ on a given contour boundary yields a set of equations for $\sigma(i,n)$.

AXISYMMETRIC COMPONENT

Differentiation of g(x) must be carried out with due concern for the nature of the improper integrals appearing in equation (4). The result is

$$g'(x_m) = \frac{1}{4\pi}\left\{ S''(x_m)\ln\tfrac{1}{4}(1-M^2) + I_m(x_m) - J_m(x_m) \right.$$

$$\left. - \frac{1}{x_m}\, S'(0) + \frac{1}{(1-x_m)}\, S'(1) - S''(0)\ln x_m - S''(1)\ln(1-x_m)\right\} \qquad M<1$$

$$g'(x_m) = \frac{1}{2\pi}\left\{ \frac{1}{2}\, S''(x_m)\ln\tfrac{1}{4}(M^2-1) - J_m(x_m) - S''(0)\ln x_m \right\} \qquad M>1$$

where

$$I_m(x_m) = \int_{x_m}^{1} \ln(x_m - t)\, S'''(t)\, dt = \sum_{m=n}^{N-1} \left[S''_{m+1} - S''_m \right] \ln(\tilde{x}_m - x_m)$$

$$J_m(x_m) = \int_{0}^{x_m} \ln(x_m - t)\, S'''(t)\, dt = \sum_{m=0}^{m-1} \left[S''_{m+1} - S''_m \right] \ln(x_m - \tilde{x}_m)$$

$$\tilde{x}_m = \tfrac{1}{2}(x_{m+1} + x_m)$$

To compute the second derivatives of the equivalent body cross sectional area required for $g'(x)$, the first derivatives at $\bar{x}_m$ are found by finite differences between x_m and x_{m+1}. Second derivatives $S''(\bar{x}_m)$ at $\bar{x}_m$ $(\bar{x}_{m+1} + \bar{x}_m)/2$ are then found by finite differences between S' at $\bar{x}_m$ and $\bar{x}_{m+1}$. Finally $S''(x_m)$ is determined by linear interpolation of $S''(\bar{x}_m)$ between $\bar{x}_m$ and $\bar{x}_{m+1}$.

PERTURBATION VELOCITIES

The axial velocity u depends on $(\partial\phi/\partial x)$ and the axisymmetric solution $g'(x)$. $(\partial\phi/\partial x)$ is obtained by differentiation of the integral in equation (3) to first obtain an exact expression which is then approximated by evaluating the result over the segmented boundary.

The derivation of $\partial\phi/\partial x$ must take into account the fact that the path of integration in equation (3) is a function of x. Referring to figure 1 increments of a dependent variable taken along C(x) are denoted by $d(\ )$ and increments taken normal to C are denoted by $\delta(\ )$. Differentiation of equation (3) then yields

$$\frac{\partial\phi}{\partial x} = -2\,\mathrm{Re}\left\{ \oint \frac{\delta\sigma}{\delta x} \ln(Z-\zeta)\,ds - \oint \frac{\sigma(\zeta)}{Z-\zeta} \frac{\delta\zeta}{\delta x}\,ds + \oint \sigma(\zeta) \ln(Z-\zeta) \frac{\delta(ds)}{\delta x} \right\} \tag{8}$$

From figure 1

$$\delta(ds) = \delta\nu\,d\theta = \delta\nu \frac{ds}{h(\zeta)} \tag{9}$$

where $h(\zeta)$ is the radius of curvature of C(x) at ζ. In addition, we have from figure 1

$$\frac{\delta\zeta}{\delta x} = \frac{\delta\nu}{\delta x} e^{i(\theta - \frac{1}{2}\pi)} \tag{10}$$

To evaluate $\frac{\delta\sigma}{\delta x}$ we note,

$$\frac{\delta\sigma}{\delta x} = \lim_{\delta x \to 0} \frac{\sigma(i,n+1) - \sigma(i,n)}{\delta x} \tag{11}$$

Introducing equations (9), (10), and (11) into equation (8),

$$\frac{\partial\phi}{\partial x} = -2\,\mathrm{Re}\left\{ \oint \left[\left(\frac{\delta\sigma}{\delta x}\right)_o + \frac{\sigma}{h}\frac{\delta\nu}{\delta x} \right] \ln(z-\zeta)\,d\Delta + i\oint \left[\sigma\frac{\delta\nu}{\delta x}\right]\frac{d\zeta}{z-\zeta} \right\}$$

Again, assuming that quantities in the brackets of the integrands are constant over i,i+1,

$$\left(\frac{\partial\phi}{\partial x}\right)_{j,n} = 2\sum_i \left\{ \left[\left(\frac{\delta\sigma}{\delta x}\right)_o + \frac{\sigma}{h}\frac{\delta\nu}{\delta x} \right]_{i,n} \frac{\Delta\phi(i,j,n)}{\sigma(i,n)} - \sigma(i,n)\left(\frac{\delta\nu}{\delta x}\right)_{i,n} \delta(i,j,n) \right\}$$

where

$$\frac{\Delta\phi(i,j,n)}{\sigma(i,n)} = \left\{ \vec{R}(i+1,j,n)\cdot\vec{u}(i,n)\,\ln R(i+1,j,n) - \vec{R}(i,j,n)\cdot\vec{u}(i,n)\,\ln R(i,j,n) - \vec{R}(i,j,n)\cdot\vec{n}(i,n)\,\delta(i,j,n) + \ell(i,n) \right\}$$

The radius of curvature h(i,n) and the derivatives $\delta\sigma/\delta x$, $\delta\nu/\delta x$ are approximated at the mid points of the segments i,i+1 as follows

a) $\delta\sigma/\delta x$ - the derivative at the mid-point $\tilde{x}_n$ of the interval x_n, x_{n+1} is set equal to the divided difference between $\sigma(i,n)$ and $\sigma(i,n+1)$. Linear interpolation between these derivatives then yields $\delta\sigma/\delta x$ at x_n.

b) $\delta\nu/\delta x$ - referring to figure 4 , the displacement $\delta\eta$ is determined by linear interpolation between $\delta\zeta_{i,n}$ and $\delta\zeta_{i+1,n}$. $\delta\eta/(x_{n+1} - x_n)$ then represents $\delta\nu/\delta x$ at $\tilde{x}_n$. Linear interpolation between the stations x'_n then yields $\delta\nu/\delta x$ at x_n .

c) $1/h$: - θ at $P_{i,n}$ is determined by interpolation between values of $\theta(i,n)$ at $\tilde{P}_{i,n}$. The curvature 1/h at $\tilde{P}_{i,n}$ is then set equal to the divided difference between θ at $P_{i+1,n}$ and θ at $P_{i,n}$.

The lateral and vertical perturbation velocities, v and ω , are obtained from

$$v - i\omega = -2\oint \frac{\sigma(\zeta)}{z-\zeta}\, ds$$

Integration over the boundary with constant segment source density yields:

$$v(j,n) - i\,\omega(j,n) = 2\sum_i \sigma(i,n)\, e^{i\theta(i,n)} \left\{ \ln \frac{R(i+1,j,n)}{R(i,j,n)} - i\,\delta(i,j,n) \right\}$$

Thus

$$v \equiv \phi_y = 2\sum_i \sigma(i,n) \left\{ \ln \frac{R(i+1,j,n)}{R(i,j,n)} \cos\theta(i,n) - \delta(i,j,n) \sin\theta(i,n) \right\}$$

$$\omega \equiv \phi_z = 2\sum_i \sigma(i,n) \left\{ \ln \frac{R(i+1,j,n)}{R(i,j,n)} \sin\theta(i,n) - \delta(i,j,n) \cos\theta(i,n) \right\}$$

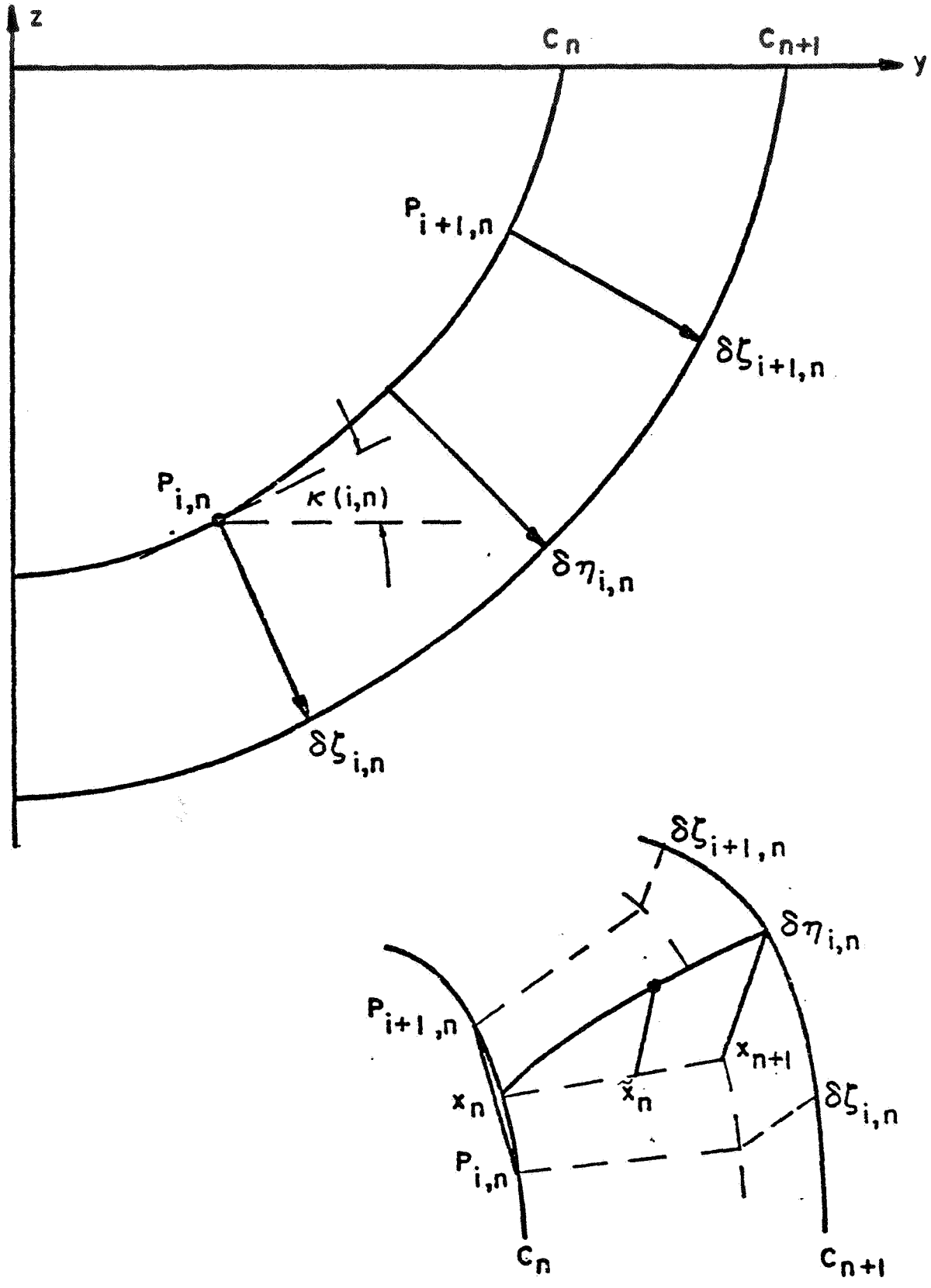

Figure 4. Interpolation Procedure for Determination of $(\delta\nu/\delta x)_{i,n}$

SURFACE SOLUTION

The wing, canard, vertical and horizontal tail are simulated by a system of swept tapered chord plane source and vortex panels with two edges parallel to the free stream. The coordinates of the panel corners are specified with respect to an (x,y,z) system having its x axis in the free stream direction and its z axis in the lift direction. The panel influence equations are written in terms of a coordinate system having a z axis normal to the panel and an x axis along one of the two parallel edges. A coordinate transformation is necessary to obtain the coordinates in the panel reference system. If the plane of the panel is inclinded at an angle θ_p with respect to the y, z plane, a transformation into the panel coordinate system (x_p,y_p,z_p) is accomplished as follows:

$$x_p = x$$

$$y_p = y\cos\theta_p + z\sin\theta_p$$

$$z_p = -y\sin\theta_p + z\cos\theta_p$$

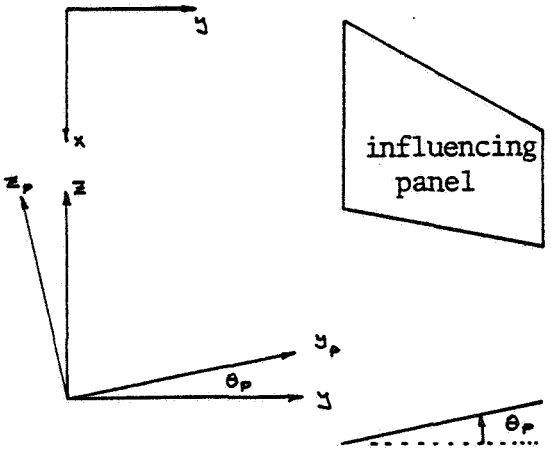

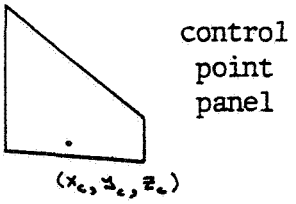

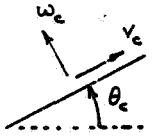

$$u_c = u_p$$

$$V_c = V_p\cos(\theta_c-\theta_p) + \omega_p\sin(\theta_p-\theta_c)$$

$$\omega_c = -V_p\sin(\theta_c-\theta_p) + \omega_p\cos(\theta_p-\theta_c)$$

A transformation of the (u_p,v_p,w_p) velocities into the coordinate system of the panel on which the control point is located (u_c,v_c,w_c) results in the axial, binormal and normal velocities induced on the panel.

For the image of the influencing panel, the signs of y, θ_c and v_c are changed while using the same calculation procedure.

PANEL SINGULARITY STRENGTHS

The source singularity strengths may be found directly by equating each source panel strength to the slope of the thickness distribution at its control point. For panel i

$$\sigma_i = \left(\frac{dz_t}{dx}\right)_i$$

where Z_t refers to the shape of the thickness distribution. The influence equations for the source panels can then be used to obtain the velocities induced by the source panels anywhere in the flow.

The determination of the vortex panel singularity strengths are the final step in the solution procedure. They are obtained by solving a set of simultaneous equations utilizing the vortex panel influence equations to relate the singularity strengths to the boundary conditions at the control points of the vortex panels. The boundary conditions permit the condition of tangential flow to be satisfied.

Each vortex panel j having singularity strength C_{p_j} induces a set of velocities (A^u_{ij}, A^v_{ij}, A^ω_{ij}) on panel i. Therefore a set of influence equations can be written:

$$u_{c_i} = \sum_j A^u_{ij} C_{p_j} + u_{o_i}$$

$$v_{c_i} = \sum_j A^v_{ij} C_{p_j} + v_{o_i}$$

$$\omega_{c_i} = \sum_j A^\omega_{ij} C_{p_j} + \omega_{o_i}$$

where (u_{oi}, v_{oi}, w_{oi}) refer to the velocities induced by all other body and source singularities, and written in the coordinate system of the panel containing the control point. Since the resultant velocity along the normal at a panel control point must be zero,

$$\vec{U}\cdot\vec{n} = U\left[\vec{e}_x + u_c\vec{e}_x + v_c\vec{e}_b + \omega_c\vec{e}_n\right]\cdot\vec{n}$$

$$= U\left[(1+u_c)\vec{e}_x\cdot\vec{n} + \omega_c\right] = 0$$

$$(1+u_c)\vec{e}_x\cdot\vec{n} \approx -\left(\frac{dz_c}{dx}\right)_i$$

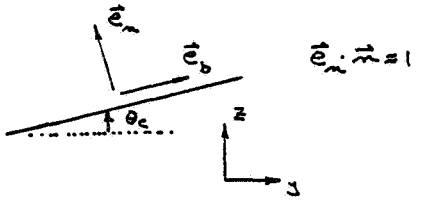

$\vec{e}_n\cdot\vec{n} = 1$

$$\omega_{c_i} = \left(\frac{dz_c}{dx}\right)_i$$

and the following system of equations results

$$\sum_j A^{\omega}_{ij} C_{p_j} = \left(\frac{dz_c}{dx}\right)_i - \omega_{o_i}$$

This set of linear equations can be solved for the C_{p_j} and, since it assumes symmetrical panel loading, can be used to determine the longitudinal characteristics. A similar set of equations exist for the calculation of the lateral/directional characteristics. This set assumes an antisymmetrical panel loading and has a correspondingly different set of influence coefficients A_{ij}.

BOUNDARY CONDITIONS

Several types of basic and unit boundary conditions are considered and can be classified as either symmetric or antisymmetric. Linearized theory allows the superposition of these basic unit solutions. The p, q and r rotary derivative boundary conditions are the result of placing the configuration at $\alpha = 0$, $\beta = 0$ in a flow field rotating at one radian per second.

Symmetric:

1) basic $\quad (dz_c/dx) - \omega_{o_B} - \omega_{o_s}$

(dz_c/dx) = surface slope due to twist and camber

ω_{o_B} = normalwash induced by slender body thickness and camber

ω_{o_s} = normalwash induced by source panels

2) Unit alpha $-\frac{\pi}{180}\cos\theta_c - \omega_{\alpha_B}$

ω_{α_B} = normalwash induced by slender body at unit alpha

3) Unit q rotation $-\frac{2}{c}(x - x_{c/4})\cos\theta_c - \omega_{q_B}$

ω_{q_B} = normalwash induced by slender body undergoing unit q rotation

4) Unit flap $-\frac{\pi}{180}\sigma$

σ = 1. for flap panel

σ = 0. for others

Antisymmetric:

1) Unit beta $-\frac{\pi}{180}\sin\theta_c - \beta_B$

β_B = normalwash induced by slender body at unit sideslip

2) Unit p rotation $-\frac{2}{b}(y - y_{c/4})\cos\theta_c - \frac{2}{b}(z - z_{c/4}) - \omega_{p_B}$

ω_{p_B} = normalwash induced by slender body undergoing unit p rotation

3) Unit r rotation $\frac{2}{b}(x - x_{c/4})\sin\theta_c - \omega_{r_B}$

ω_{r_B} = Normalwash induced by slender body undergoing unit r rotation

4) Unit flap $\frac{\pi}{180}\sigma$

σ = 1. for flap panel

σ = 0. for others

CONSTANT SOURCE AND CONSTANT VORTICITY PANEL INFLUENCE EQUATIONS

The source finite elements have a discontinuity in normal velocity across the panel surface while the vortex finite elements have a discontinuity in the tangential velocity in a direction normal to the panel leading edge. The magnitude of the discontinuity, in each case, is constant over the panel area. In addition the vortex panels have a system of trailing vorticies extending undeflected to downstream infinity.

A constant pressure or constant source panel with a quadrilateral shape can be constructed by adding or subtracting four semi-infinite triangular shaped panels[4]. These semi-infinite triangles, each determined by a corner of the quadrilateral, can be assumed to induce a velocity perturbation everywhere in the flow. However, each corner represents only an integration limit, and all four corners must be included to make any sense.

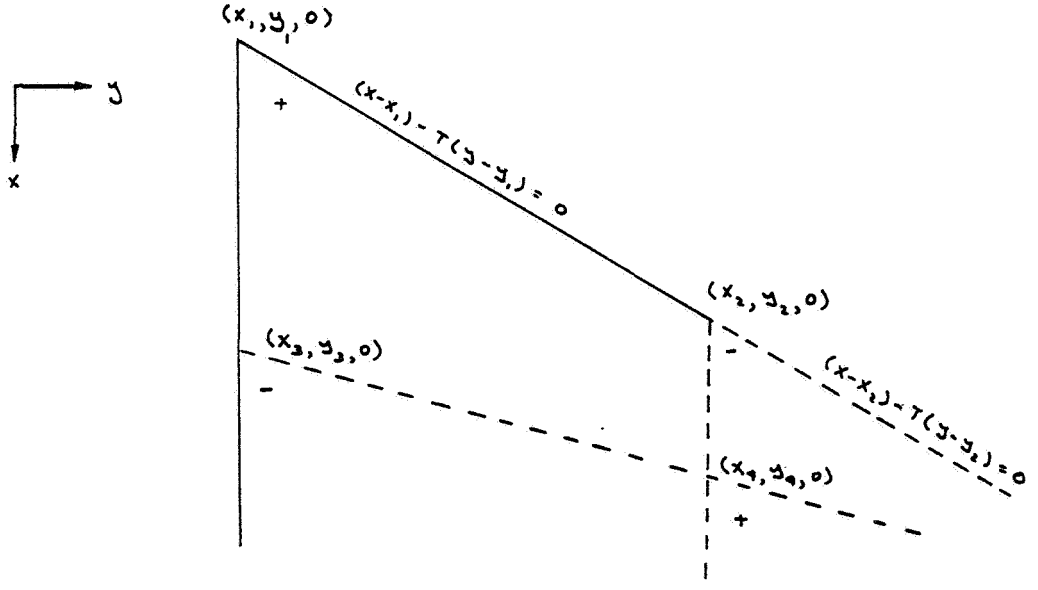

If it is kept in mind that four corners must be included, one of these triangles having sides determined by y = 0 and x-Ty = 0, induces the following perturbation velocities:

$$R^2 = x^2 + \beta^2(y^2+z^2) \qquad k = \begin{cases} 1 & M_\infty^2 < 1 \\ 2 & M_\infty^2 > 1 \end{cases}$$

$$\beta^2 = 1 - M_\infty^2$$

constant source panel

$$\Phi_s(x,y,z,T) = -\frac{\sigma k}{4\pi}\left\{ y\,\frac{1}{2}\log\frac{R+x}{R-x} + \frac{(x-Ty)}{\sqrt{T^2+\beta^2}}\,\frac{1}{2}\log\frac{\sqrt{T^2+\beta^2}\,R + (Tx+\beta^2 y)}{\sqrt{T^2+\beta^2}\,R - (Tx+\beta^2 y)} + z\tan^{-1}\frac{zR}{xy - T(y^2+z^2)}\right\}$$

$$u_s(x,y,z,T) = -\frac{\sigma k}{4\pi}\left\{ \frac{1}{\sqrt{T^2+\beta^2}}\,\frac{1}{2}\log\frac{\sqrt{T^2+\beta^2}\,R + (Tx+\beta^2 y)}{\sqrt{T^2+\beta^2}\,R - (Tx+\beta^2 y)}\right\}$$

$$v_s(x,y,z,T) = -\frac{\sigma k}{4\pi}\left\{ \frac{1}{2}\log\frac{R+x}{R-x} - \frac{T}{\sqrt{T^2+\beta^2}}\,\frac{1}{2}\log\frac{\sqrt{T^2+\beta^2}\,R + (Tx+\beta^2 y)}{\sqrt{T^2+\beta^2}\,R - (Tx+\beta^2 y)}\right\}$$

$$\omega_s(x,y,z,T) = -\frac{\sigma k}{4\pi}\left\{ \tan^{-1}\frac{zR}{xy - T(y^2+z^2)}\right\}$$

constant vorticity panel

$$\Phi_v(x,y,z,T) = \frac{c_p k}{8\pi}\left\{ Tz\,\frac{1}{2}\log\frac{R+x}{R-x} - (T^2+\beta^2)\frac{z}{\sqrt{T^2+\beta^2}}\,\frac{1}{2}\log\frac{\sqrt{T^2+\beta^2}\,R + (Tx+\beta^2 y)}{\sqrt{T^2+\beta^2}\,R - (Tx+\beta^2 y)} + (x-Ty)\tan^{-1}\frac{zR}{xy - T(y^2+z^2)}\right.$$

$$\left. - (2-k)\left[Tz\,\frac{1}{2}\log(y^2+z^2) + (x-Ty)\tan^{-1}\frac{y}{z}\right]\right\}$$

$$u_v(x,y,z,T) = \frac{c_p k}{8\pi}\left\{ \tan^{-1}\frac{zR}{xy - T(y^2+z^2)} - (2-k)\tan^{-1}\frac{y}{z}\right\}$$

$$v_v(x,y,z,T) = -\frac{c_p k}{8\pi}\left\{ T\tan^{-1}\frac{zR}{xy - T(y^2+z^2)} + \frac{zR}{(y^2+z^2)} - (2-k)\left[T\tan^{-1}\frac{y}{z} - \frac{zx}{(y^2+z^2)}\right]\right\}$$

$$\omega_v(x,y,z,T) = \frac{c_p k}{8\pi}\left\{ T\,\frac{1}{2}\log\frac{R+x}{R-x} - (T^2+\beta^2)\frac{1}{\sqrt{T^2+\beta^2}}\,\frac{1}{2}\log\frac{\sqrt{T^2+\beta^2}\,R + (Tx+\beta^2 y)}{\sqrt{T^2+\beta^2}\,R - (Tx+\beta^2 y)} + \frac{yR}{(y^2+z^2)}\right.$$

$$\left. - (2-k)\left[T\,\frac{1}{2}\log(y^2+z^2) - \frac{yx}{(y^2+z^2)}\right]\right\}$$

The total panel solution is built up by combining each of the four corners.

$$\Phi(x,y,z) = \phi(x-x_1, y-y_1, z, T_1) - \phi(x-x_2, y-y_2, z, T_1)$$
$$- \phi(x-x_3, y-y_3, z, T_3) + \phi(x-x_4, y-y_4, z, T_3)$$

$$U(x,y,z) = u(x-x_1, y-y_1, z, T_1) - u(x-x_2, y-y_2, z, T_1)$$
$$- u(x-x_3, y-y_3, z, T_3) + u(x-x_4, y-y_4, z, T_4)$$

etc.

These results hold for both subsonic and supersonic free stream velocities. In the latter case, only the real (downstream) contributions are considered.

The perturbation potential expressions are derived in Appendix A. Subsequently, verification of the perturbation velocities is presented.

LINEARLY VARYING SOURCE PANEL INFLUENCE EQUATIONS

In supersonic flow constant source panels having a sonic edge have a real singularity along an extension of this edge. The singularity occurs because:

$$\lim_{\substack{(x-x_1)\to T(y-y_1) \\ \epsilon^2=(T^2+\beta^2)\to 0}} \frac{1}{\epsilon}\left\{\frac{1}{2}\log\frac{\epsilon R_1+[T(x-x_1)+\beta^2(y-y_1)]}{\epsilon R_1-[T(x-x_1)+\beta^2(y-y_1)]}-\frac{1}{2}\log\frac{\epsilon R_2+[T(x-x_2)+\beta^2(y-y_2)]}{\epsilon R_2-[T(x-x_2)+\beta^2(y-y_2)]}\right\}=\infty$$

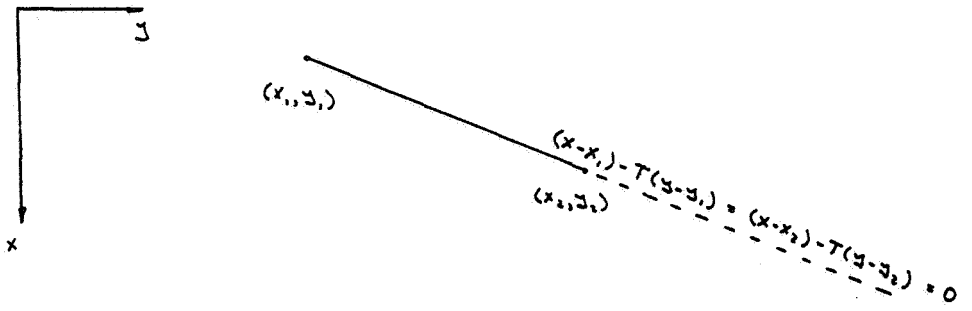

Control points which are near the extension of this edge will have large u and v velocities induced upon them. The singularity can be eliminated by using panels which have a source distribution which varies linearly in the chordwise direction. The resulting continuous source distribution eliminates the singularities. The linearly varying source panel influence equations can be found by integrating the constant source panel influence equations with respect to x.

$$u_{10}=-\frac{k}{2\pi}\left\{y\frac{1}{2}\log\frac{R+x}{R-x}+\frac{(x-Ty)}{\sqrt{T^2+\beta^2}}\frac{1}{2}\log\frac{\sqrt{T^2+\beta^2}R+(Tx+\beta^2y)}{\sqrt{T^2+\beta^2}R-(Tx+\beta^2y)}+z\tan^{-1}\frac{zR}{xy-T(y^2+z^2)}\right\}$$

$$v_{10}=-\frac{k}{2\pi}\left\{(x-Ty)\frac{1}{2}\log\frac{R+x}{R-x}-\frac{T(x-Ty)}{\sqrt{T^2+\beta^2}}\frac{1}{2}\log\frac{\sqrt{T^2+\beta^2}R+(Tx+\beta^2y)}{\sqrt{T^2+\beta^2}R-(Tx+\beta^2y)}-Tz\tan^{-1}\frac{zR}{xy-T(y^2+z^2)}-R\right\}$$

$$w_{10}=-\frac{k}{2\pi}\left\{(x-Ty)\tan^{-1}\frac{zR}{xy-T(y^2+z^2)}+Tz\frac{1}{2}\log\frac{R+x}{R-x}-z\sqrt{T^2+\beta^2}\frac{1}{2}\log\frac{\sqrt{T^2+\beta^2}R+(Tx+\beta^2y)}{\sqrt{T^2+\beta^2}R-(Tx+\beta^2y)}\right\}$$

These velocity components satisfy the same criteria as the velocity components for the constant source panels except that the source strength is proportional to x-Ty. The source panel finite elements are constructed with the following properties.

1. All panel leading and trailing edges are at constant $(\frac{x}{c})$, side edges are at constant y.

2. Each source finite element is composed of a pair of chordwise adjacent panels.

3. The source strength varies linearly with chord measured from the leading edge of a panel pair, i.e. the maximum value of the source strength is proportional to the local chord and attains this maximum on the panel edge joining the panel pair.

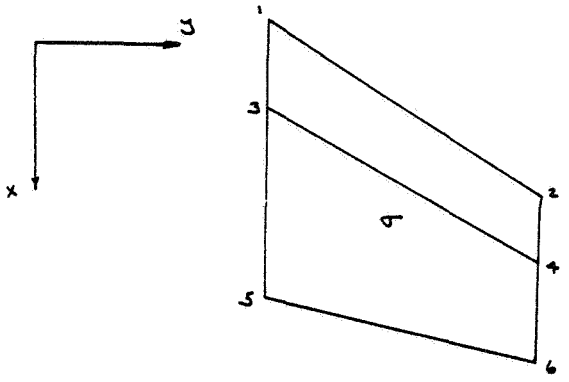

$$\Delta_{31} = \left(\frac{x}{c}\right)_3 - \left(\frac{x}{c}\right)_1 = \left(\frac{x}{c}\right)_4 - \left(\frac{x}{c}\right)_2$$

$$\Delta_{53} = \left(\frac{x}{c}\right)_5 - \left(\frac{x}{c}\right)_3 = \left(\frac{x}{c}\right)_6 - \left(\frac{x}{c}\right)_4$$

The perturbation velocities induced by this panel pair are composed of contributions from six corners.

$$\begin{aligned} u(x,y,z) = \frac{\sigma}{\Delta_{31}} \Big\{ & u_{10}(x-x_1, y-y_1, z, T_1) - u_{10}(x-x_3, y-y_3, z, T_3) \\ & - u_{10}(x-x_2, y-y_2, z, T_2) + u_{10}(x-x_4, y-y_4, z, T_4) \Big\} \\ + \frac{\sigma}{\Delta_{53}} \Big\{ & u_{10}(x-x_5, y-y_5, z, T_5) - u_{10}(x-x_3, y-y_3, z, T_3) \\ & - u_{10}(x-x_6, y-y_6, z, T_6) + u_{10}(x-x_4, y-y_4, z, T_4) \Big\} \end{aligned}$$

If there are N panels in the chordwise direction there will be N-1 singularities or unknown source strengths associated with them. The linear variation in the source distribution means the value of dz/dx must be zero at the leading and trailing edges of each span station. This may be an undesired restriction and therefore the use of linearly varying source panels is optional.

EDGE EFFECTS

The low pressure created by high velocities around a surface subsonic leading edge results in a suction force. As the edge becomes thinner or the angle of attack increases, the flow deviates from potential conditions resulting in a progressive loss of theoretical suction and an increase in drag. Generalizing a concept due to Polhamus[5], it is assumed that the leading edge vortex created by the detached flow in effect rotates the lost suction force perpendicular to the local surface.

In order to implement this philosophy, a method of determining the spanwise variation of potential suction was developed using linear thin wing theory and involves finding the coefficient of the $1/\sqrt{x}$ term in the chordwise net pressure distribution. The analysis is applicable to multiple surface problems of arbitrary planform in the presence of bodies at any Mach number. If the chordwise net pressure distribution on a thin wing at any given span station is expanded in a series

$$\Delta C_p = A_0 \cot \tfrac{1}{2}\phi + \sum_{n=1}^{N} A_n \sin n\phi$$
$$\xi = \frac{x}{c} = \tfrac{1}{2}(1 - \cos\phi) = \sin^2 \tfrac{1}{2}\phi \qquad (12)$$

it is shown in appendix B that the leading edge nondimensionalized suction force per unit length is

$$C_s(y) = \frac{\Delta \text{THRUST}}{c\,\Delta y\, q_\infty} = \frac{1}{8}\pi\sqrt{T^2+\beta^2}\,A_0^2 \qquad (13)$$

where $T = \tan \Lambda_{L.E.}$

$$\beta^2 = 1 - M_\infty^2$$

and c is the local chord

Only the first term in equation 12 contributes to the thrust, since it is the only contribution which is infinite at the leading edge. If the chordwise pressures are known at M points along the chord, the coefficients A_n are obtained by fitting a least square error curve described by N terms of the series, through the points, where N < M. The pressure distribution is obtained using constant pressure panel analysis.

The method used to compute the suction force at surface tips is similar to that for the leading edge. By using the irrotational property of the flow, it is shown in appendix B that the tip suction force is:

$$C_s(\xi) = \frac{\Delta F_\eta}{q_\infty \Delta X C_T} = \frac{\pi}{32} \frac{C_{AVG}^2}{C_T \eta_{MAX}} C_{\eta_0}^2 \left[\int_0^\xi f(x)\,dx \right]^2 \qquad (14)$$

where

C_{AVG}	surface average chord
C_T	tip chord
η_{MAX}	tip surface lateral surface dimension
ξ, x	faction of chord
C_{η_0}	$C_n(\eta) \frac{C(\eta)}{C_{AVG}} \eta_{MAX} \left[\frac{1}{2} (\eta_{MAX}^2 - \eta^2) \right]^{-1/2}$
C_n	is local section normal force coefficient

and as $\eta \rightarrow \eta_{MAX}$ the net pressure coefficient is assumed to be of the form

$$\Delta C_p(\xi, \eta) = \sqrt{\frac{1}{2}\left[1 - \left(\frac{\eta}{\eta_{MAX}}\right)^2\right]} \frac{C_{AVG}}{C(\eta)} C_{n_0} f(\xi) \qquad (15)$$

The sectional leading edge suction attained in the real flow, $\tilde{c}_s(y)$, is estimated by[6]

$$\tilde{c}_s(y) = K_s(y)\, c_s(y)$$

where

$$K_s(y) = 2 M_e^{-1}(1-M_e^2)\left[\frac{\frac{t_n}{c_n}\left(\frac{r_n}{c_n}\right)^{0.4}}{\beta_n c_{s_n}}\right]^{0.6} \leq 1$$

and

$$M_e = -\sqrt{2}\,\tilde{c}_p^{-1}\left[(1+\tilde{c}_p^2)^{1/2}-1\right]^{1/2}$$

$$\tilde{c}_p = \gamma \beta_n c_{p,LIM}, \quad \beta_n = (1-M_n^2)^{1/2}$$

$$c_{p,LIM} = -\frac{2}{\gamma M_n^2}\left[\frac{R_N \times 10^6}{R_N \times 10^{-6} + 10^{(4-5M_n)}}\right]^{.05+.35(1-M_n)^2}$$

$$R_N = R_c \frac{c_n}{c} \cos\Lambda_{LE}$$

$$c_{s,n} = c_s \frac{c}{c_n} \frac{1}{\cos^2\Lambda_{LE}}$$

$$M_n = M_\infty \cos\Lambda_{LE}$$

The chord of the normal section, C_n , is defined so as to place the maximum thickness, t , at the mid chord as indicated in the following sketch. The associated leading edge radius is designated by r_n

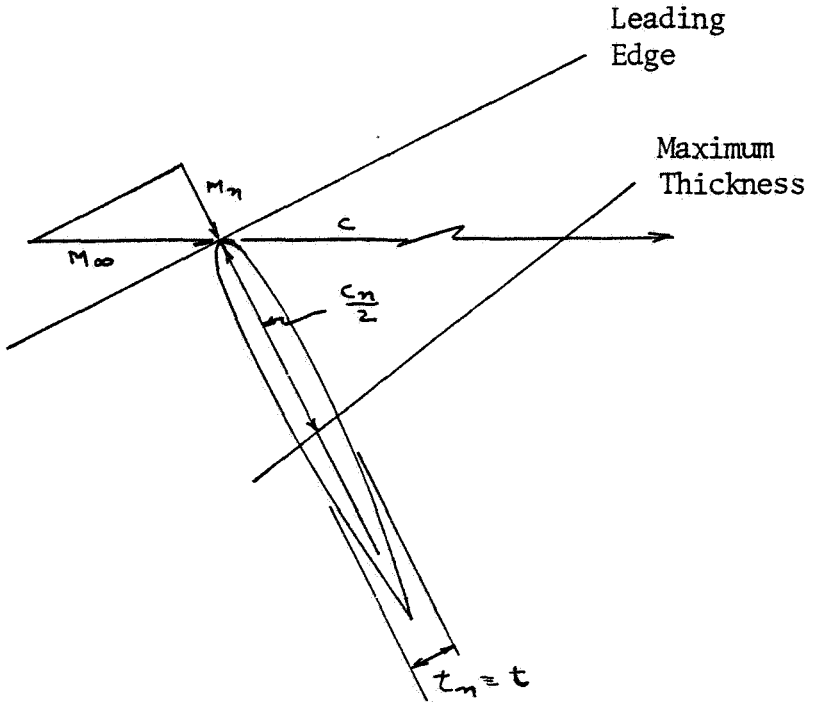

Potential tip suction is assumed to be fully rotated as a result of vortex formation in the present analysis.

AERODYNAMIC CHARACTERISTICS

Longitudinal and lateral-directional forces and moments due to thickness, twist and camber, pitch, sideslip, and the dimensionless rotary velocities $\hat{p}$, $\hat{q}$, and $\hat{r}$ are obtained from surface pressure integrations of the various configuration components.

BODIES

The pressure coefficient, to an approximation consistant with slender body theory, is

$$C_p = \frac{P-P_\infty}{q} = -2\left\{\phi_x + g'(x) + \left[\alpha + \hat{q}\,\frac{(x-CG)}{c/2} + \hat{p}\,\frac{Y}{b/2}\right]\phi_z - \left[\beta - \hat{r}\,\frac{(x-XCG)}{b/2} + \hat{p}\,\frac{(z-z_{C.G.})}{b/2}\right]\phi_y\right\} - \phi_y^2 - \phi_z^2 \tag{20}$$

The forces and moments are obtained from the surface integrations

$$\frac{F_x}{qL^2} = \int_c^1 dx \oint C_p \frac{\partial y}{\partial x}\, ds$$

$$\frac{F_y}{qL^2} = -\int_0^1 dx \oint C_p\, dz$$

$$\frac{F_z}{qL^2} = \int_0^1 dx \oint C_p\, dy$$

$$\frac{M_x}{qL^3} = -\int_0^1 dx \oint (z-z_{CG})\, C_p\, dz - \int_0^1 dx \oint y\, C_p\, dy$$

$$\frac{M_y}{qL^3} = -\int_0^1 (x-x_{CG})\, dx \oint C_p\, dy$$

$$\frac{M_z}{qL^3} = \int_0^1 (x-x_{CG})\, dx \oint C_p\, dz$$

In terms of these expressions, the commonly used aerodynamic coefficients are

$$C_x = \frac{F_x}{qL^2} \cdot \frac{L^2}{S_{REF}}$$

$$C_Y = \frac{F_Y}{qL^2} \cdot \frac{L^2}{S_{REF}}$$

$$C_z = \frac{F_z}{qL^2} \cdot \frac{L^2}{S_{REF}}$$

$$C_l = \frac{M_x}{qL^3} \quad \frac{L^3}{b\ S_{REF}}$$

$$C_m = \frac{M_Y}{qL^3} \quad \frac{L^3}{\bar{c}\ S_{REF}}$$

$$C_n = \frac{M_z}{qL^3} \quad \frac{L^3}{b\ S_{REF}}$$

where L is the body length and $\bar{c}$, b and S_{ref} are configuration reference chord, span and area, respectively.

Crosscoupling between the pitch, sideslip, and rotary motions through the product and quadratic terms in equation (20) is neglected.

PLANAR COMPONENTS

Surface pressure distributions are calculated for planar components using the first-order linearized form

$$C_p = -\frac{2u}{U} = -2\left[\frac{u}{U}_{IND} \pm \frac{C_{P_{NET}}}{4}\right]$$

The +/- signs refer to the upper and lower surfaces respectively. The term $\frac{u}{U}_{IND}$ consists of the velocities induced by the isolated bodies and other vortex and source panels. These velocities are obtained by multiplying the $\frac{u}{U}$ influence matrices by the appropriate panel strengths. The $C_{P_{NET}}/4$ term accounts for the $\frac{u}{U}$ perturbation velocity induced by the local distribution of vorticity and changes sign from upper to lower surface. The total $\frac{u}{U}$ and $C_{P_{NET}}$ values are the result of taking linear combinations of all the basic and unit solutions.

The net pressures for each of the basic and unit solutions are integrated numerically to give the section forces and moments, component forces and moments, and configuration forces and moments.

Since the vortex panels have a constant pressure distribution, a block integration scheme is employed. With the exception of drag, these basic and unit force and moment coefficients are combined in a linear manner to produce the aerodynamic characteristics for any desired flight condition. Since drag varies in a parabolic manner, it must be considered on a point by point basis as defined in a later section.

The longitudinal normal force distribution on the bodies is calculated for each solution. The load distribution on the interference shell portion of the body is given by integrating over all vortex panels at a given longitudinal station.

normal force

$$C_{n\,\frac{w}{\ell}} = \frac{C_l}{\Delta X\, L} \sum_{i=1}^{N} C_{P_{NET_i}} A_i \cos\Theta_i$$

where N is the number of panels around the shell, L is the length of the body, ΔX is the length of the interference shell segment, A_i is the panel area, and $C_1 = 2$ for a centerline body or $C_1 = 1$ for an off centerline body. This carryover load distribution is added to the previously calculated isolated body longitudinal load distribution.

The section characteristics of planar components are determined by a chordwise summation of panel data at each span station and are given by the following equations:

local normal force

$$C_n = \frac{1}{C \Delta s} \sum_{i=1}^{N_c} C_{P_{NET_i}} A_i$$

weighted normal force

$$C_n \frac{C}{C_{AVG}} = \frac{1}{\Delta s C_{AVG}} \sum_{i=1}^{N_c} C_{P_{NET_i}} A_i$$

weighted lift force

$$C_\ell \frac{C}{C_{AVG}} = \frac{1}{\Delta s C_{AVG}} \sum_{i=1}^{N_c} C_{P_{NET_i}} A_i \cos \Theta_i$$

center of pressure

$$X_{C.P.} = \frac{\frac{1}{C \Delta s C_{AVG}} \sum_{i=1}^{N_c} C_{P_{NET_i}} A_i (x_i - x_{LE})}{C_n \frac{C}{C_{AVG}}}$$

where N_c is the number of chordwise panels, and Δs is the width of the span station and is given by

$$\Delta s = \sqrt{\Delta Y^2 + \Delta Z^2}$$

Component forces and moments including edge vortex effects are given by the following equations:

lift

$$C_L S_{REF} = F_1 \sum_{i=1}^{N} C_{P_{NET_i}} A_i \cos\theta_i + \sum_{j=1}^{N_S} (1-K_{S_j}) C_{S_j} C_j \Delta S'_j \Omega_{L_j}$$

$$+ C_T^2 \sum_{k=1}^{N_{CT}} C_{S_k} \Delta \left(\frac{X}{C_T}\right)_k T_{L_k}$$

side force

$$C_Y S_{REF} = F_1 \sum_{i=1}^{N} C_{P_{NET_i}} A_i \sin\theta_i - \sum_{j=1}^{N_S} (1-K_{S_j}) C_{S_j} C_j \Delta S'_j \Omega_{Y_j}$$

$$- C_T^2 \sum_{k=1}^{N_{CT}} C_{S_k} \Delta \left(\frac{X}{C_T}\right)_k T_{Y_k}$$

rolling moment

$$C_l b S_{REF} = -F_2 \sum_{i=1}^{N} C_{P_{NET_i}} A_i \left[(Y_i - Y_{CG})\cos\theta_i + (Z_i - Z_{CG})\sin\theta_i\right]$$

$$- \sum_{j=1}^{N_S} (1-K_{S_j}) C_{S_j} C_j \Delta S'_j \left[(Y_{LE} - Y_{CG})\Omega_{L_j} + (Z_{LE} - Z_{CG})\Omega_{Y_j}\right]$$

$$- C_T^2 \sum_{k=1}^{N_{CT}} C_{S_k} \left(\frac{\Delta X}{C_T}\right)_k \left[(Y_T - Y_{CG}) T_{L_k} + (Z_T - Z_{CG}) T_{Y_k}\right]$$

pitching moment

$$C_m \bar{C} S_{REF} = - F_1 \sum_{i=1}^{N} C_{P_{NET_i}} A_i (X_i - X_{CG})\cos\theta_i$$

$$- \sum_{j=1}^{N_S} (1-K_{S_j}) C_{S_j} C_j \Delta S'_j (X_{LE_j} - X_{CG}) \Omega_{L_j} - C_T^2 \sum_{k=1}^{N_{CT}} C_{S_k} \Delta\left(\frac{X}{C_T}\right)_k T_{L_k}$$

yawing moment

$$C_n b S_{REF} = F_2 \sum_{\ell=1}^{N} C_{P_{NET_\ell}} A_\ell (x_\ell - x_{CG}) \sin\Theta_\ell$$

$$+ \sum_{j=1}^{N_S} (1 - K_{S_j}) C_{S_j} C_j \Delta S'_j (x_{LE_j} - x_{CG}) \Omega_{Y_j} + C_T^2 (x_{T_{CP}} - x_{CG}) \sum_{k=1}^{N_{CT}} C_{S_k} \Delta\left(\frac{x}{C_T}\right)_k T_{Y_k}$$

where N is the number of vortex panels on half of a symmetrical component (or total for an asymmetrical component) and F1, F2 are given by

symmetric loading	$F_1 = 1$	asymmetric geometry
	$= 2$	symmetric geometry
	$F_2 = 1$	asymmetric geometry
	$= 0$	symmetric geometry
antisymmetric loading	$F_1 = 1$	asymmetric geometry
	$= 0$	symmetric geometry
	$F_2 = 1$	asymmetric geometry
	$= 2$	symmetric geometry

For the leading and side edge vortex terms, N_S is the total number of spanwise panels for both component halves, N_{CT} is the number of tip chordwise panels, X_{TCP} is the axial location of tip vortex center of pressure, $\Delta S' = \Delta S\sqrt{1 + T^2}$ and the rotation factors Ω and T are derived in appendix B and defined below.

Leading edge vortex rotation:

$$\Omega_L = -\sin\alpha(\cos\Lambda\cos\delta) + \cos\alpha(\cos\Theta\sin\delta - \sin\Theta\sin\Lambda\cos\delta)$$

$$+ \frac{A_0}{|A_0|}\left[\sin\alpha(\cos\Lambda\sin\delta) + \cos\alpha(\cos\Theta\cos\delta + \sin\Theta\sin\Lambda\sin\delta)\right]$$

$$\Omega_Y = \cos\Theta\sin\Lambda\cos\delta + \sin\Theta\sin\delta + \frac{A_0}{|A_0|}\left[\sin\Theta\cos\delta - \cos\Theta\sin\Lambda\sin\delta\right]$$

where δ is the slope angle of the leading edge camber line and the sign of coefficient A_0(from equation 13) is used to determine the direction of vortex rotation.

Side edge vortex rotation:

$$T_L = \pm \cos\alpha \sin\theta + \frac{C_{n_o}}{|C_{n_o}|}\left(\sin\alpha \sin\delta + \cos\alpha \cos\theta \cos\delta\right)$$

$$T_Y = \pm \cos\theta + \frac{C_{n_o}}{|C_{n_o}|} \sin\theta \cos\delta$$

where δ is the slope angle of the tip camber line, $\pm$ is plus for the left side and negative for the right side of the configuration and the sign of coefficient C_{n_o} (from equation 14) is used to determine the direction of vortex rotation.

The X coordinate of the center of pressure is given by

$$X_{C.P.} = -\frac{C_m \bar{c}}{C_L} + X_{CG}$$

For interference shell components, the total forces and moments of the corresponding isolated body are added to those of the shell.

The forces and moments for the complete configuration are obtained by summing those of the individual components.

DRAG ANALYSIS

Estimation of configuration aerodynamic efficiency requires the calculation of drag. The analysis separates the computation into skin-friction and pressure drag components that are assumed to be independent of each other. The following form is considered and produces non-parabolic polars as a result of the incorporation of attainable suction considerations.

$$C_D = C_{D_{VISCOUS}} + C_{D_{WAVE}} + C_{D_{BASE}} + C_{D_{LIFT}}$$

The specific techniques used for the various drag evaluations are discussed below.

SKIN FRICTION

Several well established semiempirical techniques for the evaluation of adiabatic laminar and turbulent flat plate skin friction at incompressible and compressible speeds are used to estimate the viscous drag of advanced aircraft using a component buildup approach. A specified transition point calculation option is provided in conjunction with a matching of the momentum thickness to link the two boundary layer states. For the turbulent condition, the increase in drag due to distributed surface roughness is treated using unformly distributed sand grain results. Component thickness effects are approximated using experimental data correlations for two-dimensional airfoil sections and bodies of revolution.

Considerations such as separation, component interference, and discrete protuberances (e.g. antennas, drains, aft facing steps, etc.) must be accounted for separately if present.

In the following, a discussion is presented for a single component evaluation in order to simplify writing of the equations and eliminate multiple subscripting. The total result is obtained by a surface area weighted summation of the various component analyses as described on page 63.

Laminar/Transition

A specified transition option is provided in the program. The principal function of the calculation is to provide the conditions required to initialize the turbulent solution. In particular, the transition point length and momentum thickness Reynolds numbers are required.

$$R_{x_{TRAN}} = R \frac{x_{TRAN}}{L} L$$

$$R_{\theta_{TRAN}} = 0.664 \sqrt{R_{x_{TRAN}} C^*}$$

where

$$C^* = \frac{\mu^*}{\mu_\infty} \frac{T_\infty}{T^*}$$

$$\frac{T^*}{T_\infty} = 1 + 0.72 \left[\frac{T_r}{T_\infty} - 1 \right]$$

$$\frac{T_r}{T_\infty} = 1 + \sqrt{P_r} \frac{\gamma - 1}{2} M_\infty^2 = 1 + 0.851 \frac{\gamma - 1}{2} M_\infty^2$$

$$\mu = 2.270 \times 10^{-8} \frac{T^{3/2}}{T + 198.6} \quad \text{lb sec/ft}^2$$

This solution is based on the laminar Blasius result (8, chapter VII) in conjunction with Eckert's compressibility transformation[9]. This option permits an assessment of the reduction in skin-friction drag if laminar flow can be maintained for the specified extent. It does not establish the liklihood that such a condition will be realized in practice or to what extent.

Turbulent

Smooth and distributed rough surface options have been provided in the analysis. In either case, the solution is initialized by matching the momentum thickness at the transition point produced by the laminar/transition solution. That is, an effective origin (commonly referred to as a virtual origin) is established for the turbulent analysis.

For the hydraulically smooth case

$$C_F R_{\Delta x} = 2 R_{\theta_{TRAN}}$$

$$R_{\Delta x} = C_F R_{\Delta x} \Big/ C_F \qquad C_F \text{ from equation (21) for known } C_F R_{\Delta x}$$

$$\Delta x = R_{\Delta x} \Big/ R$$

$$\ell = L - X_{TRAN} + \Delta x$$

$$R_\ell = R \ell$$

$$\frac{0.242 \left[\sin^{-1}\alpha + \sin^{-1}\beta \right]}{\left[\frac{\gamma-1}{2} M_\infty^2 C_F' \right]^{\frac{1}{2}}} = \log_{10} \left[C_F' R_\ell \right] - \omega \log_{10} \frac{T_r}{T_\infty} \qquad (21)$$

$$C_F = \frac{2\theta_{x\to\infty}}{L} = \frac{2\theta_{T.E.}}{\ell} \frac{\ell}{L} = C_F' \frac{\ell}{L}$$

where

$$X_{TRAN} = R_{X_{TRAN}} / R$$

$$\alpha = (2A^2 - B) / \sqrt{B^2 + 4A^2}$$

$$\beta = B / \sqrt{B^2 + 4A^2}$$

$$A^2 = \frac{\gamma - 1}{2} M_\infty^2 \frac{T_\infty}{T_r}$$

$$B = \left(1 + \tfrac{1}{2}[\gamma - 1] M_\infty^2\right) \frac{T_\infty}{T_r} - 1$$

$$r = 0.88$$

$$\omega = 0.76$$

The compressible turbulent flat plate method used here is that proposed by Van Driest[10] based on the Von Karman mixing length hypothesis in conjunction with the Squire-Young formulation for profile drag (8 , chapter XXIV) as applied to a flat plate.

For the distributed rough case

$$\Delta X_1 = X_{TRAN}$$

$$C_{F_r} = \left[1.89 + 1.62 \log_{10} \frac{\Delta X}{K_s} \right]^{-2.5} \left(1 + r \frac{\gamma - 1}{2} M_\infty^2 \right)^{-1}$$

$$R_{\Delta X_{i+1}} = 2 R_{\theta_{TRAN}} / C_{F_r}$$

$$\Delta X_{i+1} = R_{\Delta X_{i+1}} / R$$

$$l = L - X_{TRAN} + \Delta X$$

$$C_F' = \left(1.89 + 1.62 \log_{10} \frac{l}{K_s} \right)^{-2.5} \left(1 + r \frac{\gamma - 1}{2} M_\infty^2 \right)^{-1}$$

$$C_F = C_F' \frac{l}{L}$$

$$C_F = MAX \left[C_{F_{SMOOTH}}, C_{F_{ROUGH}} \right]$$

The turbulent flat plate method used here is that of Schlicting (8, chapter XXI) which is based on a transposition of Nikuradse's densely packed sand grain roughened pipe data. The effect of compressibility is due to the reduction in density at the wall as proposed by Goddard.[11] The selection of the equivalent sand grain roughness for a given manufacturing surface finish is made with the aid of Table II which was taken from Clutter.[12]

TABLE II

Type of Surface	Equivalent Sand Roughness K_s (inches)
Aerodynamically smooth	0
Polished metal or wood	$0.02 - 0.08 \times 10^{-3}$
Natural sheet metal	0.16×10^{-3}
Smooth matte paint, carefully applied	0.25×10^{-3}
Standard camouflage paint, average application	0.40×10^{-3}
Camouflage paint, mass-production spray	1.20×10^{-3}
Dip-galvanized metal surface	6×10^{-3}
Natural surface of cast iron	10×10^{-3}

Thickness Corrections

The foregoing evaluations produce as estimate of the shearing forces on a flat plate (at zero angle of attack) for a variety of conditions. As an actual aircraft has a non vanishing thickness, an estimate of pressure gradient effects on skin friction and boundary layer displacement pressure drag losses is required. A common procedure for accomplishing this and the one which will be used here is based on non-lifting experimental correlations for symmetric two-dimensional airfoils and axisymmetric bodies. The following relations derived by Horner (13, chapter VI) are used, respectively.

$$\therefore K = \frac{C_d}{2C_F} = 1 + K_1 \frac{t}{c} + 60\left(\frac{t}{c}\right)^4$$

$$= \frac{C_D}{C_{DF}} = 1 + 1.5\left(\frac{d}{L}\right)^{\frac{3}{2}} + 7\left(\frac{d}{L}\right)^3$$

Horner recommends $K_1 = 2$ for airfoils with maximum thickness at 30% chord and $K_1 = 1.2$ for NACA 64 and 65 series airfoils. In this regard, the best information available to an analyst for his particular contour should be used. This is especially true for modern high performance shapes such as the supercritical airfoil, etc.

Total Viscous Drag

The aircraft total viscous-drag coefficient is estimated by a sum of the preceding analysis over all components (i.e. wing, fuselage, vertical tail, etc.). That is

$$C_{D_{VISCOUS}} = \sum_{j=1}^{N} C_{F_j} \left(\frac{S_j}{S_{REF}}\right) K_j$$

The component length used in the calculation of the skin friction coefficient is the mean chord for planar component segments and the physical length for bodies and nacelles.

BASE DRAG

Blunt base increments are estimated at subsonic and supersonic speeds by

where

$$\Delta C_{D_{BASE}} = - C_{P_{BASE}} \frac{S_{BASE}}{S_{REF}}$$

$$- C_{P_{BASE}} = 0.139 + 0.419 (M_\infty - 0.161)^2 \qquad M_\infty < 1$$

$$- C_{P_{BASE}} = 0.064 + 0.042 (M_\infty - 3.84)^2 \qquad M_\infty \geq 1$$

The expressions for the base pressure coefficient are derived from correlation of flight test results for the X-15, various lifting bodies, and the space shuttle. Power effects are treated as reductions in base area in the present analysis.

POTENTIAL DRAG

One hundred percent suction drag due to lift and supersonic wave drag due to thickness can be evaluated by integration of the momentum flux through a large circular cylinder centered on the x axis and whose radius approaches infinity.

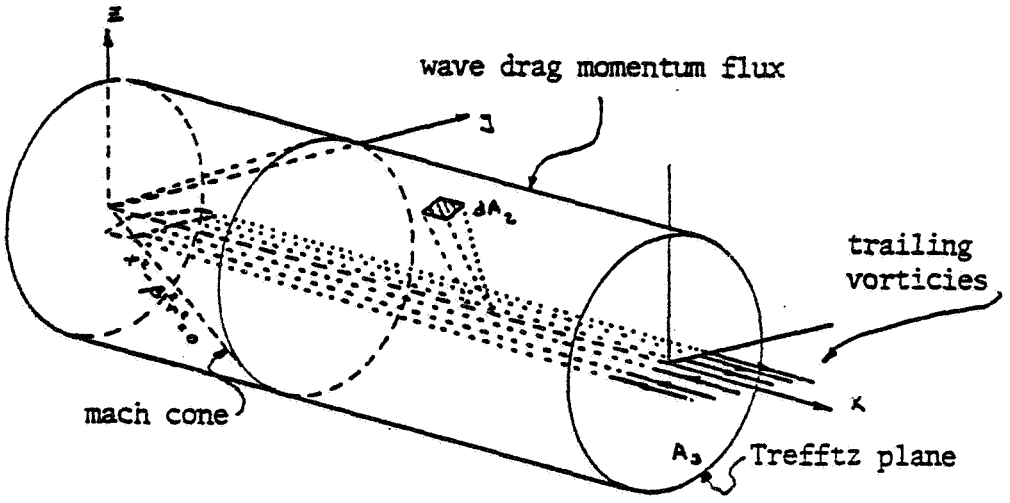

The resulting expression for the total pressure drag is as follows:

$$C_D S_{REF} = -2 \iint_{A_2} \bar{\Phi}_x \bar{\Phi}_r \, dA_2 + \iint_{A_3} (\bar{\Phi}_y^2 + \bar{\Phi}_z^2) \, dA_3 = C_{D_W} S_{REF} + C_{D_V} S_{REF}$$

The first term represents the wave drag due to momentum losses thru the side of the cylinder caused by standing pressure waves. The second term represents the vortex drag which arises from the kinetic energy left behind in the Trefftz plane by the system of trailing vorticies.

Vortex Drag

The vortex drag may be computed when the distribution of trailing vorticity in the Trefftz plane is known. The assumptions of linearized thin wing theory result in a vortex sheet which extends directly downstream of all lifting surfaces. By changing a surface integral for kinetic energy to a line integral over the vortex sheet in the Trefftz plane the following expressions for lift and drag result .

$$C_L = \frac{c_{AVG}}{S_{REF}} \int_C \bar{C}_N(\eta) \cos\theta(\eta)\, d\eta$$

$$C_{D_v} = \frac{c_{AVG}}{S_{REF}} \int_C \bar{C}_N(\eta)\, \omega_\infty(\eta)\, d\eta$$

where

C	vortex sheet branches
$\bar{C}_n$	weighted section normal force coefficient $c_n c / c_{AVG}$
ω_∞	asymptotic normal velocity on the vortex sheet
η	vortex sheet branch coordinate
θ	inclination of vortex sheet with respect to y axis

The program computes the normal velocity on the vortex sheet, ω_{∞_i}, by assuming the vortex sheet is composed of finite trailing horseshoe vorticies whose strength is proportional to the local section $C_n(s)$. The normal velocity is computed at a control point located midway between the trailing vortex segments.

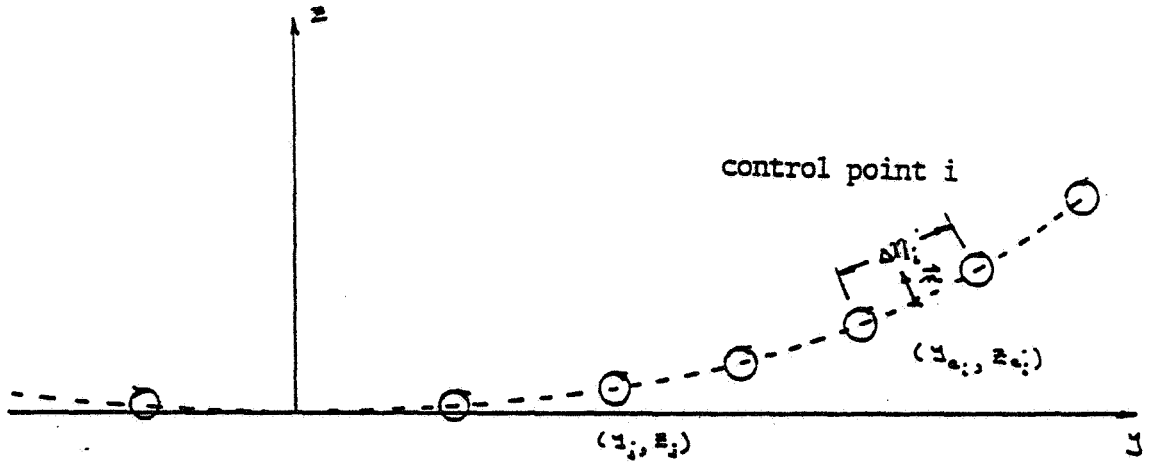

Each vortex j induces a contribution to the normal velocity at section i.

$$\vec{V} = \frac{C_{Avg}\Gamma_j}{2\pi r}\vec{e}_\phi$$

$$\Gamma_j = \frac{1}{2}\left[\bar{C}_{n_j} - \bar{C}_{n_{j+1}}\right]$$

$$\vec{r} = \left[(y_{c_i} - y_j)\vec{e}_y + (z_{c_i} - z_j)\vec{e}_z\right]$$

$$\vec{e}_\phi = \left[-(z_{c_i} - z_j)\vec{e}_y + (y_{c_i} - y_j)\vec{e}_z\right]\frac{1}{r}$$

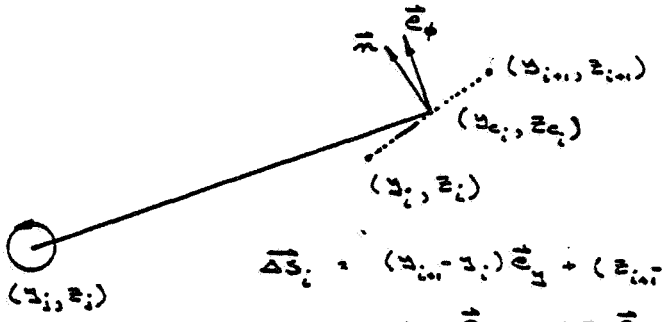

$$\vec{\Delta s}_i = (y_{j+1} - y_j)\vec{e}_y + (z_{j+1} - z_j)\vec{e}_z$$

$$= \Delta y_i \vec{e}_y + \Delta z_i \vec{e}_z$$

$$\vec{n} = \frac{1}{\Delta s_i}\left[-\Delta z_i \vec{e}_y + \Delta y_i \vec{e}_z\right]$$

$$\omega_{\infty_i} = \vec{V}\cdot\vec{n} = \frac{C_{Avg}}{2\pi r^2 \Delta s_i}\left\{(z_{c_i} - z_j)\Delta z_i + (y_{c_i} - y_j)\Delta y_i\right\}\Gamma_j = A_{ij}\Gamma_j$$

Therefore $$C_D = \sum_i \omega_{\infty_i} \bar{C}_{n_i} \Delta\eta_i \qquad \omega_{\infty_i} = \sum_j A_{ij}\Gamma_j$$

Wave Drag

The integral for wave drag

$$C_{D_w} S_{REF} = -2 \iint_{A_2} \phi_x \phi_r \, r \, dx \, d\theta$$

may be simplified by allowing the cylindrical surface of integration to recede infinitely far from the disturbance. Under these conditions, the spatial singularity simulations can be reduced to a series of one-dimensional distributions. The basis for this reduction is the finding by Hayes (14) that the potential and the gradients of interest induced by a singularity along an arbitrary trace on a distant control surface, say PP' of figure 6 (or alternately described by the cylindrical angle θ), is invariant to a finite translation along the surface of a hyperboloid emanating from the trace and passing through the singularity. As the apex of the hyperboloid is a great distance away, the aforementioned movement is along a surface which is essentially plane; it will be henceforth referred to as an "oblique plane". Since a singularity is a solution of a linear differential equation, all singular solutions which lie on the surface of the same hyperboloid (oblique plane) may thus be grouped to form a single equivalent point singularity whose strength is equal to the algebraic sum of the individual strengths and which induces the same potential (momentum) along the trace as the group of individual singularities.

This finding provides the basic technique for reducing a general spatial distribution of singularities to a series of equivalent lineal distributions. This is accomplished by surveying the three-dimensional distribution longitudinally at a series of fixed cylindrical angles, θ . At each angle, the survey produces an equivalent lineal distribution by systematically cutting the spatial distribution at a series of longitudinal stations along its length. At each cut, the group of intercepted singularities is collapsed along the "oblique plane" to form one of the equivalent point singularities comprising the lineal distribution .

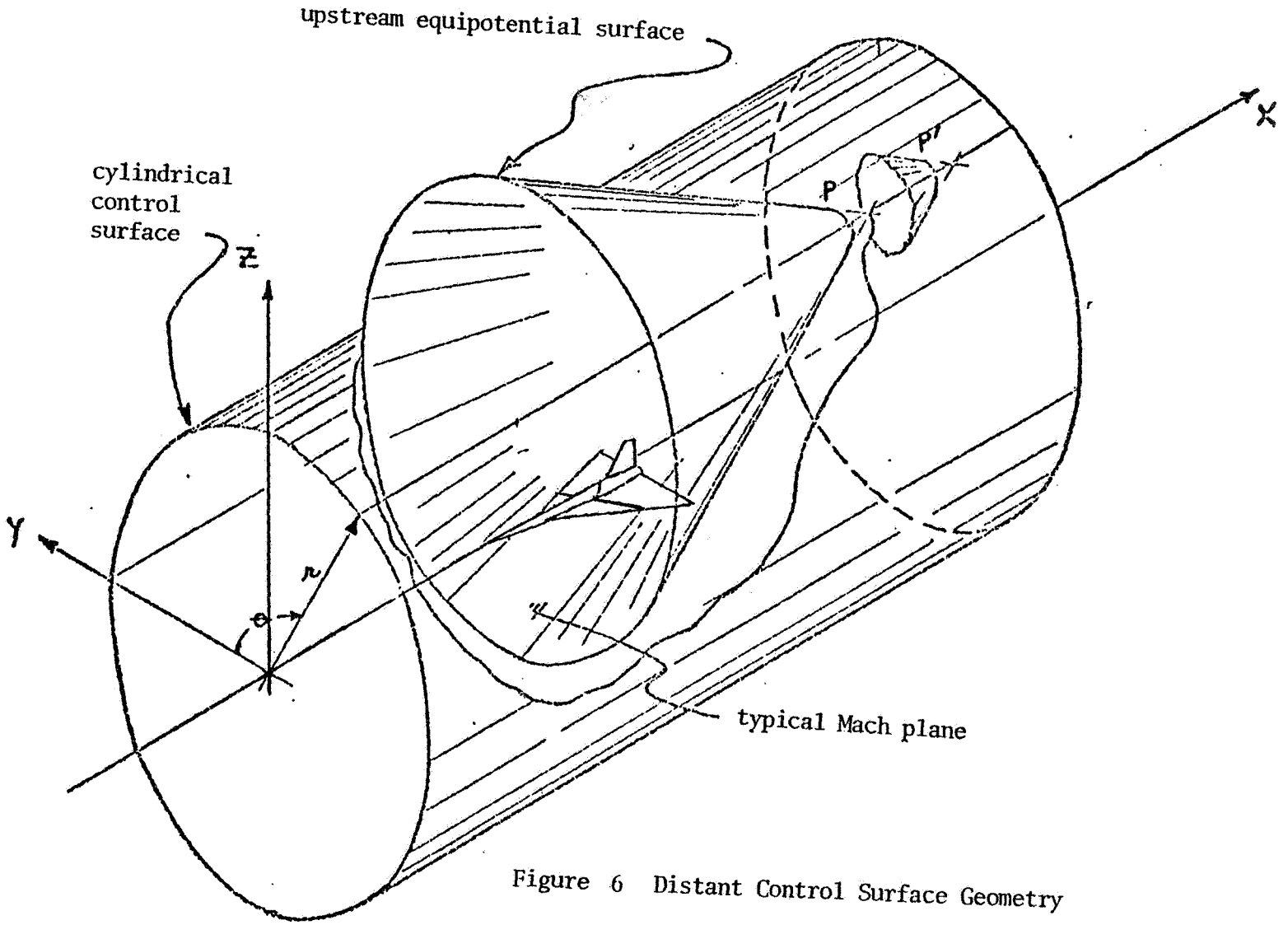

Figure 6 Distant Control Surface Geometry

The far-field expression for the wave drag of a general system of lift, and side force elements is

$$C_{D_W} S_{REF} = \frac{1}{U^2} \frac{1}{4\pi^2} \int_0^{2\pi} \int_{-\infty}^{\infty} \int_{-\infty}^{\infty} h_e'(\epsilon_1, \theta)\, h_e'(\epsilon_2, \theta) \ln|\epsilon_1 - \epsilon_2|\, d\epsilon_1 d\epsilon_2 d\theta$$

where

$h_e(\epsilon, \theta) = f(\epsilon, \theta) - g_z(\epsilon, \theta) \sin\theta - g_y(\epsilon, \theta) \cos\theta$

is the equivalent lineal singularity strength at the cylindrical angle θ

$f(\epsilon, \theta)$ = equivalent source strength per unit length

$\frac{1}{\beta} U \; g_z(\epsilon, \theta)$ = equivalent lifting element strength per unit length

$\frac{1}{\beta} U \; g_y(\epsilon, \theta)$ = equivalent side force strength per unit length

These strengths are deduced from the three dimensional singularity distributions by application of the superposition principle along equipotential surfaces. For a distant observer such surfaces are planar in the vicinity of the singularity configuration. The individual singularity strengths are related to the object under consideration by the requirement of flow tangency at the solid boundary. Lomax (15) derived the following approximate expressions between the equivalent singularity strengths and a slender lifting object.

$$f(\epsilon, \theta) = U \frac{\partial}{\partial \epsilon} A(\epsilon, \theta)$$

$$g_z(\epsilon, \theta) = \frac{1}{2} \beta U \int_c C_p\, dy$$

$$g_y(\epsilon, \theta) = \frac{1}{2} \beta U \int_c C_p\, dz$$

where (see figure 7)

$A(\epsilon, \theta)$ is the Y-Z projection of the obliquely cut crossectional area

c is the contour around the surface in the oblique cut

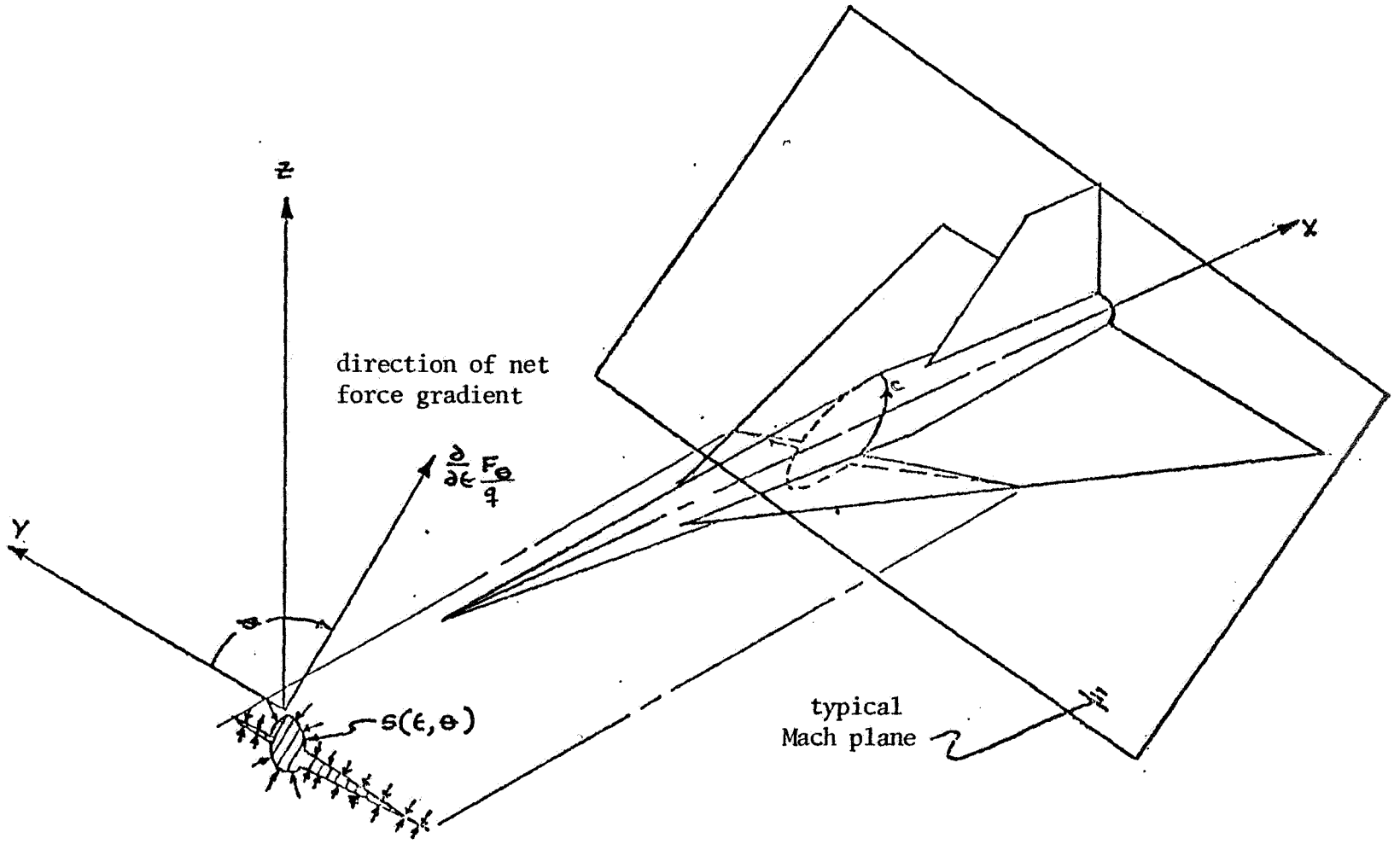

Figure 7 Areas and Forces Pertinent to the Evaluation of Wave Drag from the Far Field Point of View

Utilizing the singularity strength expressions derived by Lomax, the following expression for wave resistance based on the far field theory of Hayes is obtained

$$C_{D_W} S_{REF} = -\frac{1}{4\pi^2} \int_0^{2\pi} \int_0^{L(\theta)} \int_0^{L(\theta)} \left\{ \frac{\partial^2}{\partial \epsilon_1^2} A(\epsilon_1,\theta) - \frac{1}{2}\beta \frac{\partial}{\partial \epsilon_1} \left[\sin\theta \int_c C_p(\epsilon_1,\theta)\, dy + \cos\theta \int_c C_p(\epsilon_1,\theta)\, dz \right] \right\}$$

$$\left\{ \frac{\partial^2}{\partial \epsilon_2^2} A(\epsilon_2,\theta) - \frac{1}{2}\beta \frac{\partial}{\partial \epsilon_2} \left[\sin\theta \int_c C_p(\epsilon_2,\theta)\, dy + \cos\theta \int_c C_p(\epsilon_2,\theta)\, dz \right] \right\} \ln|\epsilon_1 - \epsilon_2|\, d\epsilon_1\, d\epsilon_2\, d\theta$$

In order to facilitate subsequent discussion, the above result is manipulated into the following form

$$C_{D_W} S_{REF} = \frac{1}{4\pi^2 L^2(\theta)} \int_0^{2\pi} \int_0^{1} \int_0^{1} \frac{\partial^2}{\partial \epsilon_1^2} A_e(\epsilon_1,\theta) \frac{\partial^2}{\partial \epsilon_2^2} A_e(\epsilon_2,\theta) \ln|\epsilon_1 - \epsilon_2|\, d\epsilon_1\, d\epsilon_2\, d\theta \quad (23)$$

where

$$A_e(\epsilon,\theta) = A(\epsilon,\theta) - \frac{1}{2}\beta \int_0^{\epsilon} \int_c C_p(\epsilon,\theta) \left[\sin\theta\, dy + \cos\theta\, dz \right] d\epsilon$$

A requirement for this transformation is that

$$A_e'(0,\theta) = A_e'(L,\theta) = 0$$

In accordance with equation 23, the wave drag of a configuration is the average of the wave drag of a series of equivalent bodies of revoluation. The drag of each of these bodies is calculated from a knowledge of its longitudinal distribution of normal cross-sectional area. For each equivalent body, these areas are defined to be the frontal projection of the areas and the accumulation of pressure force in the theta direction intercepted on the original configuration by a system of parallel oblique planes each inclined at the given Mach angle. The common trace angle (ϕ) of the system identifies the equivalent body under consideration.

Nacelles are assumed to swallow air supersonically. That is, the duct is operating at a mass flow ratio of unity. Consistent with this assumption, the equivalent body cross sectional area distribution is increased by the oblique projected duct capture area at all stations ahead of the duct which are intercepted by an oblique plane.

Blunt base components are extended (maintaining constant cross sectional area) sufficiently far downstream to prevent flow closure around the base.

In addition to a geometric description, a definition of the pressure distribution acting on the configuration is required. The vortex panel analysis is used for this purpose. The thickness pressures for planar components have tacitly been neglected under the assumption that the surfaces are sufficiently thin that the net pressure coefficient is representative of pressure acting on the oblique section.

Estimation of the wave drag based on equation 23 depends on solution of integrals of the type

$$I = \frac{1}{2\pi} \int_0^1 \int_0^1 G''(x_1)\, G''(x_2) \ln|x_1 - x_2|\, dx_1\, dx_2$$

of a numerically given function G(X). Evaluation of such forms has been studied by Eminton [16,17] for functions having G'(X) continuous on the interval (0,1) and G'(0) = G'(1) = 0. In such situations, G'(X) can be expanded in a Fourier sine series. It can then be shown that

$$I = \sum_{N=1}^{\infty} N A_N^2$$

where

$$A_N = \frac{2}{\pi} \int_0^{\pi} G'(x) \sin N\varphi \, d\varphi$$

Eminton then solved for the value of the Fourier coefficients which result in I being a minimum, subject to the condition that the resulting series for G(X) be exact for an arbitrarily specified set of points o,1, ϵ_i, i = 1,n.

This approach produces the following result

$$I = \frac{4}{\pi}\left[G(1)-G(0)\right]^2 + \pi \sum_{i=1}^{n} \sum_{j=1}^{n} C_i C_j f_{ij}$$

where

$$C_i = G(\epsilon_i) - G(0) - \left[G(1)-G(0)\right]\mu_i$$

$$\mu_i = \frac{1}{\pi}\left\{ \cos^{-1}(1-2\epsilon_i) - 2(1-2\epsilon_i)\sqrt{\epsilon_i(1-\epsilon_i)} \right\}$$

$$\epsilon_i = \frac{i}{n+1} \qquad 1 \le i \le n$$

$$f_{ij} = \left\{ P_{ij} \right\}^{-1}$$

$$P_{ij} = -\frac{1}{2}(\epsilon_i - \epsilon_j)^2 \ln \frac{\epsilon_i+\epsilon_j - 2\epsilon_i\epsilon_j + 2\sqrt{\epsilon_i\epsilon_j(1-\epsilon_i)(1-\epsilon_j)}}{\epsilon_i+\epsilon_j - 2\epsilon_i\epsilon_j - 2\sqrt{\epsilon_i\epsilon_j(1-\epsilon_i)(1-\epsilon_j)}}$$

$$+ 2(\epsilon_i+\epsilon_j-\epsilon_i\epsilon_j)\sqrt{\epsilon_i\epsilon_j(1-\epsilon_i)(1-\epsilon_j)}$$

The solution of equation 23 for wave drag is accomplished by use of the following identities.

$$G(\epsilon_i, \theta) = R_e(\epsilon_i, \theta)$$

$$C_{D_\omega}(\theta)\, S_{REF} = \frac{I(\theta)}{L^2(\theta)}$$

$$C_{D_\omega} = \frac{1}{2\pi}\int_0^{2\pi} C_{D_\omega}(\theta)\, d\theta = \frac{1}{\pi}\int_{-\pi/2}^{\pi/2} C_{D_\omega}(\theta)\, d\theta$$

ZERO SUCTION DRAG

The zero suction drag due to lift is calculated by numerically integrating the net pressure distribution times the projected area in the streamwise direction over each of the planer surfaces. The following block integration scheme is used to sum over all quadrilateral panels.

$$C_{D_o} = F_1 \frac{1}{S_{REF}} \sum_{i=1}^{N} C_{P_i} A_i \alpha_i$$

where

$$C_{P_i} = C_{P_{i_{\alpha=0}}} + \alpha \frac{\partial C_{P_i}}{\partial \alpha} + \delta \frac{\partial C_{P_i}}{\partial \delta}$$

and

$$\alpha_i = \alpha_{o_i} + \alpha + \sigma_i \delta$$

α_{o_i} is due to twist and camber, δ is the control surface deflection, and $\sigma_i = 1$ for control surface panels and $\sigma_i = 0$ for non control surface panels. $F_1 = 2$ for symmetric geometries and $F_1 = 1$ for asymmetric geometries.

Edge forces are not considered in this evaluation.

DRAG DUE TO LIFT

The drag due to lift for the total configuration is based on linearized potential (100 percent leading edge suction) calculations plus corrections to account for suction losses and associated edge vortex forces

$$C_{D_L} = C_{D_{100}} + \frac{1}{S_{REF}} \sum_{j=1}^{N_S} (1 - K_{S_j}) C_{S_j} C_j \Delta S_j' \Omega_{D_j} + \frac{C_T^2}{S_{REF}} \sum_{k=1}^{NC_T} C_{S_k} \Delta\left(\frac{x}{C_r}\right)_k T_{D_k}$$

where

$$C_{D_{100}} = C_{D_V} \qquad M < 1$$

$$= C_{D_V} + C_{D_W} - (C_{D_W})_{THICK} \qquad M \geq 1$$

and the leading edge and side edge rotation factors, Ω_D and T_D, are derived in Appendix B and defined below.

$$\Omega_D = \cos\alpha \cos\Lambda \cos\delta + \sin\alpha (\cos\theta \sin\delta - \sin\theta \sin\Lambda \cos\delta)$$

$$+ \frac{A_o}{|A_o|} \left[-\cos\alpha \cos\Lambda \sin\delta + \sin\alpha (\cos\theta \cos\delta + \sin\theta \sin\Lambda \sin\delta) \right]$$

where δ is the slope angle of the camber line perpendicular to the leading edge and the sign of coefficient A_0 (from equation 13) is used to determined the direction of vortex rotation.

$$T_D = \pm \sin\alpha \sin\theta - \frac{C_{n_o}}{|C_{n_o}|} (-\cos\alpha \sin\delta + \sin\alpha \cos\theta \cos\delta)$$

where δ is the chordwise slope angle of the tip camber line, plus refers to the left side and negative to the right side of the configuration and the sign of coefficient C_{n_0}. (from equation 14) is used to determine the direction of vortex rotation.

As estimate of the average level of leading edge suction for the complete configuration is based on the following equation:

$$\text{SUCTION} = \frac{\tilde{C}_{D_L} - C_{D_L}}{\tilde{C}_{D_L} - C_{D_{100}}} \quad \text{where } \tilde{C}_{D_L} = C_{D_L} \text{ for } K_S = 0$$

High Mach number analysis is based on non-interfering constant pressure finite element analysis[18].

An arbitrary configuration is approximated by a system of plane quadrilateral panels as indicated in the following sketch.

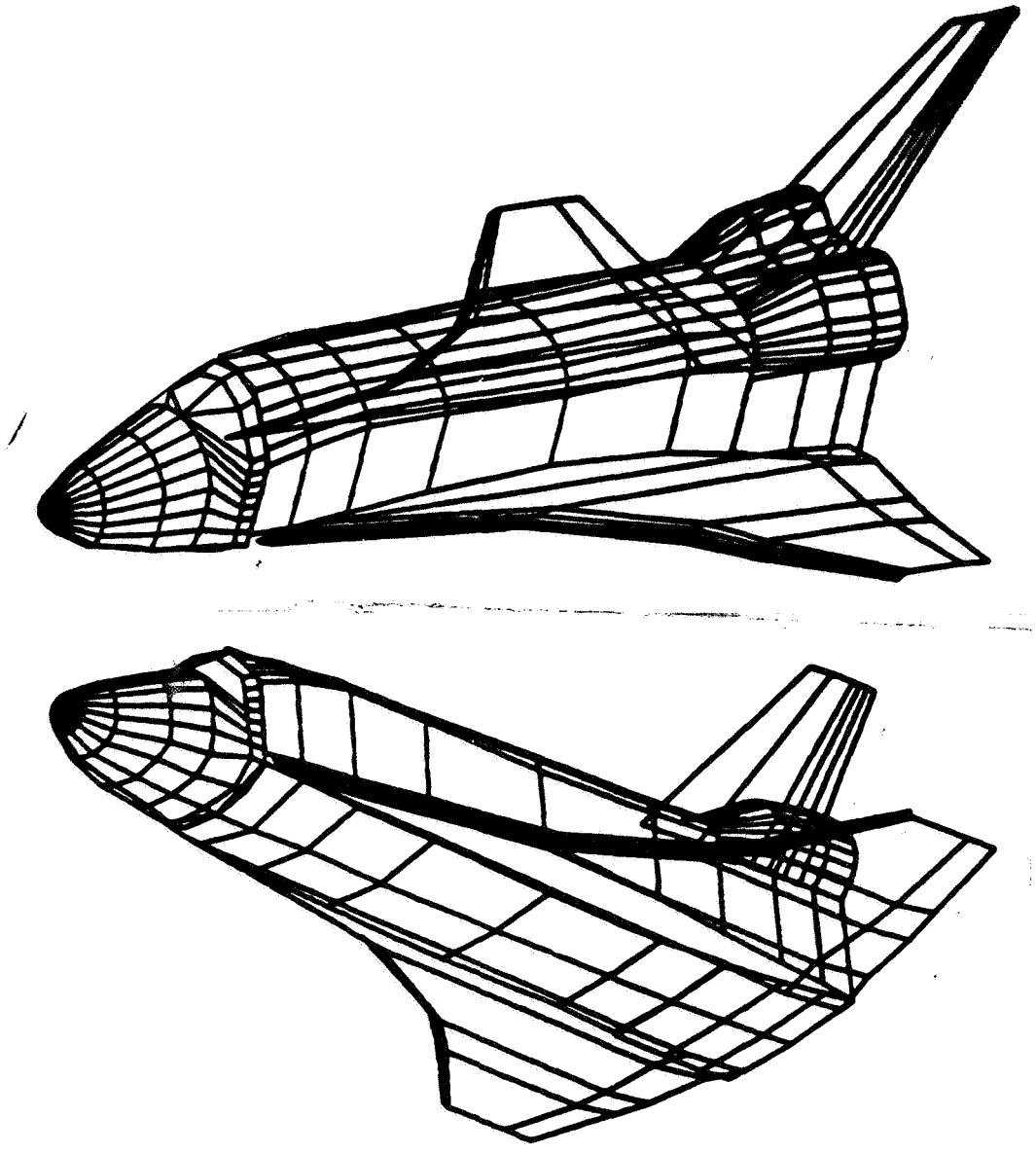

The pressure acting on each panel of a vehicle component is evaluated by a specified compression-expansion method selected from the following Table.

Impact Flow	Shadow Flow
1. Modified Newtonian	1. Newtonian (C_p = 0)
2. Modified Newtonian+Prandtl-Meyer	2. Modified Newtonian+Prandtl-Meyer
3. Tangent wedge	3. Prandtl-Meyer from free-stream
4. Tangent-wedge empirical	4. OSU blunt body empirical
5. Tangent-cone empirical	5. Van Dyke Unified
6. OSU blunt body empirical	6. High Mach base pressure
7. Van Dyke Unified	7. Shock-expansion
8. Blunt-body shear force	8. Input pressure coefficient
9. Shock-expansion	9. Free molecular flow
10. Free molecular flow	
11. Input pressure coefficient	
12. Hankey flat-surface empirical	
13. Delta wing empirical	
14. Dahlem-Buck empirical	
15. Blast wave	
16. Modified tangent-cone	

A discussion of the various methods is presented in appendix C. Specific analysis recommendations are provided by the program on a component by component basis.

In each method, the only geometric parameter required for determining panel pressure is the impact angle, δ, that the quadrilateral makes with the free-stream flow or the change in angle of a panel from a previous point where

$$\delta = \frac{\pi}{2} - \theta$$

$$\cos\theta = \frac{\bar{n} \cdot \bar{V}}{|\bar{n}|\,|\bar{V}|}$$

and

$$\bar{n} = n_X \bar{i} + n_Y \bar{j} + n_Z \bar{k}$$

$$\bar{V} = \bar{V}_\infty - \bar{\Omega} \times \bar{r}$$

$$\bar{V}_\infty = V_\infty \cos\alpha \cos\beta \; \bar{i} - V_\infty \sin\beta \; \bar{j} + V_\infty \sin\alpha \cos\beta \; \bar{k}$$

$$\bar{\Omega} = p\bar{i} - q\,\bar{j} - r\,\bar{k}$$

$$\bar{r} = (x-x_{cg})\,\bar{i} + (y-y_{cg})\,\bar{j} + (z-z_{cg})\,\bar{k}$$

Panel switching between impact or shadow conditions is based on $\delta > 0$ in the former case and $\delta < 0$ in the latter.

AERODYNAMIC CHARACTERISTICS

The pressure on each panel is calculated independent of all other panels (except the shock-expansion method). If the vehicle is rotating, the local pressure coefficient must be corrected back to free-stream conditions. That is

$$C_p = C_{p_{local}} \frac{|\bar{V}|^2}{V_\infty^2}$$

Vehicle component forces are obtained by summing panel forces

$$\Delta C_x = \frac{1}{S_{REF}} \sum C_p \, n_x A$$

$$\Delta C_y = \frac{1}{S_{REF}} \sum C_p \, n_y A$$

$$\Delta C_z = \frac{1}{S_{REF}} \sum C_p \, n_z A$$

$$\Delta C_{\ell} = \frac{1}{bS_{REF}}\left[\sum C_P\ (z-z_{cg})\ n_y A + \sum C_P\ (y-y_{cg})\ n_z A\right]$$

$$\Delta C_m = \frac{1}{\bar{c}S_{REF}}\left[\sum C_P\ (x-x_{cg})\ n_z A + \sum C_P\ (z-z_{cg})\ n_x A\right]$$

$$\Delta C_n = \frac{1}{bS_{REF}}\left[\sum C_P\ (x-x_{cg}) n_y A - \sum C_P\ (y-y_{cg})\ n_x A\right]$$

where

A = panel area

x,y,z = panel centroid

Configuration buildup and total vehicle coefficients are obtained by appropriate summation of component contributions.

The conversion of the body axis force characteristics to lift and drag coefficients is based on the standard trigonometric relations.

$$C_D = C_x \cos\alpha \cos\beta - C_y \sin\beta + C_z \sin\alpha \cos\beta$$

$$C_Y' = C_x \cos\alpha \sin\beta + C_y \cos\beta + C_z \sin\alpha \sin\beta$$

$$C_L = -C_x \sin\alpha + C_z \cos\alpha$$

The vehicle static stability derivatives in angle of attack and sideslip are calculated by the method of small perturbations. Since the basic force and moment characteristics are non-linear, these parameter vary with attitude angle

$$C_{x_\alpha} = \frac{(C_x)_{\alpha+\Delta\alpha} - (C_x)_\alpha}{\Delta\alpha}$$

$$C_{z_\alpha} = \frac{(C_z)_{\alpha+\Delta\alpha} - (C_z)_\alpha}{\Delta\alpha}$$

$$C_{m_\alpha} = \frac{(C_m)_{\alpha+\Delta\alpha} - (C_m)_\alpha}{\Delta\alpha}$$

$$C_{y_\beta} = \frac{(C_Y)_{\beta+\Delta\beta} - (C_Y)_\beta}{\Delta\beta}$$

$$C_{n_\beta} = \frac{(C_n)_{\beta+\Delta\beta} - (C_n)_\beta}{\Delta\beta}$$

The damping derivatives due to vehicle rotation rate are given in a similar manner

$$C_{m_{\hat{q}}} = \left[\frac{(C_m)_{q+\Delta q} - (C_m)_q}{\Delta q}\right] \Big/ \frac{\bar{c}}{2V}$$

etc.

The control surface derivatives are also calculated by the method of small perturbations.

$$C_{L_\delta} = \frac{(C_L)_{\delta+\Delta\delta} - (C_L)_\delta}{\Delta\delta}$$

$$C_{m_\delta} = \frac{(C_m)_{\delta+\Delta\delta} - (C_m)_\delta}{\Delta\delta}$$

$$C_{l_\delta} = \frac{(C_l)_{\delta+\Delta\delta} - (C_l)_\delta}{\Delta\delta}$$

$$C_{Y_\delta} = \frac{(C_Y)_{\delta+\Delta\delta} - (C_Y)_\delta}{\Delta\delta}$$

etc.

CONCLUSIONS

An aerodynamic configuration evaluation program has been developed and implemented on a time sharing system with an interactive graphics terminal to maximize responsiveness to the preliminary analysis problem.

The solution is based on potential theory with edge considerations at subsonic/supersonic speeds and impact type finite element analysis at hypersonic conditions. Three-dimensional configurations having multiple non-planar surfaces of arbitrary planform and bodies of non-circular contour may be analyzed. Static, rotary, and control longitudinal and lateral-directional characteristics may be generated.

CDC 175 computation time of 45 CPU seconds/Mach number at subsonic-supersonic speeds and 1 CPU second/Mach number/attitude at hypersonic conditions for a typical simulation indicates the program provides an efficient analysis for systematically performing various aerodynamic configuration tradeoff and evaluation studies.

REFERENCES

1. Ward, G. N., Linearized Theory of Steady High Speed Flow, Cambridge University Press, 1955.

2. Adams, M. C. and Sears, W. R. "Slender-Body Theory-Review and Extension," Journal of Aeronautical Sciences, February 1953.

3. Werner, J. and Krenkel, A. R., "Slender Body Theory Programmed for Bodies with Arbitrary Crossection," NASA CR 145383, February 1978

4. Woodward, F. A., "Analysis and Design of Wing-Body Combinations, at Subsonic and Supersonic Speeds," Journal of Aircraft, Vol. 5, No. 6, Nov-Dec., 1968.

5. Polhamus, E. C., "A Concept of the Vortex Lift of Sharp-Edge Delta Wings Based on a Leading-Edge-Suction Analogy," NASA TN D-3767, 1966.

6. Carlson, H. W., Mack, R. J., and Barger, R. L., "Estimation of Attainable Leading-Edge Thrust for Wings at Subsonic and Supersonic Speeds," NASA TP 1500, October 1979.

7. Tulinius, J. et al., "Theoretical Prediction of Airplane Stability Derivatives at Subcritical Speeds," NASA CR-132681, 1975.

8. Schlichting, H., Boundary Layer Theory, Fourth Edition, McGraw-Hill Book Co. Inc. 1958.

9. Eckert, E. R. G., "Survey of Heat Transfer at High Speed," WADC TR-54-70, 1954.

10. Van Driest, E. R., "The Problem of Aerodynamic Heating" Aeronautical Engineering Review, October 1956, pp. 26-41.

11. Goddard, F. E., "Effect of Uniformly Distributed Roughness on Turbulent Skin Friction Drag at Supersonic Speed," Journal Aero/Space Sciences, January 1959, pp. 1-15, 24.

12. Clutter, D. W., "Charts for Determining Skin Friction Coefficients on Smooth and Rough Plates at Mach Numbers up to 5.0 With and Without Heat Transfer," Douglas Aircraft Report No. ES-29074, 1959.

13. Hoerner, S. F., Fluid Dynamic Drag, Published by Author, 148 Busteed Drive, Midland Park, New Jersey, 1958.

14. Hayes, W. D., "Linearized Supersonic Flow," North American Aviation, Inc. Report No. AL-222, 1947.

15. Lomax, H., "The Wave Drag of Arbitrary Configurations in Linearized Flow as Determined by Areas and Forces in Oblique Planes," NACA RM A55A18, 1955.

16. Eminton, E., "On the Minimization and Numerical Evaluation of Wave Drag," RAE Report Aero 2564, 1955.

17. Eminton, E., "On the Numerical Evaluation of the Drag Integral," British R & M 3341, 1963.

18. Gentry, Arvel, E., "Hypersonic Arbitrary-Body Aerodynamic Computer Program," Douglas Report DAC 61552, Vols. I and 2, April 1968.

19. Love, E. S., Henderson, A., Jr., and Bertram, M. H., Some Aspects of the Air - Helium Simulation and Hypersonic Approximations, NASA TN D-49, October 1959.

20. Kaufman, L. G., II., Pressure Estimation Techniques for Hypersonic Flows Over Blunt Bodies, Journal of Astronautical Sciences, Volume X, No. 2, Summer 1963.

21. Ames Research Staff, Equations, Tables, and Charts for Compressible Flow, NACA TR 1135, 1953.

22. Korn, G. A., and Korn, T. M., Mathematical Handbook for Scientists and Engineers, McGraw-Hill, April 1961.

23. Liepmann, H. W., and Roshko, A., Elements of Gasdynamics, John Wiley and Sons, Inc., 1957.

24. Bertram, M. H. and Henderson, A., Jr., Recent Hypersonic Studies of Wings and Bodies, ARS Journal, Vol. 31, No. 8, August 1961.

25. Gregorek, G. M., Nark, T. C., and Lee, J. D., An Experimental Investigation of the Surface Pressure and the Laminar Boundary Layer on a Blunt Flat Plate in Hypersonic Flow, ASD-TDR-62-792, Volume I, March 1963.

26. Van Dyke, M. D., A Study of Hypersonic Small-Disturbance Theory, NACA Report 1194, 1954.

27. Shapiro, A. H., "The Dynamics and Thermodynamics of Compressible Fluid Flow," The Ronald Press, 1953.

28. Hayes, W. D., and Probstein, R. F., "Hypersonic Flow Theory, Academic Press, 1959.

29. Van Tassell, W., "Free-Molecular and Newtonian Coefficients for Arbitrary Bodies," RAD-TM-63-63, August 1963.

30. Hankey, W. L., Jr., "Optimication of Lifting Re-Entry Vehicles," ASD-TDR-62-1102, March 1963.

31. Dahlem, V. and Buck, M. L., "Experimental and Analytical Investigations of Vehicle Designs for High Lift-Drag Ratios in Hypersonic Flight," AFFDL-TR-67-138, June 1967.

32. Lukasiewicz, J., "Hypersonic Flow-Blast Analogy, AEDC-TR-61-4, June 1961.

33. Jacobs, W. F., "A Simplified Approximate Method for the Calculation of the Pressure Around Conical Bodies of Arbitrary Shape in Supersonic and Hypersonic Flow, JAS, December 1961, pp 987-988.

APPENDIX A

SUBSONIC/SUPERSONIC FINITE ELEMENT DERIVATIONS

VELOCITY PERTURBATION POTENTIAL

The expressions for the velocity potential induced by the source and vortex finite elements can be derived from the velocity potential for a point source:

Source at x_0, y_0, z_0

$$\phi_s(x, y, z) = -\frac{k\sigma}{4\pi R} \qquad R^2 = (x-x_0)^2 + \beta^2[(y-y_0)^2 + (z-z_0)^2]$$

Therefore the velocity potential for an area in the $z_0 = 0$ plane having constant source density is:

$$\phi_s(x, y, z) = -\frac{k\sigma}{4\pi} \iint_S \frac{dx_0 dy_0}{R}$$

$$\Box^2 \phi_s = 0$$

$$\Box^2 \phi_s = 0$$

$$\Box^2 = (1 - M_\infty^2)\frac{\partial^2}{\partial x^2} + \frac{\partial^2}{\partial y^2} + \frac{\partial^2}{\partial z^2}$$

A doublet at x_o, y_o, z_o. is the derivative of a point source:

$$\phi_D(x,y,z) = \frac{\partial}{\partial z_o}\cdot\phi_s = -\frac{k\sqrt{\beta^2}(z-z_o)}{4\pi R^3} = \frac{k\mu(z-z_o)}{4\pi R^3}$$

Integrating from $x_o = \bar{x}_o$ to infinity yields the potential for a line doublet or elementry horseshoe vortex.

$$\phi_H(x,y,z) = \int_{\bar{x}_o}^{\infty} \phi_D\, dx_o = \frac{k\mu}{4\pi}\frac{z}{(y-y_o)^2+z^2}\left\{(2-k)+\frac{(x-\bar{x}_o)}{R}\right\} \qquad z_o = 0$$

And an area of constant vortex strength is obtained by integrating this expression over the panel area:

$$\phi_V(x,y,z) = \frac{k\mu}{4\pi}\iint_S \frac{z}{(y-y_o)^2+z^2}\left\{(2-k)+\frac{(x-x_o)}{R}\right\} dx_o\, dy_o$$

The solution to these integrals is performed in the following sections. All integrals may be checked using tables 1 and 2 at the end of the Appendix.

The velocity expressions may be obtained by differentiating the velocity potentials using table 1.

First the integration is performed over the panels in the x_o direction.

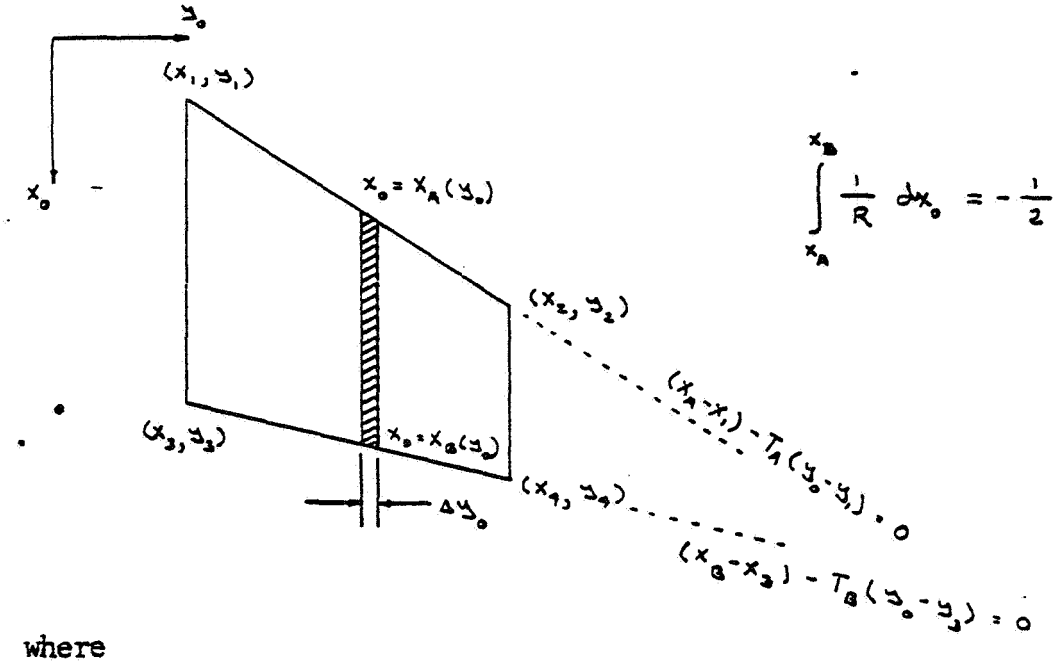

$$\int_{x_A}^{x_B} \frac{1}{R}\, dx_o = -\frac{1}{2} \log \frac{R + (x - x_o)}{R - (x - x_o)} \Bigg|_{x_A}^{x_B}$$

where

$$T_A = \frac{(x_2 - x_1)}{(y_2 - y_1)} \qquad T_B = \frac{(x_4 - x_3)}{(y_4 - y_3)}$$

To integrate with respect to y_o a change of variables is introduced:

$$\xi = (x - x_o) - T(y - y_o) \qquad (x - x_o) = \xi + \eta$$

$$\eta = T(y - y_o) \qquad (y - y_o) = \frac{1}{T}\eta$$

$$\zeta = T z \qquad z = \frac{1}{T}\zeta$$

when $x_o = x_B \quad T = T_B$

$$\xi = (x - x_B) - T(y - y_o) = (x - x_1) - T_B(y - y_1)$$

which is independent of y_o

Therefore the integral may be performed with ξ = constant

$$-\int_{y_1}^{y_2} \frac{1}{2}\log\frac{R+(x-x_0)}{R-(x-x_0)}\,dy_0 = \frac{1}{T}\int_{\eta_1}^{\eta_2}\frac{1}{2}\log\frac{R+(\xi+\eta)}{R-(\xi+\eta)}\,d\eta$$

$$= \frac{1}{T}\left\{\eta\frac{1}{2}\log\frac{R+(\xi+\eta)}{R-(\xi+\eta)} + \xi\frac{1}{B}\frac{1}{2}\log\frac{BR+(\xi+B^2\eta)}{BR-(\xi+B^2\eta)} + \xi\tan^{-1}\frac{\xi R}{\xi\eta-\xi^2}\right\}_{\eta_1}^{\eta_2}$$

$$B^2 = \frac{T^2+\beta^2}{T^2}$$

which may be checked using table 2.

Each of the four integration limits corresponds to a corner of the quadrilateral. Placing the origin of the x_0, y_0 coordinate system at one corner, the contribution to Φ becomes:

$$\phi(x,y,z,T) = -\frac{\sigma k}{4\pi}\left\{ y\frac{1}{2}\log\frac{R+x}{R-x} + \frac{(x-Ty)}{\sqrt{T^2+\beta^2}}\frac{1}{2}\log\frac{\sqrt{T^2+\beta^2}\,R+(Tx+\beta^2 y)}{\sqrt{T^2+\beta^2}\,R-(Tx+\beta^2 y)} + z\tan^{-1}\frac{zR}{xy-T(y^2+z^2)}\right\}$$

and combining each of the four corners:

$$\Phi(x,y,z) = \phi(x-x_1, y-y_1, z, T_A) - \phi(x-x_2, y-y_2, z, T_A)$$

$$- \phi(x-x_3, y-y_3, z, T_B) + \phi(x-x_4, y-y_4, z, T_B)$$

Analogous to the source panels the integration is first performed in the x_o direction.

$$\int_{x_A}^{x_B} \frac{z}{(y-y_o)^2+z^2}\left\{(2-k)+\frac{x-x_o}{R}\right\}dx_o = \frac{-z}{(y-y_o)^2+z^2}\left\{(2-k)(x-x_o)+R\right\}_{x_o=x_A}^{x_o=x_B}$$

changing variables and integrating with respect to η

$$\bullet - \int_{y_1}^{y_2} \frac{z}{(y-y_o)^2+z^2}\left\{(2-k)(x-x_o)+R\right\}dy_o = \int_{\eta_1}^{\eta_2} \frac{\xi}{(\eta^2+\xi^2)}\left\{(2-k)(\xi+\eta)+R\right\}d\eta$$

$$= (2-k)\left\{\xi \tan^{-1}\frac{\eta}{\xi} + \xi\frac{1}{2}\log(\eta^2+\xi^2)\right\}_{\eta_1}^{\eta_2}$$

$$+ \left\{\beta^2\xi\frac{1}{\beta}\frac{1}{2}\log\frac{\beta R+(\xi+\beta^2\eta)}{\beta R-(\xi+\beta^2\eta)} - \xi\frac{1}{2}\log\frac{R+(\xi+\eta)}{R-(\xi+\eta)} - \xi\tan^{-1}\frac{\xi R}{\xi\eta-\xi^2}\right\}_{\eta_1}^{\eta_2}$$

therefore for one corner or integration limit

$$\phi(x,y,z,T) = \frac{k\mu}{4\pi}\left\{(T^2+\beta^2)z\frac{1}{\sqrt{T^2+\beta^2}}\frac{1}{2}\log\frac{\sqrt{T^2+\beta^2}\,R+(Tx+\beta^2 y)}{\sqrt{T^2+\beta^2}\,R-(Tx+\beta^2 y)} - Tz\frac{1}{2}\log\frac{R+x}{R-x}\right.$$

$$\left. - (x-Ty)\tan^{-1}\frac{zR}{xy-T(y^2+z^2)} + (2-k)\left[Tz\frac{1}{2}\log(y^2+z^2)+(x-Ty)\tan^{-1}\frac{y}{z}\right]\right\}$$

and

$$\Phi(x,y,z) = \phi(x-x_1, y-y_1, z, T_A) - \phi(x-x_2, y-y_2, z, T_A)$$

$$- \phi(x-x_3, y-y_3, z, T_B) + \phi(x-x_4, y-y_4, z, T_B)$$

VERIFICATION OF THE PERTURBATION VELOCITY EXPRESSIONS

To establish that these are the correct perturbation velocities the following criteria must be met:

1. Laplace's equation must be satisfied

$$\beta^2 \bar{\Phi}_{xx} + \bar{\Phi}_{yy} + \bar{\Phi}_{zz} = 0$$

or the equivalent,

$$u_y = v_x$$

$$u_z = \omega_x$$

$$v_z = \omega_y$$

$$\beta^2 u_x + v_y + \omega_z = 0$$

2. The correct discontinuity or jump in the perturbation velocity must occur at the surface of the quadrilateral panel area. For the source panel the jump occurs in the normal or w velocity and on the vortex panel there must be a jump of constant magnitude in the u perturbation velocity over the panel area. The perturbation velocities should be continuous elsewhere, except on the trailing vortex sheet of the vortex panel.

3. The perturbation velocities must go to zero as upstream infinity is approached.

4. For the vortex panel the trailing vorticity must extend straight back to downstream infinity. This means that any discontinuity in the v velocity must be zero outside the spanwise boundaries of the panel and must be zero upstream of the panel.

The first criteria can be established by using the derivatives given in table 1.

The second criteria can be established by noting that all terms except

$$\tan^{-1}\frac{\xi R}{x y - T(y^2+z^2)} \quad \text{and} \quad \tan^{-1}\frac{y}{z}$$

are continuous at Z = 0. Consider these terms keeping in mind that the contributions from all four corners must included.

If we let

$$\xi = (x-x_1) - T(y-y_1) = (x-x_2) - T(y-y_2)$$

$$R_i^2 = (x-x_i)^2 + \beta^2[(y-y_i)^2 + z^2]$$

and use

$$\tan^{-1} A + \tan^{-1} B = \tan^{-1}\frac{A+B}{1-AB}$$

then the contributions from both corners on the leading edge can be combined as follows.

$$\tan^{-1}\frac{\xi R_1}{\xi(y-y_1) - T z^2} - \tan^{-1}\frac{\xi R_2}{\xi(y-y_2) - T z^2}$$

$$= \tan^{-1}\left\{ z\,\frac{[\xi(y-y_2) - T z^2]R_1 - [\xi(y-y_1) - T z^2]R_2}{[\xi(y-y_2) - T z^2][\xi(y-y_1) - T z^2] + z^2 R_1 R_2} \right\}$$

If we define

$$\operatorname{sgn} z = \begin{cases} 1 & z > 0 \\ -1 & z < 0 \end{cases}$$

$$\lim_{a \to 0} \tan^{-1} \frac{a}{b} = \begin{cases} 0 & b > 0 \\ \pi \operatorname{sgn} a & b < 0 \end{cases} \qquad -\pi \le \tan^{-1} c \le \pi$$

$$\Delta f(z) = \lim_{z \to 0^+} f(z) - \lim_{z \to 0^-} f(z)$$

then

$$\lim_{z \to 0} \left\{ \tan^{-1} \frac{z R_1}{\xi(y - y_1) - \tau z^2} - \tan^{-1} \frac{z R_2}{\xi(y - y_2) - \tau z^2} \right\} = \begin{cases} 0 & (y-y_1)(y-y_2) > 0 \\ -\pi \operatorname{sgn} z \operatorname{sgn} \xi & (y-y_1)(y-y_2) < 0 \end{cases}$$

$$\Delta \left\{ \tan^{-1} \frac{z R_1}{\xi(y - y_1) - \tau z^2} - \tan^{-1} \frac{z R_2}{\xi(y - y_2) - \tau z^2} \right\} = \begin{cases} 0 & (y-y_1)(y-y_2) > 0 \\ -2\pi \operatorname{sgn} \xi & (y-y_1)(y-y_2) < 0 \end{cases}$$

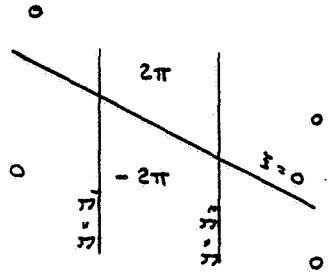

Therefore when a similar procedure is carried out for the trailing edge of a source panel we obtain the following jump in the w perturbation velocity.

$$\Delta \omega = 0$$

For the vortex panel (subsonic) we have an additional term. Considering both additional terms from the leading edge corners:

$$\tan^{-1}\frac{(y-y_1)}{z}-\tan^{-1}\frac{y-y_2}{z}=\tan^{-1}\frac{z(y_2-y_1)}{(y-y_1)(y-y_2)+z^2}$$

$$\lim_{z\to 0}\left\{\tan^{-1}\frac{(y-y_1)}{z}-\tan^{-1}\frac{y-y_2}{z}\right\}=\begin{cases}0 & (y-y_1)(y-y_2)>0\\ \pi\,\mathrm{sgn}\,z & (y-y_1)(y-y_2)<0\end{cases}$$

$$\Delta\left\{\tan^{-1}\frac{y-y_1}{z}-\tan^{-1}\frac{y-y_2}{z}\right\}=\begin{cases}0 & (y-y_1)(y-y_2)>0\\ 2\pi & (y-y_1)(y-y_2)<0\end{cases}$$

Therefore combining the terms

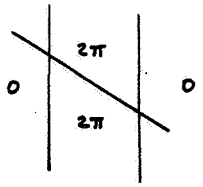

$$\Delta\left\{\tan^{-1}\frac{zR_1}{\xi(y-y_1)-\tau z^2}-\tan^{-1}\frac{zR_2}{\xi(y-y_2)-\tau z^2}-\tan^{-1}\frac{(y-y_1)}{z}+\tan^{-1}\frac{(y-y_2)}{z}\right\}$$

$$=\begin{cases}0 & (y-y_1)(y-y_2)>0\\ & \xi<0\\ -4\pi & \text{otherwise}\end{cases}$$

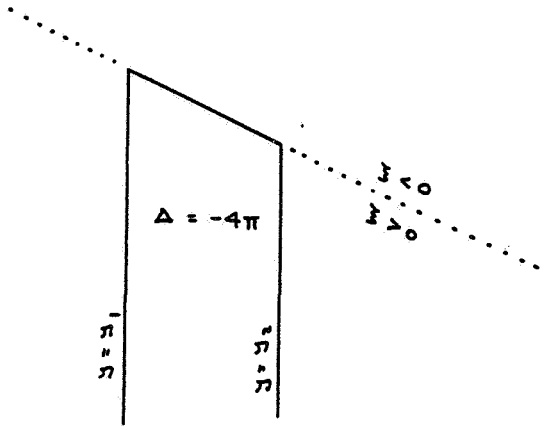

The contribution from each panel corner is:

$$\Delta u = \frac{C_p}{8\pi} \Delta \left\{ \tan^{-1} \frac{zR}{xy - T(y^2+z^2)} - \tan^{-1} \frac{y}{z} \right\}$$

$$\Delta v = -\frac{C_p T}{8\pi} \Delta \left\{ \tan^{-1} \frac{zR}{xy - T(y^2+z^2)} - \tan^{-1} \frac{y}{z} \right\}$$

Therefore summing all four panel corners

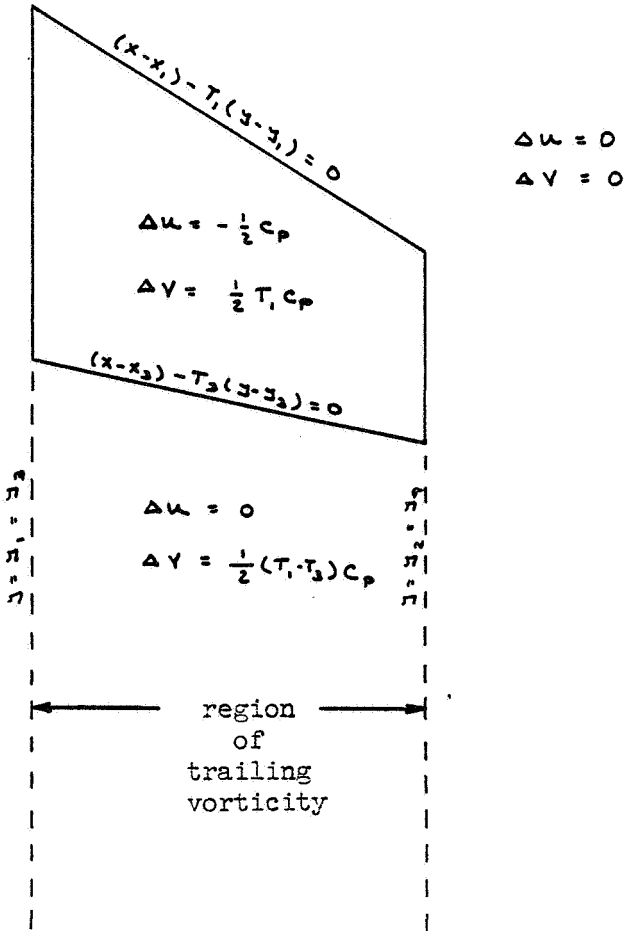

To verify the third criteria we must show that all of the functions approach zero when all four corners are considered as $x \to -\infty$

$$\frac{1}{2}\log\frac{R+x}{R-x} - \frac{1}{2}\log(y^2+z^2)$$

$$= \frac{1}{2}\log\frac{\beta^2(y^2+z^2)}{(R-x)^2} - \frac{1}{2}\log(y^2+z^2)$$

$$= -\frac{1}{2}\log(R-x)^2 + \frac{1}{2}\log\beta^2$$

Therefore considering both corners on the leading edge of the panel

$$\lim_{x\to-\infty} R = |x|$$

$$\lim_{x\to-\infty}\left\{\frac{1}{2}\log\frac{R_1+(x-x_1)}{R_1+(x-x_1)} - \frac{1}{2}\log\frac{R_2+(x-x_2)}{R_2-(x-x_2)}\right\} = \lim_{x\to-\infty}\frac{1}{2}\log\frac{(x-x_2)^2}{(x-x_1)^2} = 0$$

$$\lim_{x\to-\infty}\frac{R_1+(x-x_1)}{(y-y_1)^2+z^2} = 0$$

$$\lim_{x\to-\infty}\frac{1}{2}\log\frac{\sqrt{T^2+\beta^2}\,R+(Tx+\beta^2 y)}{\sqrt{T^2+\beta^2}\,R-(Tx+\beta^2 y)} = \frac{1}{2}\log\frac{\sqrt{T^2+\beta^2}-T}{\sqrt{T^2+\beta^2}+T}$$

and therefore this limit is also zero when both corners of the leading or trailing edges are considered. Since all terms are accounted for, the perturbation velocities are zero far upstream.

Since $$(T^2+\beta^2)R^2 - (Tx+\beta^2 y)^2 = \beta^2\left[(x-Ty)^2 + (T^2+\beta^2)z^2\right]$$

$$\frac{1}{2}\log\frac{\sqrt{T^2+\beta^2}\,R + (Tx+\beta^2 y)}{\sqrt{T^2+\beta^2}\,R - (Tx+\beta^2 y)} = \frac{1}{2}\log\frac{\left[\sqrt{T^2+\beta^2}\,R + (Tx+\beta^2 y)\right]^2}{\beta^2\left[(x-Ty)^2+(T^2+\beta^2)z^2\right]}$$

$$= -\frac{1}{2}\log\frac{\beta^2\left[(x-Ty)^2+(T^2+\beta^2)z^2\right]}{\left[\sqrt{T^2+\beta^2}\,R - (Tx+\beta^2 y)\right]^2}$$

there is an apparent singularity along the line

$$(x-Ty) = 0 \quad , \qquad z = 0$$

However this singularity may be removed by combining the contributions from both corners of the leading or trailing edges of the panel. Along either of these edges the values of

$$(x-x_i) - T(y-y_i) \quad \text{and} \quad z$$

are the same for each of the panel corners.

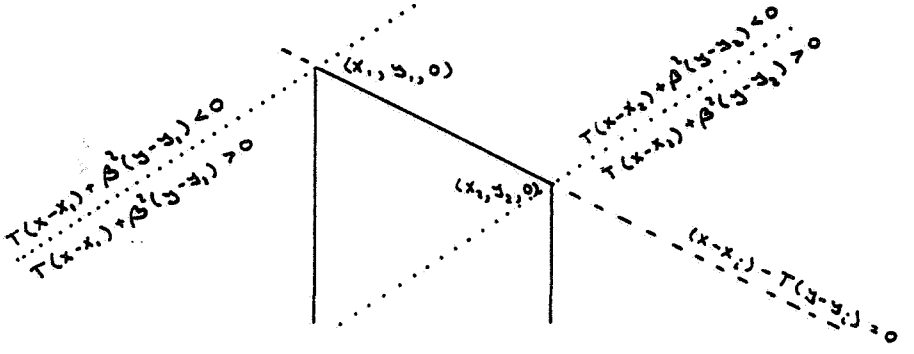

It can be seen from the above diagram that $(Tx+\beta^2 y)$ will have the same sign on a point (x,y,o) which lies outside the spanwise boundaries of the quadrilateral. Therefore outside the spanwise boundaries the term

$$\log\left[(x-Ty)^2 + (T^2+\beta^2)z^2\right]$$

can be canceled by combining both corners, and the resulting term

$$\pm\frac{1}{2}\log\frac{\sqrt{T^2+\beta^2}\,R_1 \pm \left[T(x-x_1)+\beta^2(y-y_1)\right]}{\sqrt{T^2+\beta^2}\,R_2 \pm \left[T(x-x_2)+\beta^2(y-y_1)\right]}$$

will not be singular if the correct + or - sign is chosen. Within the spanwise boundary an actual singularity occurs on the panel edge.

The term $\frac{1}{2}\log\frac{R+X}{R-X}$ also has a possible singularity. This term can be written

$$\frac{1}{2}\log\frac{R+X}{R-X} = \frac{1}{2}\log\frac{(R+X)^2}{\beta^2(y^2+z^2)}$$

For the source panel the singularity may be removed for points along $y^2+z^2=0$ which are outside of the panel boundaires.

If $(x-x_1)$ and $(x-x_3)$ have the same sign the combination of the two terms gives

$$\frac{1}{2}\log\frac{R_1+(x-x_1)}{R_1-(x-x_1)} - \frac{1}{2}\log\frac{R_2+(x-x_2)}{R_2-(x-x_2)} = \pm\frac{1}{2}\log\frac{R_1\pm(x-x_1)}{R_3\pm(x-x_3)}$$

where the correct sign is chosen to remove the singularity. On the panel edge the singularity is real and cannot be removed.

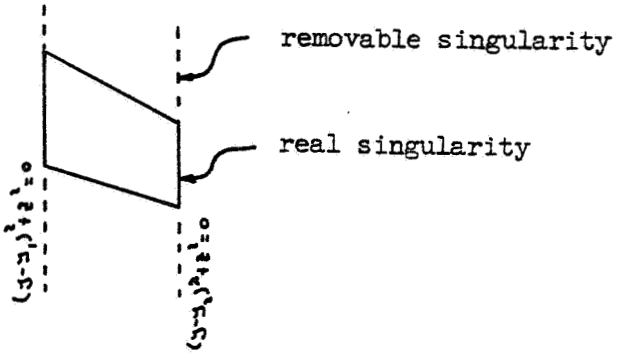

For a vortex panel the terms (subsonic)

$$\frac{1}{2}\log\frac{R+X}{R-X} - \frac{1}{2}\log(y^2+z^2) \quad \text{and} \quad \frac{y(R+x)}{(y^2+z^2)}$$

Both have real singularities for $x>0$ (downstream) and removable singularities for $x<0$ (upstream). The real singularities occur on the panel edges and on the edge of the trailing vortex sheet.

$$\text{if} \quad x<0 \qquad \lim_{(y^2+z^2)\to 0}\frac{y(R+x)}{y^2+z^2} = -\frac{1}{2}\beta^2\frac{y}{x}$$

SUPERSONIC VELOCITIES - SPECIAL CONSIDERATIONS

The velocity perturbation influence equations for supersonic flows are treated by taking only the real parts of the expressions. This means that $R = \sqrt{x^2-\beta^2(y^2+z^2)}$ is set equal to zero for points which lie outside the downstream Mach cone from any given corner. Therefore, R and $\frac{1}{2}\log\frac{R+x}{R-x}$ are zero for points which lie outside the downstream Mach cone. For $(T^2-\beta^2) > 0$, there are no problems using this method.

If $(T^2-\beta^2) < 0$ the real part of $\frac{1}{\sqrt{T^2-\beta^2}}\frac{1}{2}\log\frac{(Tx-\beta^2 y)+\sqrt{T^2-\beta^2}\,R}{(Tx-\beta^2 y)-\sqrt{T^2-\beta^2}\,R}$

is $\frac{1}{\sqrt{\beta^2-T^2}}\tan^{-1}\frac{\sqrt{\beta^2-T^2}\,R}{(Tx-\beta^2 y)}$

therefore, combining two corners

$$F2 = \frac{1}{\sqrt{\beta^2-T^2}}\tan^{-1}\frac{\sqrt{\beta^2-T^2}\left\{[T(x-x_2)-\beta^2(y-y_1)]R_1-[T(x-x_1)-\beta^2(y-y_1)]R_2\right\}}{[T(x-x_2)-\beta^2(y-y_1)][T(x-x_1)-\beta^2(y-y_1)]+(\beta^2-T^2)R_1R_2}$$

If $z = 0$ and either R_1 or R_2 is zero and we allow the other to approach zero, the value of F2 becomes

$$F2 = \begin{cases} \frac{\pi}{\sqrt{\beta^2-T^2}} & [T(x-x_1)-\beta^2(y-y_1)][T(x-x_2)-\beta^2(y-y_1)] < 0 \\ 0 & [T(x-x_1)-\beta^2(y-y_1)][T(x-x_2)-\beta^2(y-y_1)] > 0 \end{cases}$$

Therefore if R_1 and R_2 are zero but we are inside the envelope of mach cones from the leading edge (see figure 5), the value of F2 is set equal to

$$F2 = \frac{\pi}{\sqrt{\beta^2-T^2}}$$

$$\text{if} \quad \begin{cases} [T(x-x_1)-\beta^2(y-y_1)][T(x-x_2)-\beta^2(y-y_1)] < 0 \\ R_1^2 < 0 \qquad R_2^2 < 0 \\ (x-Ty)^2 > (\beta^2-T^2)z^2 \end{cases}$$

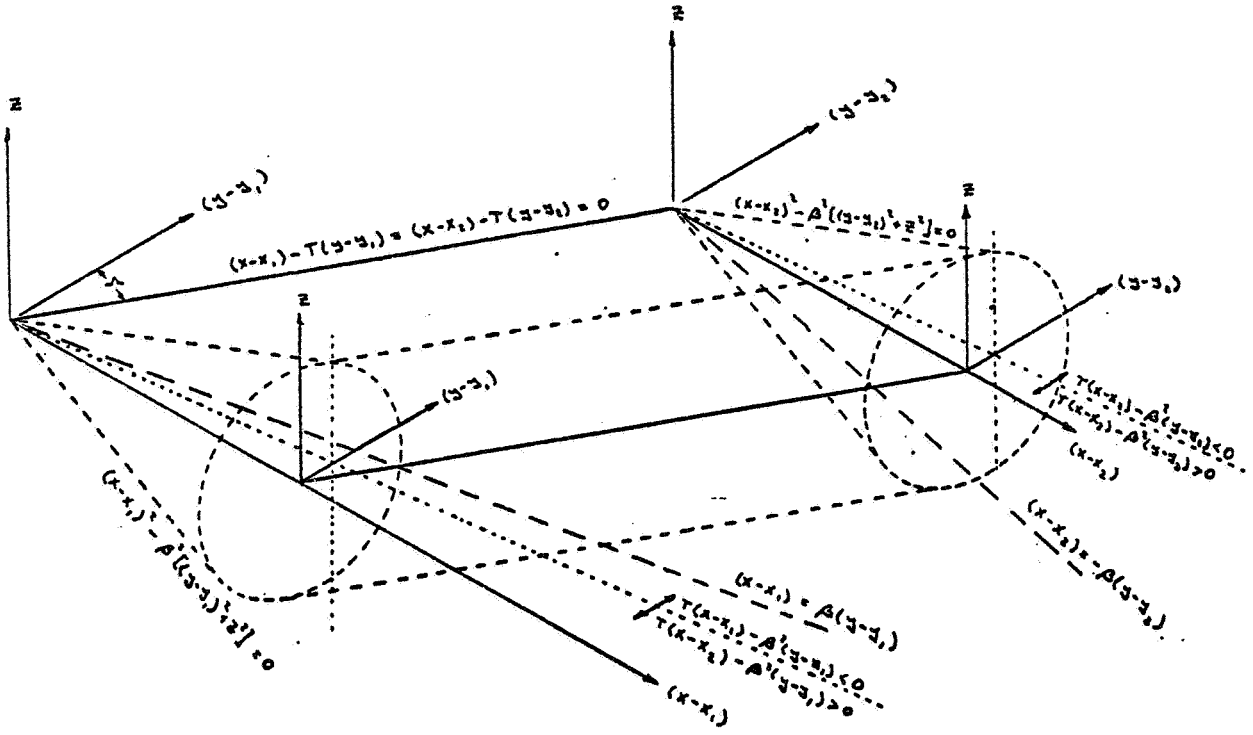

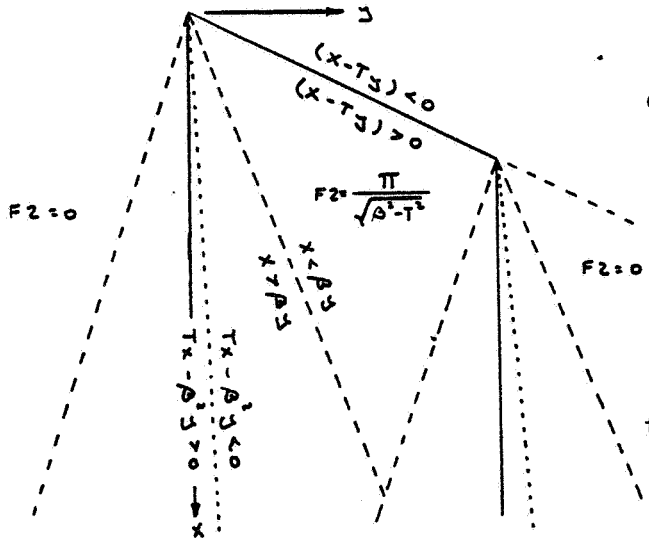

intersection of $(x-Ty)^2 = (\beta^2-T^2)z^2$

and $x^2 = \beta^2(y^2+z^2)$

occurs on the line $\begin{cases} y = ax \\ z = bx \end{cases}$

therefore $1 = \beta^2(a^2+b^2)$

$1-2aT+T^2a^2 = (\beta^2-T^2)b^2$

$\beta^2(1-2aT+T^2a^2) = (1-\beta^2a^2)(\beta^2-T^2) = \beta^2(\beta^2-T^2)b^2$

$\beta^4a^2-2\beta^2Ta+T^2 = 0 \qquad \beta^2a = T$

$\beta^4b^2 = \beta^2-T^2 \qquad \beta^2b = \pm\sqrt{\beta^2-T^2}$

therefore the line is determined by

$Tx-\beta^2y = 0 \qquad \beta^2z^2 = (\beta^2-T^2)x^2$

or $Tx-\beta^2y = 0 \qquad (x-Ty)^2 = (\beta^2-T^2)z^2$

Figure 5 Supersonic Leading Edge Mach Cone Envelope

As $T \to \beta$ (sonic leading edge) the value of $(T^2 - \beta^2) \to 0$. In this case

$$\lim_{T \to \beta} F2 = \frac{(R_1 - R_2)}{T\left[(x - x_1) - T(y - y_1)\right]} \qquad \left[(x - x_1) - T(y - y_1)\right] > 0$$

TABLE 1

TABLE OF DERIVATIVES

$$R^2 = x^2 + \beta^2(y^2+z^2)$$

$$R\frac{\partial}{\partial x}R = x$$

$$\frac{\partial}{\partial x}\ \frac{1}{2}\log\frac{R+x}{R-x} = \frac{1}{R}$$

$$\frac{\partial}{\partial x}\ \frac{1}{\sqrt{T^2+\beta^2}}\ \frac{1}{2}\log\frac{\sqrt{T^2+\beta^2}\,R+(Tx+\beta^2 y)}{\sqrt{T^2+\beta^2}\,R-(Tx+\beta^2 y)} = -\frac{xy-T(y^2+z^2)}{[(x-Ty)^2+(\beta^2+T^2)z^2]}\ \frac{1}{R}$$

$$\frac{\partial}{\partial x}\ \tan^{-1}\frac{zR}{xy-T(y^2+z^2)} = -\frac{z(Tx+\beta^2 y)}{[(x-Ty)^2+(\beta^2+T^2)z^2]}\ \frac{1}{R}$$

$$R\frac{\partial}{\partial y}R = \beta^2 y$$

$$\frac{\partial}{\partial y}\ \frac{1}{2}\log\frac{R+x}{R-x} = -\frac{xy}{(y^2+z^2)}\ \frac{1}{R}$$

$$\frac{\partial}{\partial y}\ \frac{1}{\sqrt{T^2+\beta^2}}\ \frac{1}{2}\log\frac{\sqrt{T^2+\beta^2}\,R+(Tx+\beta^2 y)}{\sqrt{T^2+\beta^2}\,R-(Tx+\beta^2 y)} = \frac{[x(x-Ty)+\beta^2 z^2]}{(x-Ty)^2+(\beta^2+T^2)z^2}\ \frac{1}{R}$$

$$\frac{\partial}{\partial y}\ \tan^{-1}\frac{zR}{xy-T(y^2+z^2)} = -\frac{xz}{y^2+z^2}\frac{1}{R}+\frac{Tz(Tx+\beta^2 y)}{(x-Ty)^2+(\beta^2+T^2)z^2}\ \frac{1}{R}$$

$$R\frac{\partial}{\partial z}R = \beta^2 z$$

$$\frac{\partial}{\partial z}\ \frac{1}{2}\log\frac{R+x}{R-x} = -\frac{xz}{y^2+z^2}\ \frac{1}{R}$$

$$\frac{\partial}{\partial z}\ \frac{1}{\sqrt{T^2+\beta^2}}\ \frac{1}{2}\log\frac{\sqrt{T^2+\beta^2}\,R+(Tx+\beta^2 y)}{\sqrt{T^2+\beta^2}\,R-(Tx+\beta^2 y)} = -\frac{z(Tx+\beta^2 y)}{(x-Ty)^2+(\beta^2+T^2)z^2}\ \frac{1}{R}$$

$$\frac{\partial}{\partial z}\ \tan^{-1}\frac{zR}{xy-T(y^2+z^2)} = \frac{xy}{y^2+z^2}\frac{1}{R}+\frac{(x-Ty)(Tx+\beta^2 y)}{(x-Ty)^2+(\beta^2+T^2)z^2}\ \frac{1}{R}$$

TABLE 2

TABLE OF DERIVATIVES

$$R^2 = (\xi+\eta)^2 + (B^2-1)(\eta^2+\xi^2) \qquad B^2 = \text{constant} = \frac{T^2+A^2}{T^2}$$

$$R\frac{\partial}{\partial \xi} R = (\xi+\eta)$$

$$\frac{\partial}{\partial \xi}\ \frac{1}{2}\log\frac{R+(\xi+\eta)}{R-(\xi+\eta)} = \frac{1}{R}$$

$$\frac{\partial}{\partial \xi}\ \frac{1}{B}\frac{1}{2}\log\frac{BR+(\xi+B^2\eta)}{BR-(\xi+B^2\eta)} = \frac{\xi^2-\xi\eta}{\xi^2+B^2\xi^2}\ \frac{1}{R}$$

$$\frac{\partial}{\partial \xi}\tan^{-1}\frac{\xi R}{\xi\eta-\xi^2} = -\frac{\xi(\xi+B^2\eta)}{(\xi^2+B^2\xi^2)}\ \frac{1}{R}$$

$$R\frac{\partial}{\partial \eta} R = (\xi+B^2\eta)$$

$$\frac{\partial}{\partial \eta}\ \frac{1}{2}\log\frac{R+(\xi+\eta)}{R-(\xi+\eta)} = \frac{(\xi^2-\xi\eta)}{(\eta^2+\xi^2)}\ \frac{1}{R}$$

$$\frac{\partial}{\partial \eta}\ \frac{1}{B}\frac{1}{2}\log\frac{BR+(\xi+B^2\eta)}{BR-(\xi+B^2\eta)} = \frac{1}{R}$$

$$\frac{\partial}{\partial \eta}\tan^{-1}\frac{\xi R}{\xi\eta-\xi^2} = -\frac{\xi(\xi+\eta)}{(\eta^2+\xi^2)}\ \frac{1}{R}$$

$$R\frac{\partial}{\partial \xi} R = (B^2-1)\xi$$

$$\frac{\partial}{\partial \xi}\ \frac{1}{2}\log\frac{R+(\xi+\eta)}{R-(\xi+\eta)} = -\frac{\xi(\xi+\eta)}{(\eta^2+\xi^2)}\ \frac{1}{R}$$

$$\frac{\partial}{\partial \xi}\ \frac{1}{B}\frac{1}{2}\log\frac{BR+(\xi+B^2\eta)}{BR-(\xi+B^2\eta)} = -\frac{\xi(\xi+B^2\eta)}{(\xi^2+B^2\xi^2)}\ \frac{1}{R}$$

$$\frac{\partial}{\partial \xi}\tan^{-1}\frac{\xi R}{\xi\eta-\xi^2} = \frac{\eta(\xi+\eta)}{(\eta^2+\xi^2)}\ \frac{1}{R} + \frac{\xi(\xi+B^2\eta)}{(\xi^2+B^2\xi^2)}\ \frac{1}{R}$$

$$T\frac{\partial}{\partial T}\ \frac{1}{2}\log\frac{BR+(\xi+B^2\eta)}{BR-(\xi+B^2\eta)} = \frac{\xi R}{B(\xi^2+B^2\xi^2)}$$

$$T\frac{\partial}{\partial T}\tan^{-1}\frac{\xi R}{\xi\eta-\xi^2} = \frac{\xi R}{(\xi^2+B^2\xi^2)}$$

APPENDIX B

SURFACE EDGE FORCES

LEADING EDGE POTENTIAL SUCTION

In the limit as the wing thickness goes to zero, the increasingly reduced pressure acting over a decreasing area results in a limiting suction force at the leading edge. If we consider the leading edge region, the force on the airfoil may be obtained by integrating over a control surface in the flow,

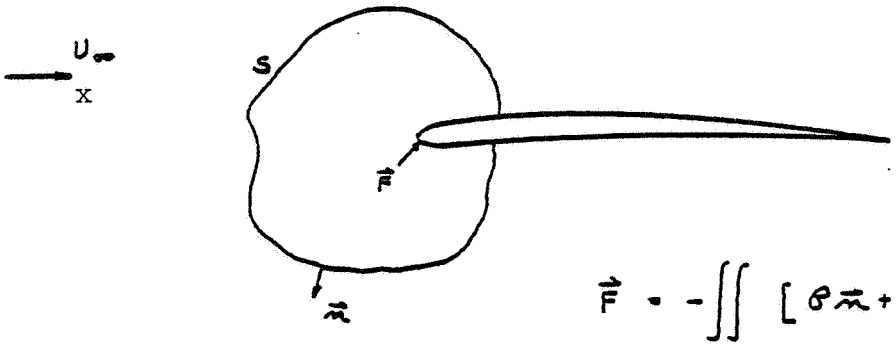

$$\vec{F} = -\iint_S \left[p\vec{n} + (\rho\vec{u})\vec{u}\cdot\vec{n} \right] dS$$

where S is a control surface into which the leading edge penetrates and $\vec{F}$ is the force on the area enclosed by S. In two dimensions the surface integral becomes a line integral and since for incompressible, irrotational flow

$$p = p_\infty - \tfrac{1}{2}\rho(u^2+v^2)$$

$$\vec{n}\,dS = dy\,\vec{e}_x - dx\,\vec{e}_y$$

$$F_x = -\int_C \left\{ \left[p_\infty - \tfrac{1}{2}\rho(u^2+v^2) \right] dy + \rho u \left[u\,dy - v\,dx \right] \right\}$$

$$= -\int_C p_\infty\,dy + \tfrac{1}{2}\rho \int_C \left[2uv\,dx + (v^2-u^2)\,dy \right]$$

where C is the contour around the leading edge of the airfoil and F_x is the force per unit of leading edge length.

As the wing thickness approaches zero, the wing becomes a line segment and the flow in the leading edge region is identical to the flow around a 180 degree corner. Incompressibly, it is described by

$$u_r = \frac{a}{\sqrt{r}} \cos\tfrac{1}{2}\theta + U_\infty \cos\theta$$

$$u_\theta = \frac{-a}{\sqrt{r}} \sin\tfrac{1}{2}\theta - U_\infty \sin\theta$$

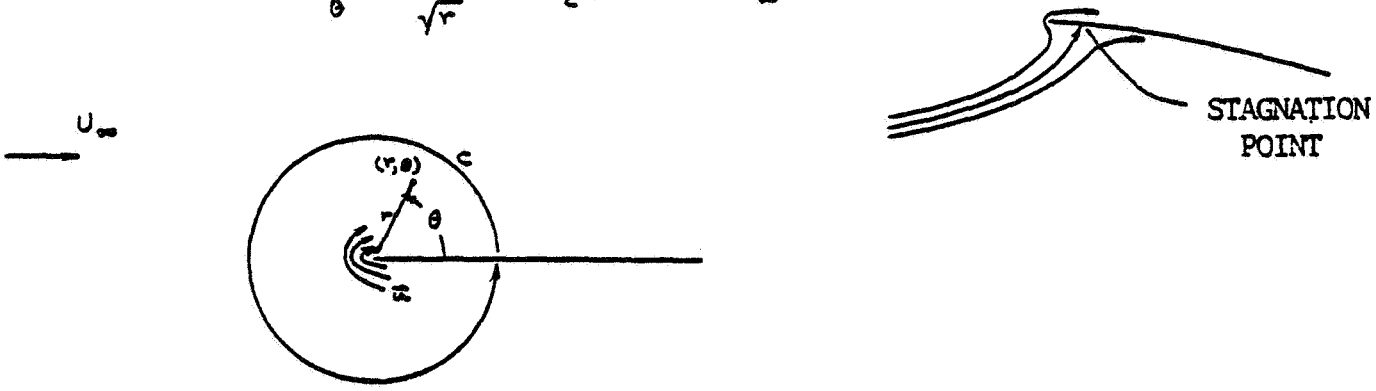

where (r,θ) is a coordinate system centered at the leading edge,

and

$$u = u_r \cos\theta - u_\theta \sin\theta$$

$$v = u_r \sin\theta + u_\theta \cos\theta$$

$$dy = R\cos\theta\, d\theta$$

$$dx = -R\sin\theta\, d\theta$$

and C is the circle $r = R$

Therefore, since

$$\int_C \rho_\infty \, dy = 0$$

as $R \to 0$

$$\sqrt{R}\,u = a\left\{\cos\tfrac{1}{2}\theta\cos\theta + \sin\tfrac{1}{2}\theta\sin\theta\right\} = a\cos\tfrac{1}{2}\theta$$

$$\sqrt{R}\,v = a\left\{\cos\tfrac{1}{2}\theta\sin\theta - \sin\tfrac{1}{2}\theta\cos\theta\right\} = a\sin\tfrac{1}{2}\theta$$

$$F_x = \tfrac{1}{2}\rho a^2 \int_0^{2\pi}\left\{-2\cos\tfrac{1}{2}\theta\sin\tfrac{1}{2}\theta\sin\theta + \left[\sin^2\tfrac{1}{2}\theta - \cos^2\tfrac{1}{2}\theta\right]\cos\theta\right\} d\theta$$

$$= -\tfrac{1}{2}\rho a^2 \int_0^{2\pi}\left[\sin^2\theta + \cos^2\theta\right] d\theta = -\tfrac{1}{2}\,2\pi\rho a^2 \qquad (1)$$

To relate $-F_X$, the leading edge suction force, to the pressure distribution near the leading edge, the ΔC_p across the line segment must be evaluated.

On the top $\theta = 0$ $\quad u = \dfrac{1}{\sqrt{x}}a + U_\infty$, $\quad v = 0$

On the bottom $\theta = 2\pi$ $\quad u = -\dfrac{1}{\sqrt{x}}a + U_\infty$, $\quad v = 0$

$$\Delta p = \tfrac{1}{2}\rho\,\frac{4aU_\infty}{\sqrt{x}}$$

and if c is the chord length $\quad \Delta C_p = \dfrac{4a}{U_\infty\sqrt{c}}\,\dfrac{1}{\sqrt{\xi}} \qquad \xi = \dfrac{x}{c}$

$$C_t = \frac{\Delta\,\text{THRUST}}{c\,\Delta z\,q_\infty} = \frac{-F_x}{c\,\frac{1}{2}\rho U_\infty^2} = \frac{2\pi}{c}\frac{a^2}{U_\infty^2} = \frac{1}{8}\pi\left\{\frac{4a}{\sqrt{c}\,U_\infty}\right\}^2$$

or $\quad \Delta C_p = A\dfrac{1}{\sqrt{\xi}} \qquad C_t = \dfrac{1}{8}\pi A^2 \qquad A = \dfrac{4a}{U_\infty\sqrt{c}}$

These expressions relate the leading edge thrust coefficient to the net distribution, ΔC_p, at the leading edge.

In general we can write

$$C_p(\phi) = A_0 \cot\tfrac{1}{2}\phi + \sum_{n=1}^{\infty} A_n \sin n\phi$$

where

$$\xi = \frac{x}{c} = \tfrac{1}{2}(1-\cos\phi) = \sin^2\tfrac{1}{2}\phi$$

$$\cot\tfrac{1}{2}\phi = \frac{\cos\frac{1}{2}\phi}{\sin\frac{1}{2}\phi} = \frac{\sqrt{1-\sin^2\frac{1}{2}\phi}}{\sin\phi} = \frac{\sqrt{1-\xi}}{\sqrt{\xi}}$$

A_0 is the coefficient of the $\xi^{-1/2}$ term and therefore determines the leading edge suction force since only the term which is infinite at the leading edge contributes to the suction.

$$C_t = \frac{1}{8}\pi A_0^2 \qquad M_\infty = 0$$

For linearized compressible flow the following Mach number correction must be applied

$$C_t = \frac{1}{8}\beta\pi A_0^2 \qquad \beta^2 = 1 - M_\infty^2$$

To derive the expression for a swept wing, an infinitely skewed wing is considered.

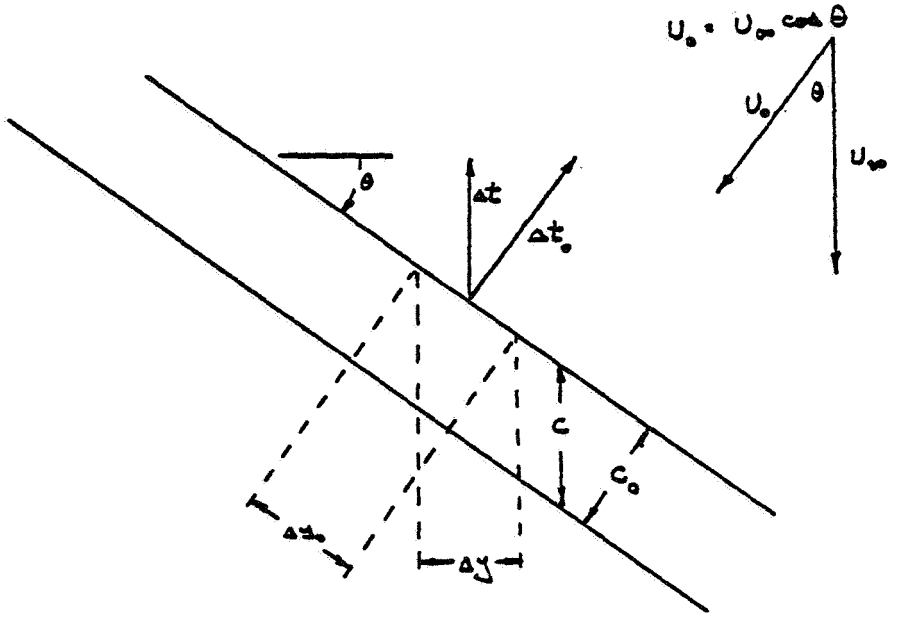

Let the subscript or supercript o denote the variables normal to the leading edge. Then

$$\Delta C_p^\circ = \mathring{A}_0 \cot\tfrac{1}{2}\phi + \sum_{m=1}^{\infty} \mathring{A}_m \sin m\phi$$

and

$$C_{t_0} = \frac{1}{8}\pi\beta_0 \mathring{A}_0^2 = \frac{\Delta t_0}{c_0 \Delta y_0 q_\infty^\circ}$$

the ratio of thrust per unit length is identical in either system

$$c_0 C_{t_0} q_\infty^\circ = c C_t q_\infty = \frac{\Delta t_0}{\Delta y_0} = \frac{\Delta t}{\Delta y}$$

ΔC_p and C_t in the freestream coordinate system are based on freestream dynamic pressure q_∞. Thus

$$q_\infty^\circ = q_\infty \cos^2\theta$$

$$\Delta C_p = \Delta C_p^\circ \frac{q_\infty^\circ}{q_\infty} = \Delta C_p^\circ \cos^2\theta$$

and $$C_t c = C_{t_0} c_0 \frac{q_\infty^\circ}{q_\infty} = C_{t_0} c_0 \cos^2\theta$$

therefore $$A_m = \mathring{A}_m \cos^2\theta$$

and $$\beta_0^2 = 1 - M_0^2 = \cos^2\theta \left[\frac{1}{\cos^2\theta} - M_\infty^2\right] = \cos^2\theta\left[\tan^2\theta + (1 - M_\infty^2)\right]$$

$$= \cos^2\theta \left[\tan^2\theta + \beta^2\right]$$

therefore combining terms

$$C_t(y) = \frac{\Delta t}{c \Delta y q_\infty} = \frac{1}{8} \pi \beta_0 \mathring{A}_0^2 \frac{q_\infty^\circ}{q_\infty} \frac{c_0}{c}$$

$$= \frac{1}{8} \pi \cos\theta \sqrt{\tan^2\theta + \beta^2} \frac{A_0^2}{\cos^2\theta} \cos^2\theta \cos\theta$$

$$= \frac{1}{8} \pi \sqrt{\tan^2\theta + \beta^2} \; A_0^2$$

when ΔC_p is given by

$$\Delta C_p = A_0 \cot \tfrac{1}{2}\phi + \sum_{m=1}^{\infty} A_m \sin m\phi$$

SIDE EDGE POTENTIAL SUCTION

The method used to compute the suction force at surface tips is similar to that used for the leading edge. Since the flow is irrotational

$$\frac{\partial}{\partial y} \Delta u = \frac{\partial}{\partial x} \Delta V$$

$$\frac{\partial}{\partial x} \Delta V(x,y) = -\frac{1}{2} \frac{\partial}{\partial y} \Delta C_p(x,y)$$

introduce a change of coordinates

let $\bar{x}$ be the fraction of chord

T be the slope of a constant $\bar{x}$ line $\quad T = T(\bar{x},\eta)$

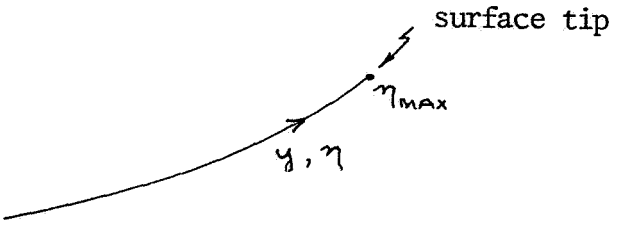

$$d\bar{x} = \frac{1}{c}[dx - T\,dy]$$

$$d\eta = dy$$

$$\left(\frac{\partial}{\partial x}\right)_y = \left(\frac{\partial \bar{x}}{\partial x}\right)_y \left(\frac{\partial}{\partial \bar{x}}\right)_\eta + \left(\frac{\partial \eta}{\partial x}\right)_y \left(\frac{\partial}{\partial \eta}\right)_{\bar{x}} = \frac{1}{c}\left(\frac{\partial}{\partial \bar{x}}\right)_\eta$$

$$\left(\frac{\partial}{\partial y}\right)_x = \left(\frac{\partial \bar{x}}{\partial y}\right)_x \left(\frac{\partial}{\partial \bar{x}}\right)_\eta + \left(\frac{\partial \eta}{\partial y}\right)_x \left(\frac{\partial}{\partial \eta}\right)_{\bar{x}} = \frac{1}{c}\left[-T\left(\frac{\partial}{\partial \bar{x}}\right)_\eta + c\left(\frac{\partial}{\partial \eta}\right)_{\bar{x}}\right]$$

or $$\left(\frac{\partial}{\partial \bar{x}}\right)_\eta \Delta V(\bar{x},\eta) = \frac{1}{2}\left[T\left(\frac{\partial}{\partial \bar{x}}\right)_\eta - c(\eta)\left(\frac{\partial}{\partial \eta}\right)_{\bar{x}}\right]\Delta C_p(\bar{x},\eta)$$

$$= \frac{1}{2}\left(\frac{\partial}{\partial \bar{x}}\right)_\eta [T(\bar{x},\eta)\Delta C_p(\bar{x},\eta)]$$

$$-\frac{1}{2}\left(\frac{\partial T}{\partial \bar{x}}\right)_\eta \Delta C_p(\bar{x},\eta) - \frac{c(\eta)}{2}\left(\frac{\partial}{\partial \eta}\right)_{\bar{x}} \Delta C_p(\bar{x},\eta)$$

then integrating

$$\Delta V(\bar{x},\eta) = \frac{1}{2}T(\bar{x},\eta)\Delta C_p(\bar{x},\eta) - \frac{1}{2}\int_0^{\bar{x}} \left\{\left(\frac{\partial T}{\partial \bar{x}}\right)_\eta + c(\eta)\left(\frac{\partial}{\partial \eta}\right)_{\bar{x}}\right\}\Delta C_p(\bar{x},\eta)\,d\bar{x} \qquad (2)$$

Near the tip, we assume a net pressure coefficient of the form

$$\Delta C_p(\xi,\eta) = \frac{\sqrt{\frac{1}{2}(\eta_{MAX}^2 - \eta^2)}}{\eta_{MAX}} \frac{C_{AVG}}{C} C_{N_0} f(\xi) , \qquad \int_0^1 f(\xi)\,d\xi = 1$$

where

$$C_N \frac{C}{C_{AVG}} = \frac{\sqrt{\frac{1}{2}(\eta_{MAX}^2 - \eta^2)}}{\eta_{MAX}} C_{N_0}$$

Differentiating

$$\frac{\partial}{\partial \eta}\Delta C_p(\xi,\eta) = -\frac{1}{2}\frac{\eta}{\eta_{MAX}} \frac{1}{\sqrt{\frac{1}{2}(\eta_{MAX}^2 - \eta^2)}} \frac{C_{AVG}}{C} C_{N_0} f(\xi)$$

Then as $\eta \to \eta_{max}$, equation 2 gives (keeping only the largest term)

$$\Delta V(\xi,\eta) = \frac{1}{4} \frac{C_{AVG}}{\sqrt{\eta_{MAX}(\eta_{MAX} - \eta)}} C_{N_0} \int_0^{\xi} f(x)\,dx$$

$$U_\infty \Delta V(\xi,\eta) = \frac{2a(\xi)}{\sqrt{(\eta_{MAX} - \eta)}} \Rightarrow a(\xi) = \frac{U_\infty}{8} \frac{C_{AVG} C_{N_0}}{\sqrt{\eta_{MAX}}} \int_0^{\xi} f(x)\,dx$$

Using the expression derived for flow around a corner (equation 1) in conjunction with this relation, the suction force at the tip is given by

$$C_S(\xi) = \frac{\Delta F_\eta}{C_T \Delta x\, q_\infty} = \frac{2\pi}{C_T q_\infty} \frac{1}{2}\rho_\infty a^2 = \frac{\pi}{32} \frac{C_{AVG}^2}{C_T \eta_{MAX}} C_{N_0}^2 \left\{ \int_0^{\xi} f(x)\,dx \right\}^2$$

$$\frac{F_\eta}{C_T^2 q_\infty} = \frac{\pi}{32} \frac{C_{AVG}^2}{C_T \eta_{MAX}} C_{N_0}^2 \int_0^1 \left\{ \int_0^{\xi} f(x)\,dx \right\}^2 d\xi$$

$$\frac{F_\eta}{S_{REF} q_\infty} = \frac{\pi}{32} \frac{C_{AVG}^2 C_T}{\eta_{MAX} S_{REF}} C_{N_0}^2 \int_0^1 \left\{ \int_0^{\xi} f(x)\,dx \right\}^2 d\xi$$

EDGE FORCE AND MOMENT INCREMENTS

To account for edge vortex effects, the linearized forces and moments are corrected to reflect losses in suction and the associated formation of vortex forces for leading and side edges. The corrections are applied to the standard lift, side force and drag coefficients. The corresponding increments in the total moment coefficients are calculated by applying the above force increments at the appropriate X,Y,Z coordinates for the leading edge stations and center of pressure for the side edges.

For leading edge force calculations, the lost suction force for each span station is given by

$$C_s \, c \, \Delta s' (1 - K_s)$$

where C_s is the coefficient of leading edge suction, c is the local chord, $\Delta s'$ is the local span station width and K_s is the leading edge suction recovery factor. This force is subtracted from the direction normal to the section leading edge and re-entered as a force component rotated $\pm 90°$ about the leading edge. The sign of the rotation is determined by the sign of the coefficient A_0 in the equation for leading edge suction.

The change in the total lift, side force and drag is calculated for each span station and is written as a function of four coordinate system rotations whose rotation angles are known from the leading edge geometry. The origin of each coordinate system is located at the leading edge of the section camber line.

The first transformation involves the rotation of the system (X_4, Y_4, Z_4), whose X axis is tangent to the local normal camber line, to the system (X_3, Y_3, Z_3), whose X axis is tangent to the corresponding chord plane as indicated in the following sketch:

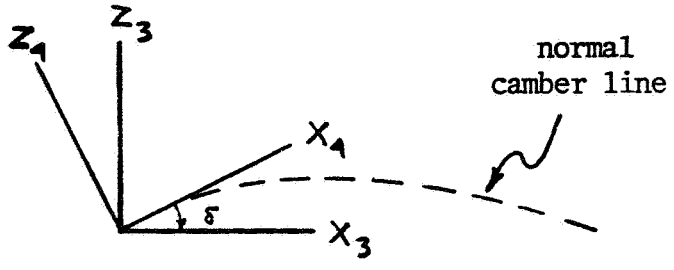

where $\delta = TAN^{-1}\{[(dz/dx)_c + (dz/dx)_\epsilon + (dz/dx)_{\delta_F}]/COS\Lambda\}$

$(dz/dx)_c$ is streamwise slope due to camber

$(dz/dx)_\epsilon$ is streamwise slope due to twist

$(dz/dx)_{\delta_F}$ is streamwise slope due to flap deflection

and

Λ is the local leading edge sweep angle.

The sweep term converts the total streamwise slope to a slope measured in the direction normal to the leading edge.

The two coordinates systems are related by the following transformation matrix:

$$\begin{Bmatrix} C_{x_3} \\ C_{y_3} \\ C_{z_3} \end{Bmatrix} = \begin{bmatrix} \cos\delta & 0 & -\sin\delta \\ 0 & 1 & 0 \\ \sin\delta & 0 & \cos\delta \end{bmatrix} \begin{Bmatrix} C_{x_4} \\ C_{y_4} \\ C_{z_4} \end{Bmatrix}$$

The second transformation involves the rotation of the system (X_3, Y_3, Z_3), whose Y axis is tangent to the leading edge, to the system (X_2, Y_2, Z_2), whose Y axis is normal to the configuration center line and in the plane of the surface.

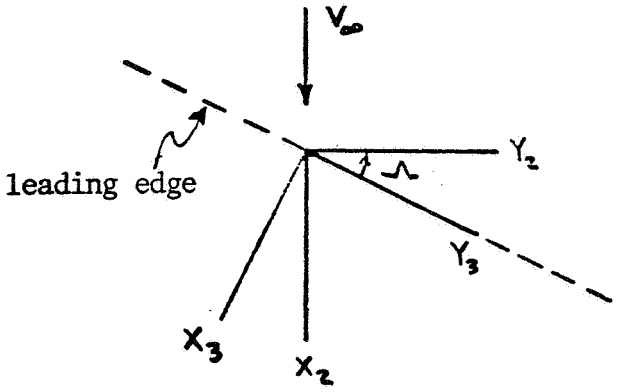

The two coordinates systems are related by the following transformation matrix:

$$\begin{Bmatrix} C_{X_2} \\ C_{Y_2} \\ C_{Z_2} \end{Bmatrix} = \begin{bmatrix} \cos\Lambda & \sin\Lambda & 0 \\ -\sin\Lambda & \cos\Lambda & 0 \\ 0 & 0 & 1 \end{bmatrix} \begin{Bmatrix} C_{X_3} \\ C_{Y_3} \\ C_{Z_3} \end{Bmatrix}$$

The third transformation involves the rotation of the system (X_2, Y_2, Z_2), whose Z axis is normal to the local surface plane, to the sytem (X_1, Y_1, Z_1), whose X, Y, and Z axes are in the body axes direction.

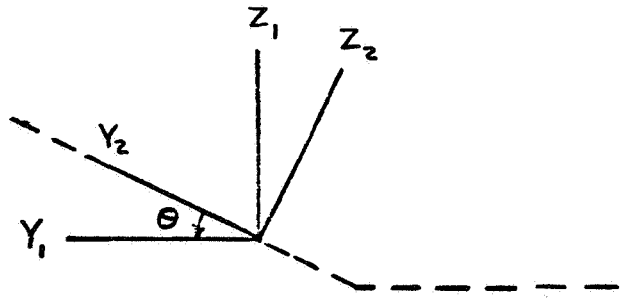

The rotation is about the X_2, X_1 axis and of magnitude Θ, the local dihedral angle. The two coordinate systems are related by the following transformation matrix:

$$\begin{Bmatrix} C_{X_1} \\ C_{Y_1} \\ C_{Z_1} \end{Bmatrix} = \begin{bmatrix} 1 & 0 & 0 \\ 0 & \cos\Theta & -\sin\Theta \\ 0 & \sin\Theta & \cos\Theta \end{bmatrix} \begin{Bmatrix} C_{X_2} \\ C_{Y_2} \\ C_{Z_2} \end{Bmatrix}$$

The fourth and final transformation involves the rotation of the body axis system (X_1, Y_1, Z_1) to the wind axes system (D, Y, L).

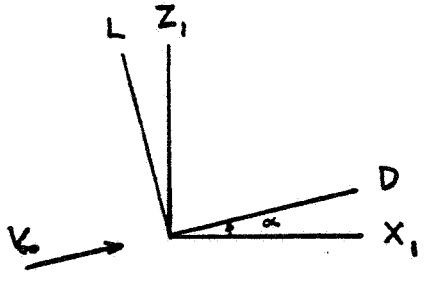

The rotation is about the Y_1, Y axis and of magnitude α, the angle of attack. The two coordinate systems are related by the following transformation matrix:

$$\begin{Bmatrix} C_D \\ C_Y \\ C_L \end{Bmatrix} = \begin{bmatrix} \cos\alpha & 0 & \sin\alpha \\ 0 & 1 & 0 \\ -\sin\alpha & 0 & \cos\alpha \end{bmatrix} \begin{Bmatrix} C_{X_1} \\ C_{Y_1} \\ C_{Z_1} \end{Bmatrix}$$

The composite transformation between the (X_4, Y_4, Z_4) coordinate system and the (D, Y, L) coordinate system can then be expressed as

$$\begin{Bmatrix} C_D \\ C_Y \\ C_L \end{Bmatrix} = \begin{bmatrix} \\ \Omega \\ \\ \end{bmatrix} \begin{Bmatrix} C_{X_4} \\ C_{Y_4} \\ C_{Z_4} \end{Bmatrix}$$

where Ω is the rotation matrix obtained from multiplication of the four previously specified transformation matrices.

Expressing C_{X4}, C_{Y4} and C_{Z4}, in terms of the leading edge suction parametors,

$$C_{X_4} = C_s c \Delta s' (1 - K_s)$$

$$C_{Y_4} = 0$$

$$C_{Z_4} = \frac{A_o}{|A_o|} C_s c \Delta s' (1 - K_s)$$

we can now write the change in drag, side force and lift resulting from the force rotation at each span station:

$$\Delta C_D = C_s c \Delta s' (1 - K_s) \Omega_D$$

$$\Delta C_Y = C_s c \Delta s' (1 - K_s) \Omega_Y$$

$$\Delta C_L = C_s c \Delta s' (1 - K_s) \Omega_L$$

where

$$\Omega_D = \left[\cos\alpha(\cos\Lambda\cos\delta) + \sin\alpha(-\sin\Theta\sin\Lambda\cos\delta + \cos\Theta\sin\delta)\right] + \frac{A_o}{|A_o|}\left[\cos\alpha(-\cos\Lambda\sin\delta) + \sin\alpha(\sin\Theta\sin\Lambda\sin\delta + \cos\Theta\cos\delta)\right]$$

$$\Omega_Y = \left[\cos\Theta\sin\Lambda\cos\delta + \sin\Theta\sin\delta\right] + \frac{A_o}{|A_o|}\left[-\cos\Theta\sin\Lambda\sin\delta + \sin\Theta\cos\delta\right]$$

and

$$\Omega_L = \left[-\sin\alpha(\cos\Lambda\cos\delta) + \cos\alpha(-\sin\Theta\sin\Lambda\cos\delta + \cos\Theta\sin\delta)\right] + \frac{A_o}{|A_o|}\left[-\sin\alpha(-\cos\Lambda\sin\delta) + \cos\alpha(\sin\Theta\sin\Lambda\sin\delta + \cos\Theta\cos\delta)\right]$$

For side edge force calculations, the lost suction force at each chord station is give by

$$C_S\, c_T^2\, \Delta\frac{X}{C}$$

where C_S is the coefficient of side edge suction, C_T is the tip chord and $\Delta\frac{X}{C}$ is the local nondimensional chord increment over which C_S is acting. This force is subtracted from the direction normal to the tip chord and re-entered as a force component rotated $\pm 90°$ about the tip chord. The sign of the rotation is determined by the sign of the coefficient C_{n_0} in the equation for side edge suction.

In a manner similar to that for the leading edge forces, the change in the total lift, side force and drag coefficients is calculated for each chord increment and is written as a function of three coordinate system rotations whose angles are known from the tip geometry. The origin of each coordinate system is located on the chord line at the beginning of each chord increment.

The first transformation involves the rotation of the system (X_3, Y_3, Z_3), whose X axis is parallel to the local camber line, to the system (X_2, Y_2, Z_2), whose X axis is tangent to the tip chord.

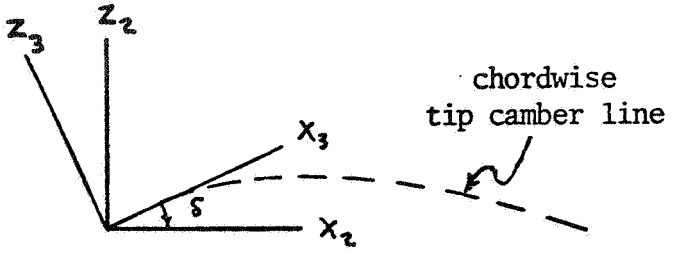

where $$\delta = TAN^{-1}\left\{ (dz/dx)_c + (dz/dx)_\epsilon + (dz/dx)_{\delta_F} \right\}$$

$(dz/dx)_c$ is streamwise slope due to camber

$(dz/dx)_\epsilon$ is streamwise slope due to twist

and

$(dz/dx)_{\delta_F}$ is streamwise slope due to flap deflection

The two coordinate systems are related by the following transformation matrix:

$$\begin{Bmatrix} C_{X_2} \\ C_{Y_2} \\ C_{Z_2} \end{Bmatrix} \quad \begin{bmatrix} \cos\delta & 0 & -\sin\delta \\ 0 & 1 & 0 \\ \sin\delta & 0 & \cos\delta \end{bmatrix} \quad \begin{Bmatrix} C_{X_3} \\ C_{Y_3} \\ C_{Z_3} \end{Bmatrix}$$

The second transformation involves the rotation of the system (X_2, Y_2, Z_2), whose Y axis is normal to the tip chord, to the system (X_1, Y_1, Z_1), whose X, Y, and Z axes are in the body axes direction.

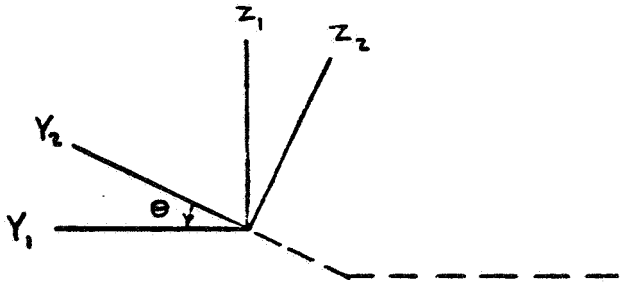

The rotation is about the X_2, X_1 axis and of magnitude Θ, the local dihedral angle. The two coordinate systems are related by the following transformation matrix:

$$\begin{Bmatrix} C_{x_1} \\ C_{y_1} \\ C_{z_1} \end{Bmatrix} \quad \begin{bmatrix} 1 & 0 & 0 \\ 0 & \cos\Theta & -\sin\Theta \\ 0 & \sin\Theta & \cos\Theta \end{bmatrix} \quad \begin{Bmatrix} C_{x_2} \\ C_{y_2} \\ C_{z_2} \end{Bmatrix}$$

The third and final transformation involves the rotation of the body axes system (X_1, Y_1, Z_1) to the wind axes system (D, Y, L).

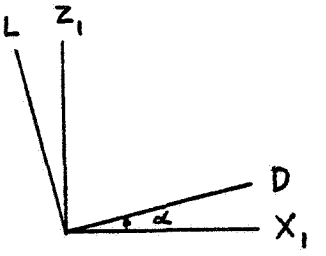

The rotation is about the Y_1, Y axis and of magitude α, the angle of attack. The two coordinate systems are related by the following transformation matrix:

$$\begin{Bmatrix} C_D \\ C_Y \\ C_L \end{Bmatrix} \quad \begin{bmatrix} \cos\alpha & 0 & \sin\alpha \\ 0 & 1 & 0 \\ -\sin\alpha & 0 & \cos\alpha \end{bmatrix} \quad \begin{Bmatrix} C_{x_1} \\ C_{y_1} \\ C_{z_1} \end{Bmatrix}$$

The transformation between the (X_3, Y_3, Z_3) coordinate system and the (D,Y,L) coordinate system can then be expressed as

$$\begin{Bmatrix} C_D \\ C_Y \\ C_L \end{Bmatrix} \quad \begin{bmatrix} \quad T \quad \end{bmatrix} \quad \begin{Bmatrix} C_{x_3} \\ C_{y_3} \\ C_{z_3} \end{Bmatrix}$$

where T is the rotation matrix obtained from multiplication of the three previously specified transformation matrices.

Expressing C_{X_3}, C_{Y_3} and C_{Z_3} in terms of the side edge suction parametors,

$$C_{X_3} = 0$$

$$C_{Y_3} = -C_s c_T^2 \Delta\frac{X}{C}$$

$$C_{Z_3} = \frac{C_{n_o}}{|C_{n_o}|} C_s c_T^2 \Delta\frac{X}{C}$$

we can now write the change in drag, side force and lift resulting from the force rotation at each side edge station:

$$\Delta C_D = C_s c_T^2 \Delta\frac{X}{C} T_D$$

$$\Delta C_Y = C_s c_T^2 \Delta\frac{X}{C} T_Y$$

$$\Delta C_L = C_s c_T^2 \Delta\frac{X}{C} T_L$$

where

$$T_D = \mp \sin\alpha \sin\Theta + \frac{C_{n_o}}{|C_{n_o}|}\left[-\cos\alpha \sin\delta + \sin\alpha \cos\Theta \cos\delta\right]$$

$$T_Y = \mp \cos\Theta + \frac{C_{n_o}}{|C_{n_o}|} \sin\Theta \cos\delta$$

$$T_L = \mp \cos\alpha \sin\Theta + \frac{C_{n_o}}{|C_{n_o}|}\left[\sin\alpha \sin\delta + \cos\alpha \cos\Theta \cos\delta\right]$$

The minus sign on the first term of each equation is for the right side of the configuration and the positive sign is for the left side. These force increments are numerically integrated along each tip chord to obtain the total change in lift, side force and drag due to side edge force roation.

APPENDIX C

HYPERSONIC FINITE ELEMENT ANALYSIS

High Mach number analysis has a number of optional methods for calculating the pressure coefficient. In each method the only geometric parameter required is the element impact angle, δ, or the change in the angle of an element from a previous point.

The methods to be used in calculating the pressure in impact ($\delta > 0$) and shadow ($\delta < 0$) regions may be specified independently. A summary of the program pressure options is presented below.

Impact Flow	Shadow Flow
1. Modified Newtonian	1. Newtonian ($C_p = 0$)
2. Modified Newtonian+Prandtl-Meyer	2. Modified Newtonian+Prandtl-Meyer
3. Tangent wedge	3. Prandtl-Meyer from free-stream
4. Tangent-wedge empirical	4. OSU blunt body empirical
5. Tangent-cone empirical	5. Van Dyke Unified
6. OSU blunt body empirical	6. High Mach base pressure
7. Van Dyke Unified	7. Shock-expansion
8. Blunt-body shear force	8. Input pressure coefficient
9. Shock-expansion	9. Free molecular flow
10. Free molecular flow	
11. Input pressure coefficient	
12. Hankey flat-surface empirical	
13. Delta wing empirical	
14. Dahlem-Buck empirical	
15. Blast wave	
16. Modified tangent-cone	

A brief review of these methods will be presented in the following text.

MODIFIED NEWTONIAN

This method is probably the most widely used of all the hypersonic force analysis techniques. The major reason for this is its simplicity. Like all the force calculation methods, however, its validity in any particular application depends upon the flight condition and the shape of the vehicle or component being considered. Its most general application is for blunt shapes at high hypersonic speed. The usual form of the modified Newtonian pressure coefficient is

$$C_p = K \sin^2 \delta$$

In true Newtonian flow ($M = \infty$, $\gamma = 1$) the parameter K is taken as 2. In the various forms of modified Newtonian theory, K is given values other than 2 depending on the type of modified Newtonian theory used. K is frequently taken as being equal to the stagnation pressure coefficient. In other forms it is determined by the following relationship (Reference 19).

$$K = \frac{C_{p_{nose}}}{\sin^2 \delta_{nose}}$$

where

$C_{p_{nose}}$ = the exact value of the pressure coefficient at the nose or leading edge

δ_{nose} = impact angle at the nose or leading edge

In other work K is determined purely on an empirical basis.

$$K = \text{fn}(M, \alpha, \text{shape})$$

When modified Newtonian theory is used, the pressure coefficient in shadow regions (δ is negative) is usually set equal to zero.

MODIFIED NEWTONIAN PLUS PRANDTL-MEYER

This method, described as the blunt body Newtonian + Prandtl-Meyer technique, is based on the analysis presented by Kaufman in Reference 20. The flow model used in this method assumes a blunt body with a detached shock, followed by an expansion around the body to supersonic conditions. This method uses a combination of modified Newtonian and Prandtl-Meyer expansion theory. Modified Newtonian theory is used along the body until a point is reached where both the pressure and the pressure gradients match those that would be calculated by a continuing Prandtl-Meyer expansion.

The calculation procedure derived for determining the pressure coefficient using the blunt body Newtonian + Prandtl-Meyer technique is outlined below.

1. Calculate free-stream static to stagnation pressure ratio

$$P = \frac{p_\infty}{p_o} = \left[\frac{2}{(\gamma + 1) M_\infty^2}\right]^{\frac{\gamma}{\gamma - 1}} \left[\frac{2\gamma M_\infty^2 - (\gamma - 1)}{\gamma + 1}\right]^{\frac{1}{\gamma - 1}}$$

2. Assume a starting value of the matching Mach number, M_q (for $\gamma = 1.4$ assume $M_q = 1.35$)

3. Calculate matching point to free-stream static pressure ratio

$$Q = \frac{p_q}{p_o} = \left[\frac{2}{2 + (\gamma - 1) M_q^2} \right]^{\frac{\gamma}{\gamma - 1}}$$

4. Calculate new free-stream static to stagnation pressure ratio

$$P_c = Q \left[1 - \frac{\gamma^2 M_q^4 Q}{4(M_q^2 - 1)(1 - Q)} \right]$$

5. Assume a new matching point Mach number (1.75) and repeat the above steps to obtain a second set of data.

6. With the above two tries use a linear interpolation equation to estimate a new matching point Mach number. This process is repeated until the solution converges.

7. Calculate the surface slope at the matching point

$$\sin^2 \delta_q = \frac{Q - P}{1 - P}$$

8. Use the Prandtl-Meyer expansion equations to find the Mach number on the surface element, M_δ

9. Calculate the surface pressure ratio

$$\frac{p_\delta}{p_o} = \eta_c \left[1 + \frac{\gamma - 1}{2} M_\delta^2 \right]^{-\frac{\gamma}{\gamma - 1}}$$

where

η_c is provided as an empirical correction factor

p_δ is the pressure on the element of interest

10. Calculate the surface to free-stream pressure ratio

$$\frac{p_\delta}{p_\infty} = \left(\frac{1}{P}\right) \left(\frac{p_\delta}{p_o}\right)$$

11. Calculate the surface pressure coefficient

$$C_{P_\delta} = \frac{2}{\gamma M_\infty^2}\left(\frac{p_\delta}{p_\infty} - 1\right)$$

The results of typical calculations using the above procedure are shown in Figure 1. Note that the calculations give a positive pressure coefficient at a zero impact angle. As pointed out in several references these results correlate well with test data for blunt shapes. However, if the surface curvature changes gradually to zero slope some distance from the blunt stagnation point the pressure calculated by this method will be too high. This is caused by characteristics near the nose intersecting the curved shock system and being reflected back onto the body. If the zero slope is reached near the nose (such as in a hemisphere or a cylinder) this effect has not had time to occur.

TANGENT-WEDGE

The tangent-wedge and tangent-cone theories are frequently used to calculate the pressures on two-dimensional bodies and bodies of revolution, respectively. These methods are really empirical in nature since they have no firm theoretical basis. They are suggested, however, by the results of more exact theories that show that the pressure on a surface in impact flow is primarily a function of the local impact angle. In this program the tangent-wedge pressures are calculated using the oblique shock relationships of NACA TR-1135 (Reference 21). The basic equation used is the cubic given by

$$\left(\sin^2\theta_s\right)^3 + b\left(\sin^2\theta_s\right)^2 + c\left(\sin^2\theta_s\right) + d = 0 \quad \text{or}$$

$$R^3 + b R^2 + c R + d = 0$$

where

θ_s = shock angle

δ = wedge angle

$$b = -\frac{M^2 + 2}{M^2} - \gamma \sin^2\delta$$

$$c = \frac{2M^2 + 1}{M^4} + \left[\frac{(\gamma+1)^2}{4} + \frac{\gamma - 1}{M^2}\right]\sin^2\delta$$

$$d = -\frac{\cos^2\delta}{M^4}$$

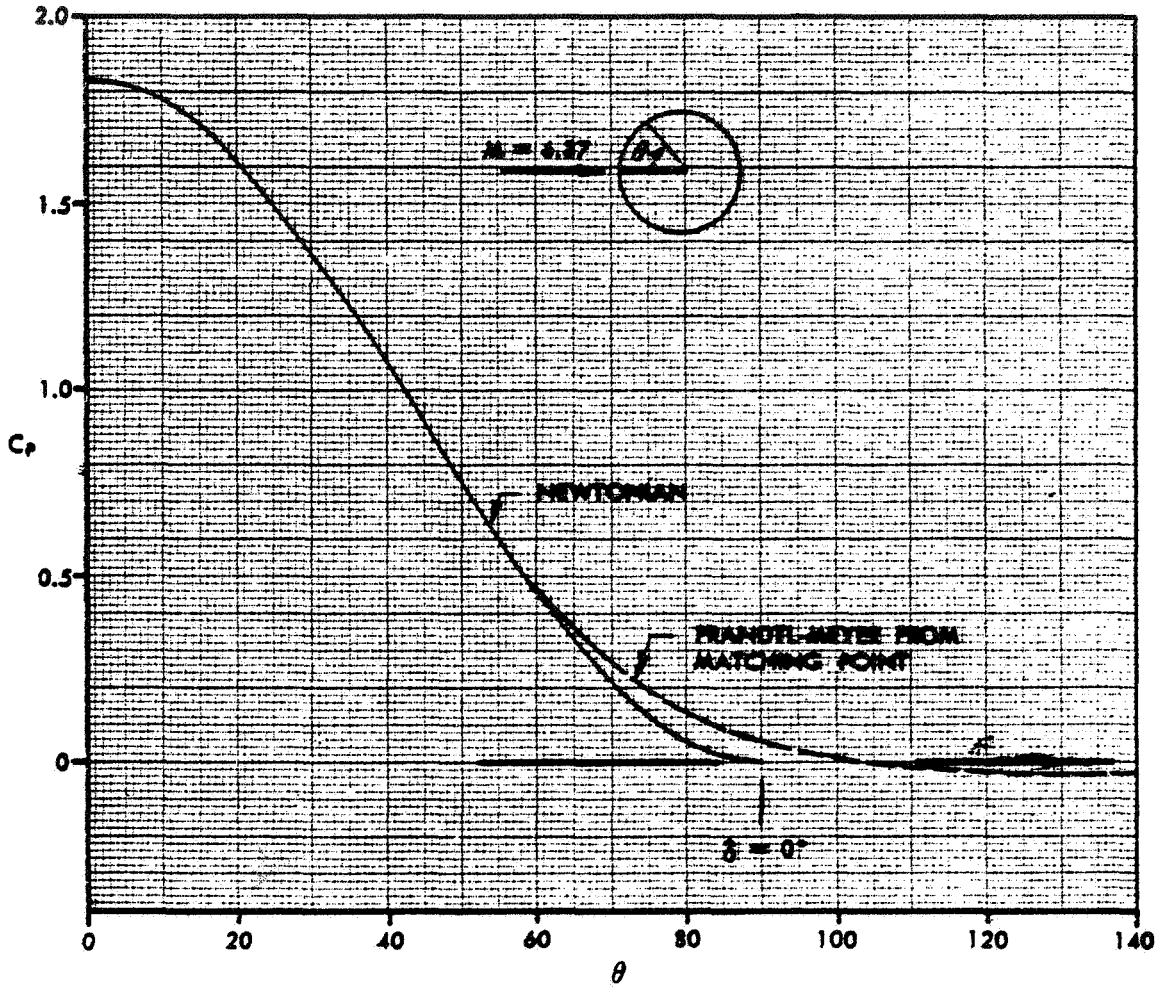

Figure 1. Blunt Body Newtonian + Prandtl-Meyer Pressure Results

The roots of the above cubic equation may be obtained by using the trigonometric solution procedure (see Reference 22) as indicated below.

$$y_1 = 2\sqrt{-p/3}\cos(\omega/3) - b/3$$

$$y_2 = -2\sqrt{-p/3}\cos(\omega/3 + 60°) - b/3$$

$$y_3 = -2\sqrt{-p/3}\cos(\omega/3 - 60°) - b/3$$

$$R_1 = y_1 - b/3$$

$$R_2 = y_2 - b/3$$

$$R_3 = y_3 - b/3$$

where

y_i = roots of the reduced cubic equation

$$p = -\frac{b^2}{3} + c$$

$$q = 2(b/3)^3 - \frac{bc}{3} + d$$

$$\cos\omega = -\frac{q}{2\sqrt{-(p/3)^3}}$$

$R_i = \sin^2\theta_s$ = roots of the cubic equation

The smallest of the three roots corresponds to a decrease in entropy and is disregarded. The largest root is also disregarded since it never appears in physical actuality.

For small deflections, the cubic solution becomes very sensitive to numerical accuracy; that is, to the number of significant digits carried. Since this is dependent on the particular machine employed, an alternate procedure is used.

When the flow deflection angle is equal to or less than 2.0 degrees, the following equation is used instead of the above cubic relationships (Reference 23):

$$\sin^2 \theta_s = \frac{1}{M^2} + \frac{\gamma + 1}{2} \frac{\delta}{\sqrt{M^2 - 1}}$$

Once the shock angle is obtained the remaining flow properties may be found from the relationships of Reference 21.

$$\text{density} = \rho_2 = \rho \left[\frac{6 M^2 \sin^2 \theta_s}{M^2 \sin^2 \theta_s + 5} \right]$$

$$\text{temperature} = T_2 = T \left[\frac{7(M^2 \sin^2 \theta_s - 1)(M^2 \sin^2 \theta_s + 5)}{36 M^2 \sin^2 \theta_s} \right]$$

$$\text{pressure coefficient} = C_p = \frac{\left[\frac{7M^2 \sin^2 \theta_s - 1}{6} \right]}{0.7 M^2}$$

where

$( )_2$ = conditions behind the shock

Oblique shock detachment conditions are reached when no solution may be found to the above cubic relationships. Under these conditions the program uses the Newtonian + Prandtl-Meyer method for continued calculations.

TANGENT-WEDGE, TANGENT-CONE, AND DELTA WING NEWTONIAN EMPIRICAL METHOD

The tangent-cone and the tangent-wedge Newtonian empirical methods used in this program are based on the empirical relationships derived below.

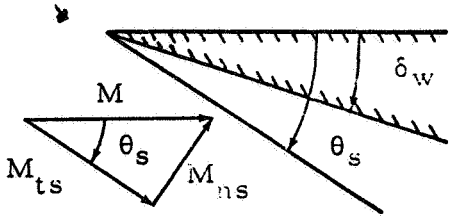

For wedge flow

$$\sin \theta_s = \frac{\sin \delta_w}{(1 - \epsilon) \cos (\theta_s - \delta_w)}$$

where

$$\epsilon = \frac{\rho}{\rho_2} = \frac{\gamma - 1}{\gamma + 1} \left[1 + \frac{2}{(\gamma - 1) M_{ns}^2} \right]$$

For cone flow (thin shock layer assumption)

$$\sin \theta_s \cong \frac{\sin \delta_c}{(1 - \frac{\epsilon}{2}) \cos (\theta_s - \delta_c)}$$

In the limit as $M \to \infty$, $\epsilon = \epsilon_{lim} = \frac{\gamma - 1}{\gamma + 1}$ and $\cos (\theta_s - \delta) = 1$

Therefore

wedge: $\sin \theta_s = \frac{\gamma + 1}{2} \sin \delta_w$ cone: $\sin \theta_s = \frac{2(\gamma + 1)}{\gamma + 3} \sin \delta_c$

These limiting expressions for θ may now be compared with the data of TR-1135 (Reference 21) at $\gamma = 7/5$ using the following similarity parameters. The exact equations contain three variables — θ_s, δ, and ϵ. Noting that for γ = constant, $\epsilon = \text{fn}(M_{ns})$ only, the preceding equations may be rewritten in the following form:

wedge

$$M_{ns} = \frac{M \sin \delta_w}{(1 - \epsilon) \cos (\theta_s - \delta_w)}$$

cone

$$M_{ns} = \frac{M \sin \delta_c}{(1 - \frac{\epsilon}{2}) \cos (\theta_s - \delta_c)}$$

The parameter $(\theta - \delta)$ is approximately constant and independent of M except near the shock detachment condition. The equations essentially contain only two variables, M_{ns} and M sin δ. These are used as coordinates to plot the data for wedge flow shown in Figure 2. A similar plot could be obtained for cone flow. From the figure it is seen that the data are nearly normalized with the use of these coordinates.

For rapid calculations we need relationships for M_{ns} as a function of M sin δ that satisfy the following requirements:

1. The effect of shock detachment is neglected
2. At M sin δ = 0, $M_{ns} = 1$
3. The solution asymptotically approaches the $M = \infty$ line
4. Have the correct slope, $\frac{d M_{ns}}{d\, M \sin\delta}$ at M sin δ = 0

These conditions lead to equations of the following form

$$\text{wedge} \quad M_{ns} = K_w M' + e^{-\frac{K_w}{2} M'}$$

$$K_w = \frac{\gamma + 1}{2}$$

$$\text{cone} \quad M_{ns} = K_c M' + e^{-K_c M'}$$

where

$$M' = M \sin \delta$$

$$K_c = 2 (\gamma + 1)/(\gamma + 3)$$

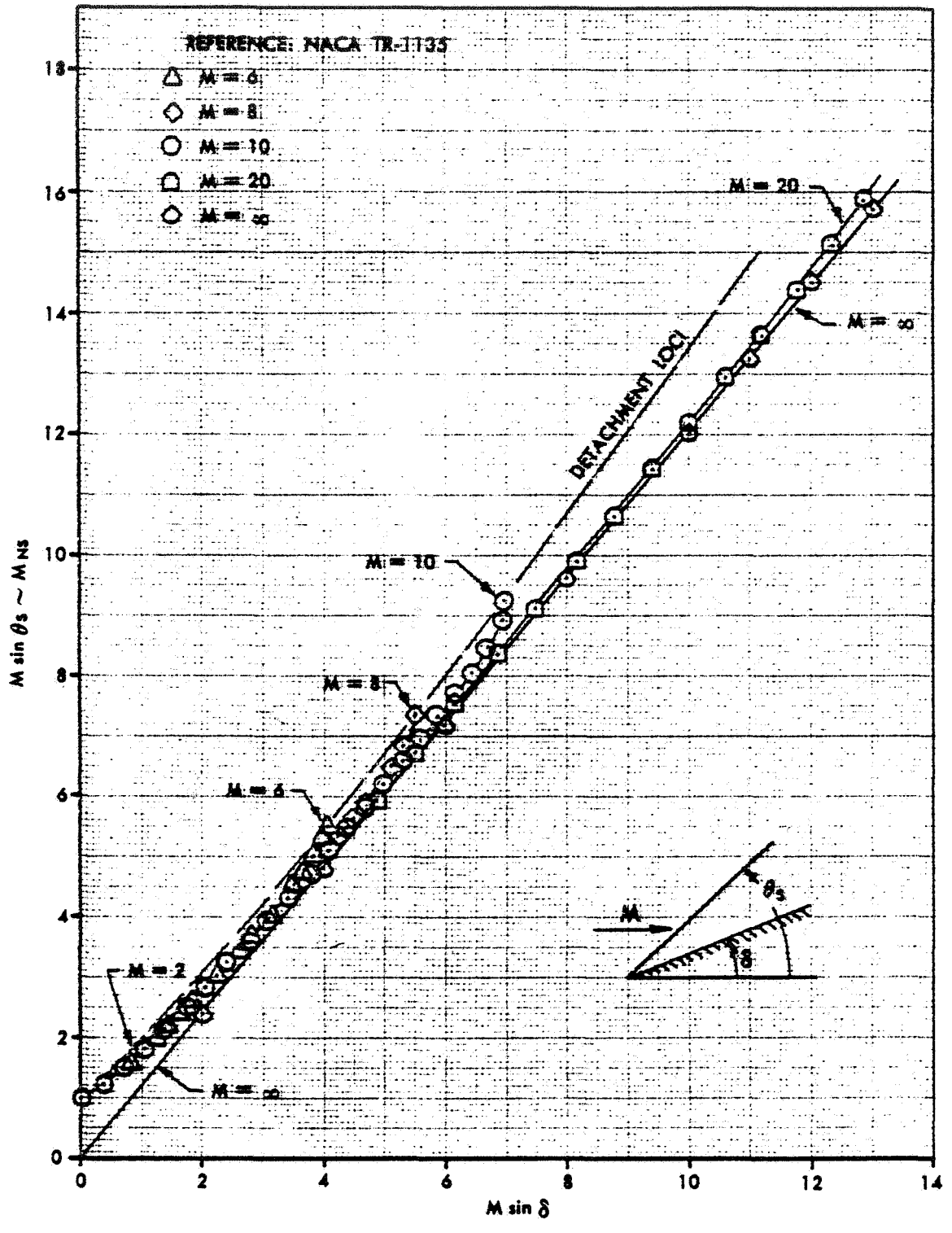

Figure 2. Wedge Flow Shock Angle

These expressions are compared with the data of TR-1135 in Figures 3 and 4. The cone data are also shown in Figure 5 with the same scales as in Figure 2.

The pressure coefficient may now be obtained by the following relationships for a wedge and cone respectively.

$$C_p = \left(\frac{4}{\gamma + 1}\right) (M_{ns}^2 - 1) \; / \; M^2$$

$$C_p = 2 \sin^2 \delta \left[1 - \frac{(\gamma - 1) \; M_{ns}^2 + 2}{4 \; (\gamma + 1) \; M_{ns}^2}\right]^{-1}$$

Experimental results have shown the pressure on the centerline of a delta wing to be in agreement with two-dimensional theory at small values of the similarity parameter ($M' < 3.0$) and with conical flow theory at higher values. The previous expressions derived for wedge and cone flows have been combined to give these features. The resulting relationships are given below.

$$M_{ns} = K_C \, M' + e^{-(K_C - \frac{K_w}{2}) \; M'}$$

For $\gamma = 7/5$

$$M_{ns} = 1.09 \, M \sin \delta + e^{-0.49 \, M \sin \delta}$$

The similarity parameter relationship for pressure is

$$M^2 \, C_p = \left(\frac{4}{\gamma + 1}\right) \left(M_{ns}^2 - 1\right)$$

The shock angle and pressure coefficient calculated from the above equations are compared with the experimental results (Reference 28) in Figures 6 and 7, respectively.

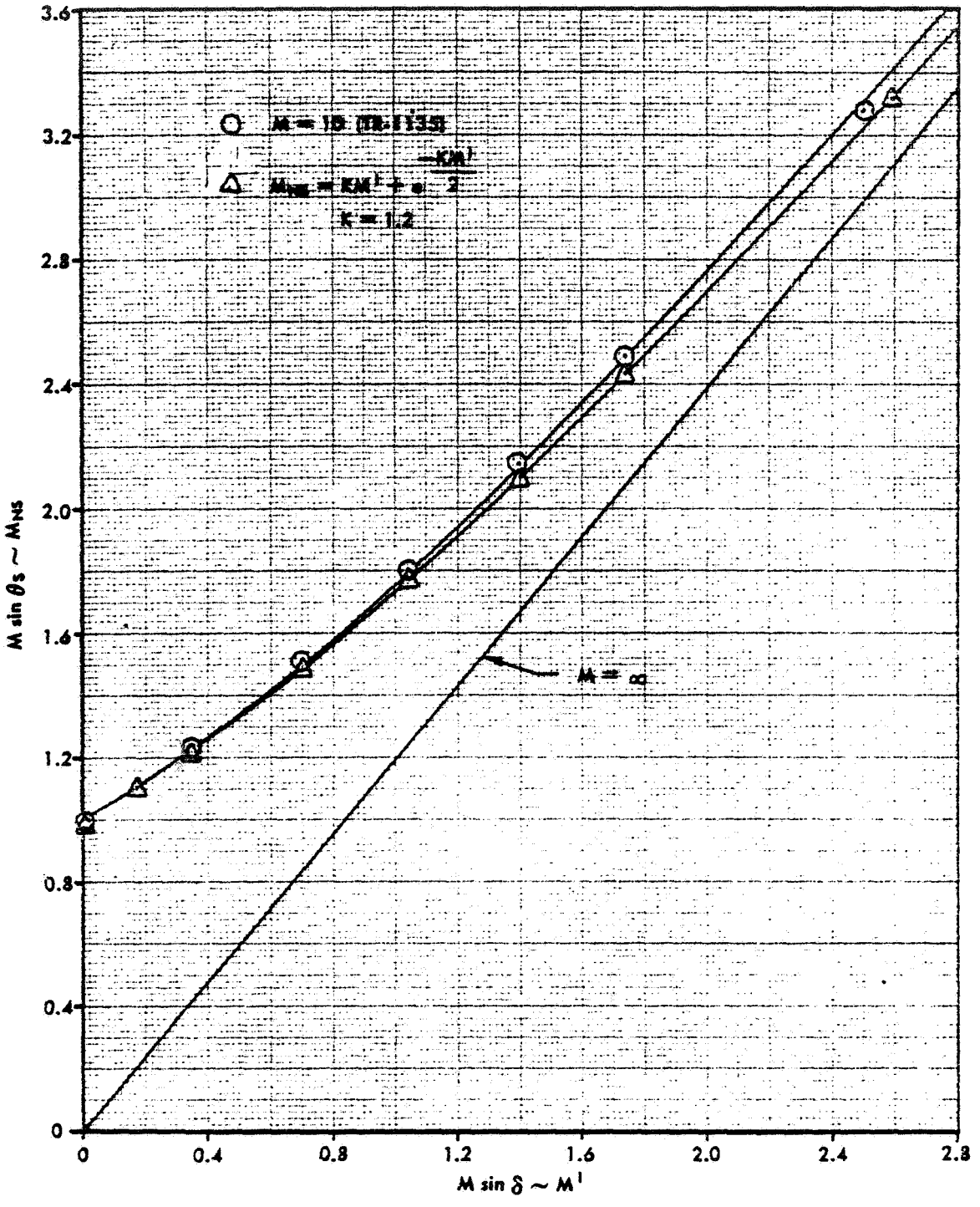

Figure 3. Wedge Flow Shock Angle Empirical Correlation

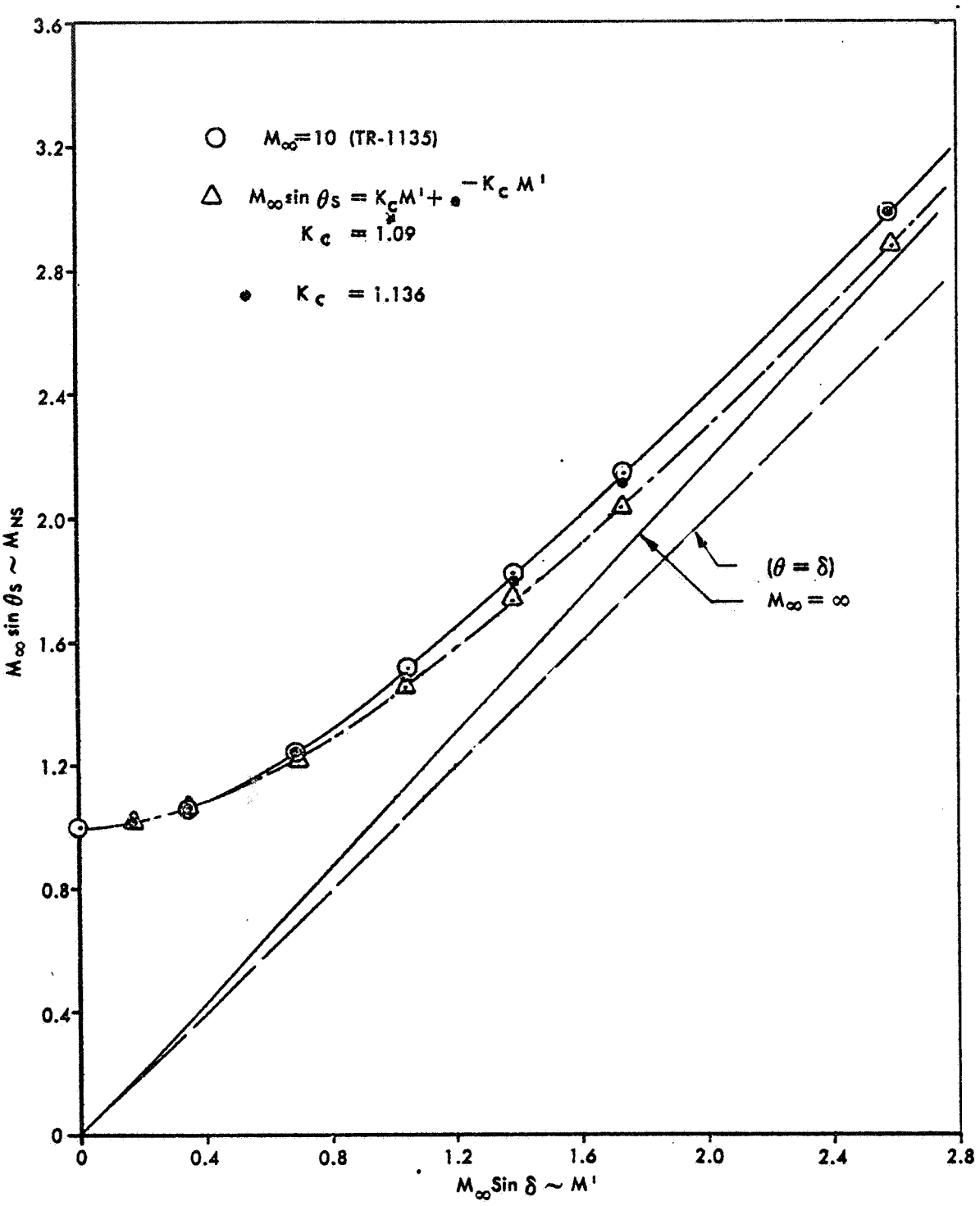

Figure 4. Conical Flow Shock Angle Empirical Correlation

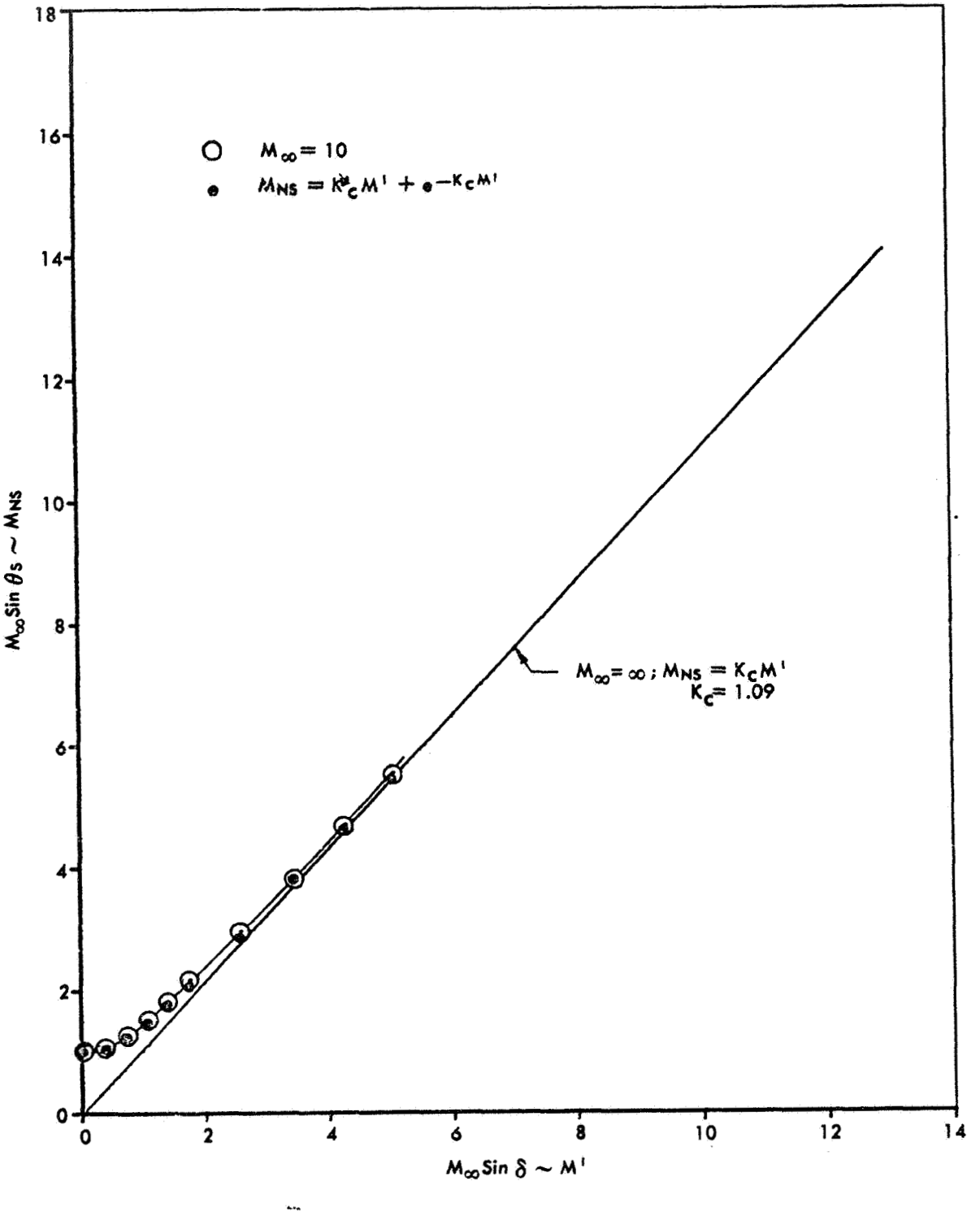

Figure 5. Conical Flow Shock Angle Empirical Correlation

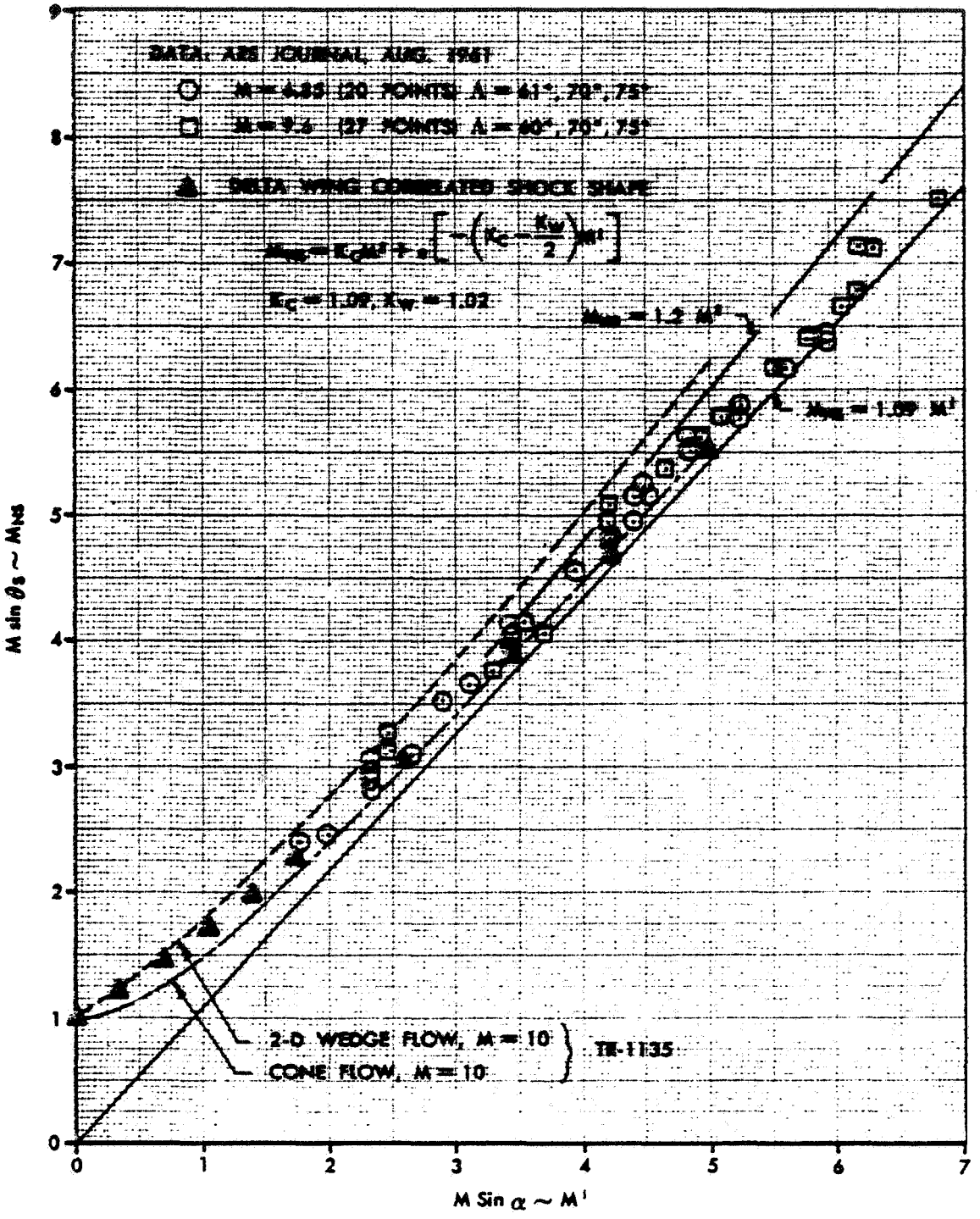

Figure 6. Delta Wing Centerline Shock Angle Correlation

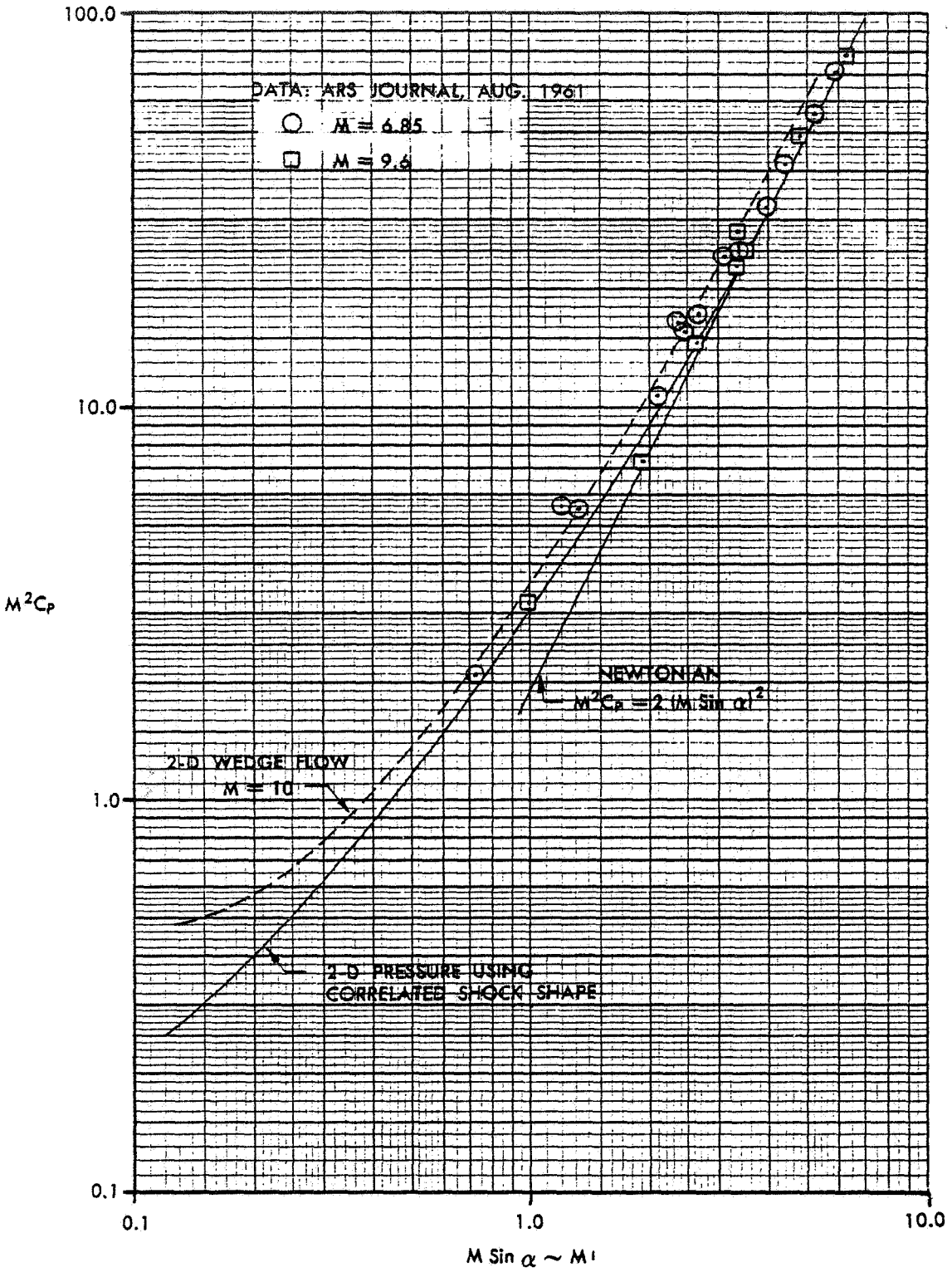

Figure 7. Delta Wing Centerline Pressure Coefficient Correlation

OSU BLUNT BODY EMPIRICAL METHOD

The OSU (Ohio State University) blunt body empirical equation describes the pressure distribution about cylinders in supersonic flow. The equation was presented in Reference 25) and was stated to match "all the data obtained on the cylinders in the present test series with a maximum deviation of 2.5 percent." The expression used is

$$\frac{p_1}{p_{t_\infty}} = 0.32 + 0.455 \cos\theta + 0.195 \cos 2\theta + 0.035 \cos 3\theta - 0.005 \cos 4\theta$$

where

θ = peripheral angle on a cylinder (= 0 at the stagnation point) = $90° - \delta$

p_1 = surface pressure

p_{t_∞} = total pressure rise through normal shock

The pressure coefficient is calculated from the relationship

$$C_p = \left[\left(\frac{p_1}{p_{t_\infty}}\right)\left(\frac{p_{t_\infty}}{p_\infty}\right) - 1\right] \Big/ \left(\frac{\gamma}{2} M^2\right)$$

where

$$\frac{p_{t_\infty}}{p_\infty} = K \frac{\gamma}{2} M^2 + 1$$

K = stagnation pressure coefficient = $C_{p_{stag}}$

p_∞ = freestream pressure

γ = ratio of specific heats = 1.4

VAN DYKE UNIFIED METHOD

This force calculation method is based on the unified supersonic-hypersonic small disturbance theory proposed by Van Dyke in Reference 26 as applied to basic hypersonic similarity results. The method is useful for thin profile shapes and as the name implies extends down to the supersonic speed region.

The similarity equations that form the basis of this method are derived by manipulating the oblique shock relations for hypersonic flow. The basic derivations are shown on pages 753 and 754 of Reference 31. The result obtained for a compression surface under the assumption of a small deflection angle and large Mach number is (hypersonic similarity equation).

$$C_p = \delta^2 \left[\frac{\gamma + 1}{2} + \sqrt{\left(\frac{\gamma + 1}{2} \right)^2 + \frac{4}{H^2}} \right]$$

where H is the hypersonic similarity parameter given by $M\delta$. The contribution by Van Dyke in Reference 26 suggests that this relationship will also be valid in the realm of supersonic linear theory if the hypersonic similarity parameter $M\delta$ is replaced by the unified supersonic-hypersonic parameter $\left(\sqrt{M^2 - 1}\right)\delta$. This latter parameter is used in the calculations for this force option in the arbitrary body program.

A similar method may also be obtained for a surface in expansion flow with no leading edge shock such as on the upper side of an airfoil. The resulting equation is

$$C_p = \delta^2 \frac{2}{\gamma H^2} \left[\left(1 - \frac{\gamma - 1}{2} H \right)^{\frac{2\gamma}{\gamma - 1}} - 1 \right]$$

where again H is taken to be $\left(\sqrt{M^2 - 1}\right)\delta$ in the unified theory approach.

SHOCK-EXPANSION METHOD

This force calculation method is based on classical shock-expansion theory (see Reference 27). In this method the surface elements are handled in a "strip-theory" manner. The characteristics of the first element of each longitudinal strip of elements may be calculated by oblique shock theory, by conical flow theory, or by a Prandtl-Meyer expansion. Downstream of this initial element the forces are calculated by a Prandtl-Meyer expansion.

By a proper selection of the element orientation the method may be used for both wing-like shapes and for more complex body shapes. In this latter case the method operates in a hypersonic shock-expansion theory mode.

FREE MOLECULAR FLOW METHOD

At very high altitudes conventional continuum flow theories fail and one must begin to consider the general macroscopic mass, force, and energy transfer problem at the body surface. This condition occurs when the air is sufficiently rarefied so that the mean free path of the molecules is much greater than a characteristic body dimension. This condition is known as free molecular flow and the method of analysis selected for this program is described in Reference 28. This method was also used in Reference 29. The equations used were taken from these references and are presented below.

Pressure coefficient

$$C_p = \frac{1}{S^2}\left\{\left[\frac{2-f_n}{\sqrt{\pi}} S \sin\delta + \frac{f_n}{2}\sqrt{\frac{T_b}{T_\infty}}\right] e^{-(S\sin\delta)^2} + \left[(2-f_n)(S^2\sin^2\delta + \frac{1}{2}) + \frac{f_n}{2}\sqrt{\pi}\sqrt{\frac{T_b}{T_\infty}} S\sin\delta\right]\left[1+\mathrm{erf}(S\sin\delta)\right]\right\}$$

Shear force coefficient

$$C_f = \frac{(\cos\delta) f_t}{\sqrt{\pi} S}\left\{e^{-(S\sin\delta)^2} + \sqrt{\pi} S \sin\delta\left[1+\mathrm{erf}(S\sin\delta)\right]\right\}$$

where

S = speed ratio = $\sqrt{\gamma/2}\ M_\infty$

f_n = normal momentum accommodation coefficient (= 1.0 for Newtonian and = 0. for completely diffuse reflection)

δ = impact angle

T_b = body temperature, °K

T_∞ = free-stream temperature, °K

erf = error function $\mathrm{erf}(x) = \frac{2}{\sqrt{\pi}}\int_0^x e^{-x^2}\,dx$

f_t = tangential momentum accommodation coefficient (= 0. for Newtonian flow and 1.0 for completely diffuse reflection)

The pressure force acts perpendicular to the surface and this direction is readily obtained since the element normal has already been determined in the geometry subroutines. The shear force acts in the direction of the tangential velocity component on the surface and this direction is determined by taking successive vector products as follows.

The procedure is illustrated in the accompaning sketch where the incident velocity vector is defined as

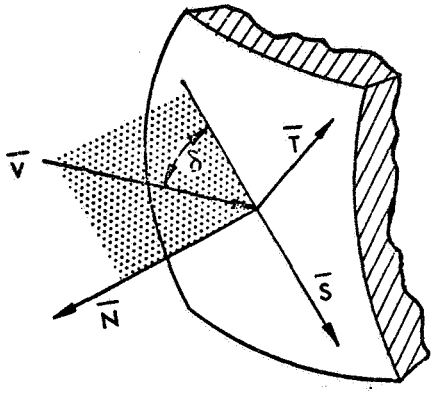

$$\bar{V} = V_X \bar{i} + V_Y \bar{j} + V_X \bar{k}$$

and the surface normal as

$$\bar{N} = N_X \bar{i} + N_Y \bar{j} N_Z \bar{k}$$

First, a surface tangent vector ($\bar{T}$) is defined by the cross product of the normal and velocity vectors;

$$\bar{T} = T_X \bar{i} + T_Y \bar{j} + T_Z \bar{k}$$

where

$$T_X = N_Y V_Z - N_Z V_Y$$

$$T_Y = N_Z V_X - N_X V_Z$$

$$T_Z = N_X V_Y - N_Y V_X$$

Then the direction of the shear force ($\bar{S}$) is given by the cross product of the surface tangent and normal vectors;

$$\bar{S} = S_X \bar{i} + S_Y \bar{j} + S_Z \bar{k}$$

where

$$S_X = T_Y N_Z - T_Z N_Y$$

$$S_Y = T_Z N_X - T_X N_Z$$

$$S_Z = T_X N_Y - T_Y N_X$$

The final components of the shear force in the vehicle axis system are given by

$$SHEAR_X = (SHEAR)\left(S_X\right) / STOTAL$$

$$SHEAR_Y = (SHEAR)\left(S_Y\right) / STOTAL$$

$$SHEAR_Z = (SHEAR)\left(S_Z\right) / STOTAL$$

where

SHEAR is the shear force as calculated by the free molecular flow equations.

$$STOTAL = \left(S_X^2 + S_Y^2 + S_Z^2\right)^{1/2}$$

In using the free molecular flow method the above analysis must be carried out over the entire surface of the shape including the base, shadow regions, etc. When the free molecular flow method is selected, it is used for both impact and shadow region.

The plane formed by the velocity vector and the surface normal is referred to as the velocity plane (shaded region in the sketch), since both the incident and surface velocity are in this plane. This definition is correct for two-dimensional flow, however, it is only an approximation to the shear direction in the general arbitrary-body case.

HANKEY FLAT-SURFACE EMPIRICAL METHOD

This method uses an empirical correlation for lower surface pressures on blunted flat plates. The method, derived in Reference 30, approximates tangent-wedge at low impact angles and approaches Newtonian at high impact angles. The pressure coefficient is given by

$$C_p = 1.95 \sin^2 \delta + 0.21 \cos \delta \sin \delta$$

DAHLEM-BUCK EMPIRICAL METHOD

This is an impact method that has been derived such that tangent-cone and Newtonian results are approximated, respectively, at low and high values of the impact angle. The empirical relationships presented in Reference 31 are

for $\delta < 22.5^{\circ}$ $\quad C_p = \dfrac{1 + (\sin 4\delta)^{3/4}}{(4 \cos \delta \cos 2\delta)^{3/4}} (\sin \delta)^{5/4}$

for $\delta \geq 22.5^{\circ}$ $\quad C_p = 2.0 \sin^2 \delta$

BLAST WAVE PRESSURE INCREMENTS

This method uses conventional blast-wave parameters to calculate the overpressure due to bluntness effects. Force contributions determined by this procedure must be added to the regular inviscid pressure forces (tangent-wedge, tangent-cone, Newtonian, etc.) calculated over the same vehicle geometry. The specific blast wave solutions used in the Program were derived by Lukasiewicz in Reference 32:

$$\frac{P}{P_\infty} = A M_\infty^2 \left\{ \frac{(C_D)^{\frac{1}{1+j}}}{(X_o - X)/d} \right\}^{\frac{2+j}{3}} + B$$

where

C_D is the nose drag coefficient

d is the nose diameter or thickness

X_o is a coordinate reference point

and the coefficients A, B are

Flow	j	A	B
Two-Dimensional	0	0.121	0.56
Axisymmetric	1	0.067	0.44

MODIFIED TANGENT-CONE METHOD

This method, originally developed for use on cones with elliptical cross-sections, modifies the tangent-cone result by an increment representing the deviation from an average pressure divided by an average Mach number. More specifically, the following equations are used (after Jacobs, Reference 33):

$$C_p = C_{p_{tc}} - \frac{C_{p_{tc}} - C_{p_{avg}}}{M_{avg}}$$

where C_p is the surface pressure coefficient

$C_{p_{tc}}$ is the conventional tangent-cone pressure coefficient

$C_{p_{avg}}$ is the average pressure coefficient

$= \sum C_{p_t} A / \sum A$, A is element area

M_{avg} is the average Mach number, defined for an equivalent cone having pressure coefficient $C_{p_{avg}}$.

HIGH MACH BASE PRESSURES

For a body in high speed flow it might be expected that any base regions would experience total vacuum. That is,

$$C_p = - \frac{1}{\frac{\gamma}{2} M_\infty^2}$$

However, the viscosity of real gases causes some pressure to be felt in base region and experimental data have shown this to be roughly 70% vacuum for air. Therefore, the expression

$$C_p = - \frac{1}{M_\infty^2}$$

has been included in the program.

1. Report No.	2. Government Accession No.	3. Recipient's Catalog No.
NASA CR-165627		

4. Title and Subtitle	5. Report Date
Aerodynamic Preliminary Analysis System II Part I - Theory	January 1981
	6. Performing Organization Code

7. Author(s)	8. Performing Organization Report No.
E. Bonner, W. Clever, K. Dunn	NA-80-374
	10. Work Unit No.

9. Performing Organization Name and Address	11. Contract or Grant No.
Rockwell International Corporation North American Aircraft Division Los Angeles, California 90009	NAS1-15674
	13. Type of Report and Period Covered
12. Sponsoring Agency Name and Address	Contractor Report
National Aeronautics and Space Administration Langley Research Center Hampton, Virginia 23665	14. Sponsoring Agency Code

15. Supplementary Notes

Langley technical monitor: Alan W. Wilhite
Part I Final Report

16. Abstract

An aerodynamic analysis program based on potential theory with edge considerations at subsonic/supersonic speeds and impact type finite element analysis at hypersonic conditions is described. Three dimensional configurations having multiple non-planar surfaces of arbitrary planform and bodies of non-circular contour may be analyzed. Static, rotary, and control longitudinal and lateral-directional characteristics may be generated.

The analysis has been implemented on a time sharing system in conjunction with an input tablet digitizer and an interactive graphics input/output display and editing terminal to maximize its responsiveness to the preliminary analysis problem. CDC 175 computation time of 45 CPU seconds/Mach number at subsonic-supersonic speeds and 1 CPU second/Mach number/attitude at hypersonic conditions for a typical simulation indicates that program provides an efficient analysis for systematically performing various aerodynamic configuration tradeoff and evaluation studies.

17. Key Words (Suggested by Author(s))	18. Distribution Statement
aerodynamic analysis subsonic supersonic hypersonic	Unclassified - Unlimited

19. Security Classif. (of this report)	20. Security Classif. (of this page)	21. No. of Pages	22. Price*
		124	